WILL

ANNUAL REPORT 1990

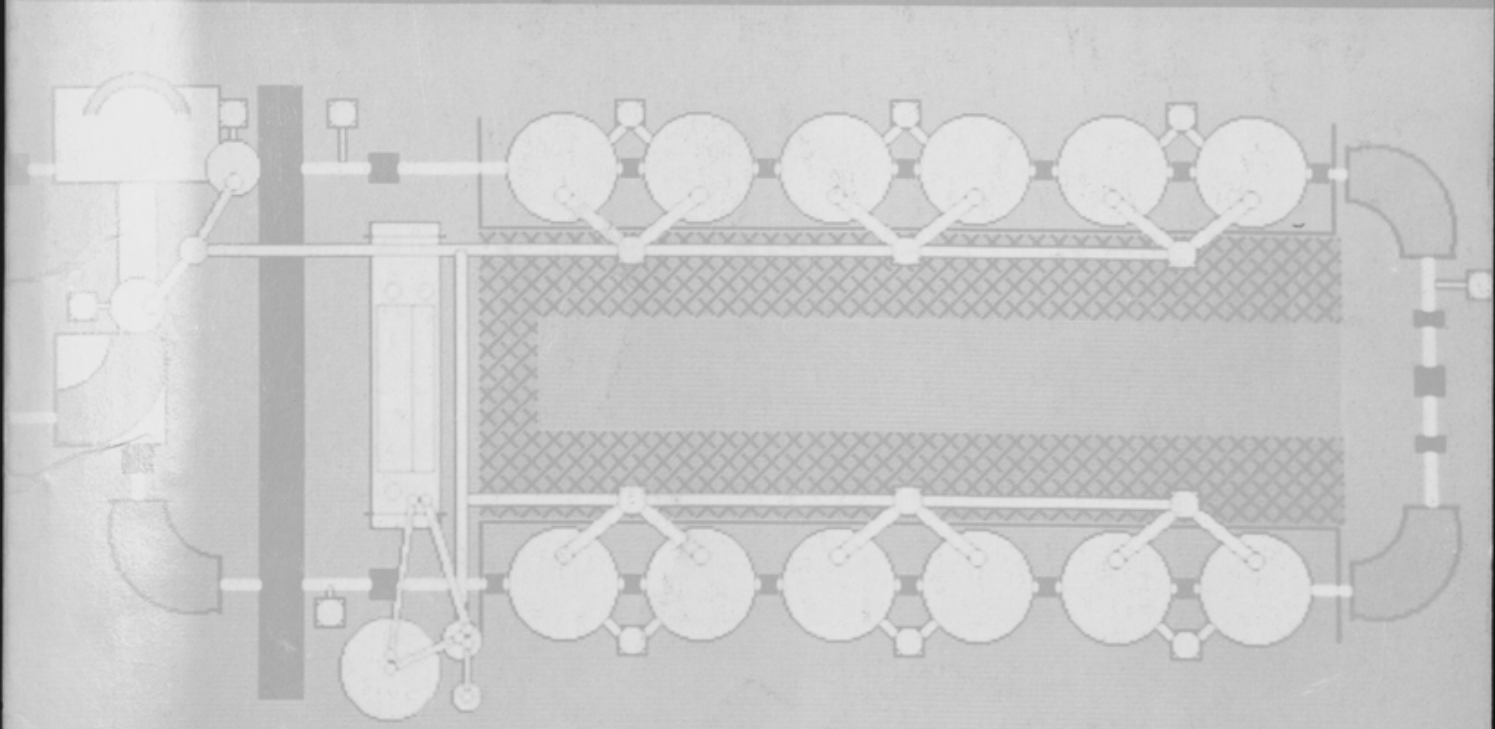

NUCLEAR PHYSICS LABORATORY
UNIVERSITY OF WASHINGTON

ANNUAL REPORT

Nuclear Physics Laboratory
University of Washington
April, 1990

Supported in part by the United States Department of Energy
under contract DE-AC06-8lER40048 and grant DE-FG06-90ER40537

Cover Photo

Our cover photo is a monochrome montage of two touch-screen color displays that are part of the control system for our booster. When the cover is opened one sees on the upper left of the back cover the injector deck where two of the ion sources are now located. Also indicated below the tandem injection line is the new polarized ion source. On the front cover the booster itself is seen. The beam completes a loop starting at upper left and eventually exiting to the experimental areas (not shown) above the crossover. Touching any of the elements seen, such as cryostats, magnets, pumping stations or diagnostic elements, calls up new display pages which enables one to check the status of or change the parameters of the elements involved.

The display was generated by Mark Howe and photographed by Mary Levine. The cover was designed by Michael Strong of the Office of University Publications.

INTRODUCTION

We continue to exploit our complex of accelerators and ion-sources over a wide range of energy and mass. We are using light- and medium-mass nuclei from the booster to study nucleus-nucleus collisions and the statistical properties of excited nuclei. Polarized and unpolarized protons and deuterons were used this year, chiefly at low energies, to study few body systems and to produce polarized β-emitting nuclei. Accelerator mass spectrometry (AMS) of ^{14}C with the tandem has improved steadily, and now has a precision and accuracy of 1%, limited by counting statistics. Recently, we have used the injector deck to accelerate molecular clusters containing deuterium, in a search for tepid fusion events in the bombardment of deuterated titanium. In our non-accelerator research, we continue to develop powerful instrumentation, notably the parallel plate avalanche counters for LEAR and the Eöt-Wash torsion balance.

In our studies of the shapes of highly excited nuclei from giant dipole resonance (GDR) decay measurements, we are presently concentrating on measurements and interpretation of γ-ray angular distributions. We expect our $^{90}Zr^{*}$ -$^{92}Mo^{*}$ results to be well described by the rotating liquid drop model. Thus these results will form a benchmark test of our ability to quantitatively understand the γ-ray anisotropies through the inclusion of thermal shape and orientation fluctuations. Last year we reported the inference from GDR decay studies of large nuclear isospin mixing in light nuclei at high excitation energies. Further measurements confirm the assumption of statistical decay, and hence the isospin mixing results remain a puzzle theoretically.

Investigation of the total reaction cross sections of the fragile projectiles $^{6,7}Li$ and ^{9}Be has shown the expected large breakup cross section in mass 7 and 9. However, the analysis reveals a surprising discrepancy between the absorption radius and the charge radius for ^{6}Li. A detailed study of rainbow scattering may provide new insights into this problem.

We have continued to exploit our new electrostatic separator to measure gamma ray multiplicities for fusion events tagged by evaporation residues. This device has allowed us to make measurements at lower subbarrier energies than previously. We have demonstrated the existence of the barrier bump in the mean spin for the $^{28}Si + ^{154}Sm$ system.

Our studies of hard photons have continued on two fronts. We have completed analysis of an experiment with a 35 MeV/u ^{14}N beam on a Ag target (measured at MSU). These data, together with data on the emission of pre-equilibrium neutrons and protons confirms the importance of the nucleon momentum tails in determining the spectrum of nucleon-nucleon collisions during the early stage of a heavy ion collision. We have also looked for hard photons previously reported with a surprisingly large decay probability in the spontaneous fission of ^{252}Cf. We have set an upper limit considerably lower than the value reported, but in agreement with our theoretical expectations.

We continue the study of polarization phenomena, both with the polarized ion source (PIS) and the analysis of polarization produced in nuclear reactions. In particular, we find large polarizations in the $^{59}Co(^{3}He, \overrightarrow{p})$ reaction. With the PIS, we have begun measurements of the angular distribution of the $^{2}H(\overrightarrow{d}, \gamma)^{4}He$ reaction at $E_d = 1$ MeV. The angular distribution and analyzing powers are sensitive to D-state components in ^{4}He and non E2 radiation amplitudes. We are working to optimize the production of polarized β-emitters in order to measure the beta asymmetry in mixed Fermi and Gamow-Teller transitions in $T = 1/2$ mirror pairs. This work is in collaboration with a

group from Argonne National Laboratory. We will also use the $\vec{d}$ beam to calibrate a deuteron tensor polarimeter from TRIUMF, which is intended for polarization measurements in π-d elastic scattering.

Considerable effort has gone into planning a new β-decay experiment in mass-8 that is expected to provide the most precise semi-leptonic tests of time-reversal invariance, conservation of the vector current, and second class currents.

We are continuing experiments to determine properties of resonances that should dominate explosive nucleosynthesis. Our (^{3}He, n) time-of-flight measurements have greatly profited from the new tandem buncher developed for linac injection.

The AMS group, in collaboration with colleagues in the UW School of Oceanography, is studying $^{14}CH_4$ concentrations in methane from wetland environments and the atmosphere. This work has demonstrated that the ^{14}C content of atmospheric methane is increasing at about 1.4% per year, probably due in large part to $^{14}CH_4$ released from nuclear reactors.

The Eöt-Wash group continues to improve the sensitivity of their rotating torsion balance search for new macroscopic forces. The balance is presently sensitive to a rotational excitation of the pendulum of 10^{-29} eV/atom. The limits obtained on new forces coupling either to baryon number or to baryon$-$lepton number are roughly two orders of magnitude better than the best previous results for interactions with ranges between 1 m and 3×10^{10} m.

In May, 1989, a first comparison of antiproton and proton masses was achieved by the PS 196 collaboration at CERN. Using the temperature of axial motion in a Penning trap of antiprotons and electrons as a signal, we were able to set an upper limit of 2×10^{-6} on the mass asymmetry. Resonant detection of antiproton cyclotron motion in the trap has now been implemented. Using this technique, the asymmetry upper limit has recently been reduced to about a part in 10^7, with a cloud of $\sim 1000\overline{p}$. Refinement of the trap quality and reduction of the cloud size to order one $\overline{p}$ should provide an asymmetry measurement at the 1 part per billion scale.

We have joined the APEX collaboration, which intends to carry out a series of experiments using the ATLAS accelerator facility at Argonne to determine the origin of correlated e^+e^- pairs produced in heavy ion collisions, as observed at GSI. The APEX apparatus is a solenoid electron spectrometer based on the EPOS spectrometer at GSI, but with more complete kinematic information, and designed for a factor 20 greater count rate.

The analysis of our data from the comparison of inclusive scattering of positive and negative pions from medium and heavy nuclei has been improved. We are developing a semi-classical model to relate the spectra and angular distributions to the pion-nucleon interaction and the nuclear geometry. Progress with a new experiment to study inclusive photo-production of pions on a variety of nuclei has been limited by difficulties with the Saskatoon Accelerator. During the past year the prototype counter has been built and tested with a bremsstrahlung beam, and we are awaiting an opportunity to perform further tests with the tagger. We are able to identify pions produced by the bremsstrahlung beam; with the tagger we will be able to make a quantitative measurement of the efficiency of the counter for pion identification, and we will also get a useful measure of the backgrounds expected for the experiment.

The proposed Pegasys experiment at SLAC passed several milestones in the past year. A conceptual design report (CDR) and budget were submitted to the DOE. A joint SLAC, DOE technical review committee examined the CDR in Jan 1990. This experiment proposes to measure the hadronic cascade formed in deep inelastic electron scattering. Chief among many goals for this experiment is the study of the formation length of hadrons. At the UW, we have continued our responsibility for the time-of-flight wall. We are confident that with either the existing PEP ring, or a proposed 'B-factory' there is an exciting program of research for the Pegasys experiment.

The Nuclear Physics Laboratory provides charged particle and neutron beams for a variety of research groups outside the University. During the past year, four groups from the Boeing Company used our facilities, primarily to test the ability of various electronics components to withstand radiation. In addition, we radiated bearing materials for a group from Rocketdyne developing radioisotope techniques to monitor rocket engine bearing wear.

Our superconducting booster has been in regular operation during the year ending February 28, 1990. Improvements have been made in the booster control system, permitting faster tuning, and component reliability has improved. Graduate students are being trained to operate the booster. We have begun work aimed at improving resonator plating, in order to increase the maximum energy available from the accelerator.

As always, we welcome applications from outsiders for the use of our facilities. As a convenient reference for potential users, the table on the following page lists the vital statistics of our accelerator. For further information, please write or telephone Dr. W.G. Weitkamp, Technical Director, Nuclear Physics Laboratory, University of Washington, Seattle, WA 98195; (206) 543-4080.

We close this introduction with a reminder that the articles in this report describe work in progress and are not to be regarded as publications or quoted without permission of the authors. In each article, the names of the investigators have been listed alphabetically, with the primary author underlined.

We thank María Ramírez and Ida Tess for producing this report.

Charles Hyde-Wright
Editor

TANDEM VAN DE GRAAFF ACCELERATOR

A High Voltage Engineering Corp. Model FN purchased in 1966 with NSF funds; operation funded primarily by the U.S. Department of Energy. See W.G. Weitkamp and F.H. Schmidt, "The University of Washington Three Stage Van de Graaff Accelerator," Nucl. Instrum. Meth. **122**, 65 (1974).

Available Energy Analyzed Beams

Ion	*Max. Current* (pμA)	*Max. Practical Energy* MeV
p,d	10	18
polarized p,d	0.1	18
He	2	27
Li	1	36
C	3	63
O	2	72
Si	0.3	90
Ni	0.2	99
I	0.01	108

BOOSTER ACCELERATOR

Our linac Booster Accelerator has become operational during the past year. We give in the following table maximum beam energies and expected intensities for several representative ions.

Available Energy Analyzed Beams

Ion	*Max. Current* (pμA)	*Max. Energy (MeV)*
p	> 1	35
d	> 1	37
He	0.2	65
^{6}Li	0.1	94
C	0.6	170
N	0.03	198
O	0.2	205
O	0.1	220
Si	0.1	300
^{35}Cl	0.02	358
Ni	0.001	395

Contents

1 GIANT RESONANCES

1.1 Giant Dipole Radiation and Isospin Purity in Highly Excited Compound Nuclei

J.A. Behr, Z.M. Drebi, C.A. Gossett, J.H. Gundlach, M.S. Kaplan, M. Kicinska-Habior* and K.A. Snover

We have continued our studies of isospin violation in highly excited light compound nuclei. We look for γ decay of the Giant Dipole Resonance built on excited states. Since the E1 operator is isovector, T=0 to T=0 transitions are isospin forbidden. So the statistical GDR γ-yield from a T=0 compound nucleus will come from isospin mixing of the initial states into T=1 states, from isospin-allowed decays to T=1 final states, and from daughter nuclei populated by particle decay. (Statistical decay does not depend on the isospin mixing of the final states reached by γ decay.) For example, our statistical calculation of the GDR γ-ray yield from ^{28}Si at an excitation energy E*=47 MeV changes by a factor of 8 depending on whether isospin is pure or completely mixed. The GDR γ-ray yield of an N$\neq$Z nucleus is much less sensitive to isospin mixing, because all γ-decay channels are isospin allowed.[1]

The experimental GDR γ-ray yields of T=0 ^{28}Si at E*=47 and 63 MeV are greater by factors of 2–3 than if isospin were pure, as determined by comparison with statistical model calculations and with the experimental yield from N$\neq$Z ^{30}Si. This can be explained by including isospin mixing in the calculation, characterized by one parameter, the spreading width $\Gamma_0^{\downarrow}$ for T=0 states to mix to T=1 states. The statistical assumption $\Gamma_1^{\downarrow} = \Gamma_0^{\downarrow}\,\rho_0/\rho_1$ then yields the spreading width $\Gamma_1^{\downarrow}$ for T=1 states to mix to T=0 states, a quantity which can be compared to other experimental results. (For N$\neq$Z nuclei, $\Gamma_0^{\downarrow}$ and $\Gamma_1^{\downarrow}$ are the spreading widths of the states with T=$|T_3|$ and T=$|T_3|$+1, respectively.) These spreading widths together with the compound nuclear widths then imply a fraction α^2 of T=0 states which mix to T=1 states. The results are shown in the figure. The spreading widths at E*=47 and 63 MeV are large compared to values deduced from other compound nuclear experiments at lower excitation energies,[2] including the value for ^{28}Si at E*=34 MeV determined previously at this lab.[3] They are also large compared to isobaric analog resonance spreading widths. However, there is little theoretical guidance for what the coulomb spreading widths should be in compound nuclei, particularly at such high excitation energy.

The results shown for each E* assume a constant $\Gamma_1^{\downarrow}$ for both the initial compound nucleus and the daughters formed after particle decay. Allowing the daughters in the E*=47 MeV case, for example, to have a smaller $\Gamma_1^{\downarrow}$ (as suggested by other results at lower excitation energy[2]) would make their contribution smaller. A $\Gamma_1^{\downarrow}$ 40% higher for the parent ^{28}Si would then be necessary to explain the observed γ-ray yield.

To test the statistical nature of the γ-ray production, we have measured and compared the yields from the ^{14}N+^{14}N and ^{16}O+^{12}C reactions forming ^{28}Si at the same E*=47 MeV. These reactions have different Q-values so the bombarding energies are very different (40 MeV and 72

*Present address: Institute of Experimental Physics, University of Warsaw, Poland.

[1]Nuclear Physics Laboratory Annual Report, University of Washington (1989) p. 7.

[2]H.L. Harney, A. Richter, H.A. Weidenmüller, Rev. Mod. Phys. 58, 607 (1986).

[3]M.N. Harakeh, D.H. Dowell, G. Feldman, R. Loveman, J.L. Osborne and K.A. Snover, Phys. Lett. B176, 297 (1986.)

MeV, respectively). The experimental result is the same within 10 percent, consistent with a statistical reaction mechanism. This helps exclude possible γ-ray production from nonstatistical mechanisms like nuclear bremsstrahlung, as well as entrance-channel isospin violation by Coulomb excitation, both of which should depend strongly on bombarding energy.

The figure also shows our measurements of mixing in the odd-odd T=0 nucleus ^{26}Al, made by comparing its yield to N$\neq$Z ^{26}Mg (formed by ^{14}N+^{12}C and ^{13}C+^{13}C reactions, respectively) and to statistical model calculations. We have yet to understand the relation of these results to those in ^{28}Si.

One feature in the analysis which our measurements do not test, and to which the inferred isospin mixing is sensitive, is the ratio of T=1 to T=0 level densities in ^{28}Si and other N=Z nuclei. Our current investigations are focussed on the question of how well we know this ratio, and whether in fact it might be larger than previously assumed, which would help explain our measurements without the need for large mixing.

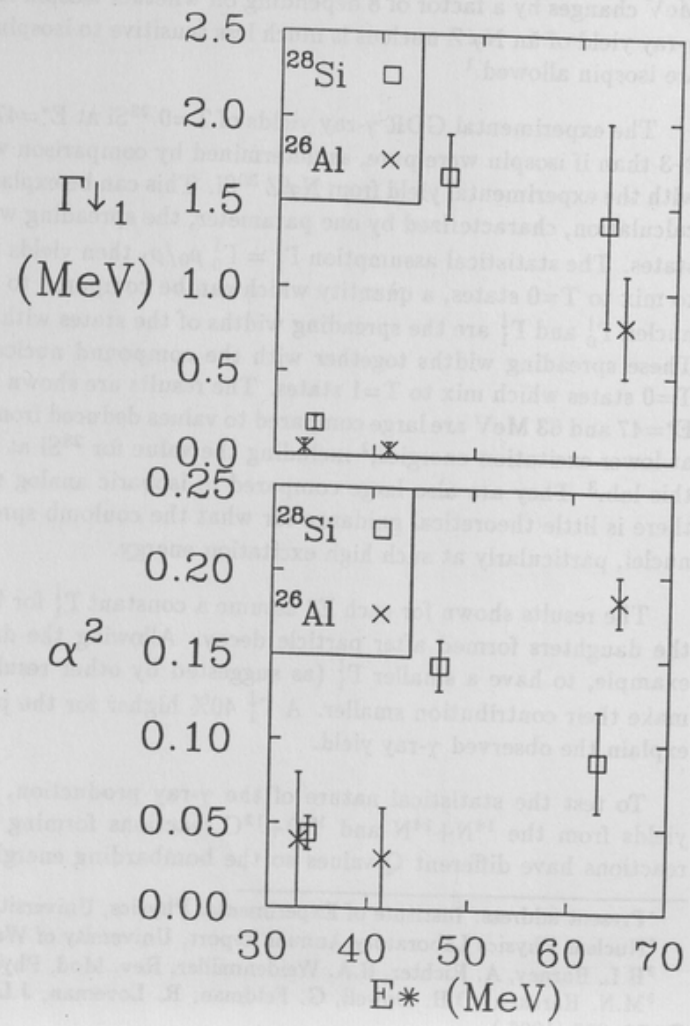

Fig. 1.1-1 Isospin mixing width $\Gamma_1^{\downarrow}$ of T=1 states, and fraction α^2 of mixed T=0 states. Error bars include systematic uncertainties deduced using different level density prescriptions.

1.2 Giant Dipole Resonance Decays of $^{45}Sc^*$ at High Spin

J.A. Behr, Z.M. Drebi, C.A. Gossett, J.H. Gundlach, M. Kicinska-Habior* and K.A. Snover

We have extended our earlier measurements[1] of Giant Dipole decays in rotating compound nuclei near A = 40 to higher energies and spins. New measurements of the high energy γ-ray spectrum shape and angular distribution in the $^{18}O + {}^{27}Al \rightarrow {}^{45}Sc^*$ have been made at E_{lab} = 89 and 110 MeV, corresponding to initial excitation energies in ^{28}Si of 77 and 89 MeV, using the UW tandem plus linac. The reactions correspond to average final-state spins of 22 and 25$\hbar$, and final-state temperatures of 1.8 and 2.1 MeV, respectively, for states populated by GDR decay with $E_\gamma \approx E_D \approx 17$ MeV.

At these energies the spectrum shape indicates the GDR width is extremely broad, ≈15–18 MeV, due presumably to deformation splitting (which is, however, not resolved due to the large deformation fluctuations).

The measured spectra contain a 15.1 MeV peak whose position shifts with angle consistent with emission from a source moving with a velocity intermediate between the projectile velocity and the center of mass velocity. Based on the simple assumption of isotropic emission in a rest frame moving at a single intermediate velocity, a consistent correction was obtained for this contaminant at all angles. The corrected spectra are forward-backward symmetric ($a_1 = 0$ within errors) in the center of mass frame for E_γ >11 MeV, consistent with statistical decay.

The measured a_2 coefficients in the center of mass are negative for E_γ = 11–20 MeV, and relatively large in magnitude, reaching values of −0.2. These results suggest the excited nuclei have rotating shapes with large deformations, since −0.25 is the maximum (negative) value possible, and are qualitatively consistent with the large oblate liquid-drop-like deformations expected for these spins and temperatures. Preliminary a_2 calculations, including fluctuations, when compared to the data suggest $\beta_o \approx 0.4$, which is similar to the deformation obtained in a Strutinsky shell-corrected potential energy surface calculated[2] for this system. More detailed analysis is underway.

---

*Present address: Institute of Experimental Physics, University of Warsaw, Poland.

[1] M. Kicinska-Habior *et al.*, Nuclear Physics Laboratory Annual Report, University of Washington (1989) p. 4; Phys. Rev. C, in press.

[2] Y. Alhassid and B. Bush (private communication).

1.3 Giant Dipole Resonance of ^{59}Cu Formed in the ^{32}S + ^{27}Al Reaction

J.A. Behr, Z.M. Drebi, M.S. Kaplan and K.A. Snover

The shapes of composite nuclei with very large angular momenta and high excitation energies are largely unknown. One of the interesting predictions of several theoretical treatments of hot highly rotating nuclei is large spin-induced deformations.

In the past few years, systems in the mass region A=60 have been studied. In particular, energy spectra and angular distributions of light particles emitted in the statistical decay of ^{59}Cu formed in the reaction ^{32}S + ^{27}Al at 100–150 MeV bombarding energies have been measured. Adjustments to the phase space of the statistical model needed to fit these spectra suggest a large deformation in this system.[1] However, quantitative and more direct information about the deformation is needed.

It has been proved that spectral shapes of GDR gammas emitted from hot highly rotating nuclei, together with their angular distributions, constitutes an excellent "tool" for studying compound nuclear shapes and shape evolution. Therefore, we plan to use this tool to study ^{59}Cu system formed in the same entrance channel ^{32}S + ^{27}Al. We have measured spectral shapes and angular distributions at 100 MeV bombarding energy, with analysis in progress, we plan measurements at 150 to 250 MeV bombarding energies.

[1] G. Viesti *et al.*, Phys. Rev. **C38**, 2640 (1988).

1.4 Shapes and Thermal Shape Fluctuations in Highly Excited, Rotating Nuclei around A = 90

J.A.Behr, C.A. Gossett, J.H. Gundlach, M. Kicinska-Habior,* K.T. Lesko† and K.A. Snover

We investigated nuclear matter under extreme conditions such as elevated temperature and rapid rotation. In particular we concentrated on the evolution of the nuclear shape as a function of these parameters in nuclei close to the quasi doubly magic nucleus ^{90}Zr. We used the GDR γ-decay spectrum shape and the angular distribution to quantitatively study the quadrupole shape induced by rotation and the shape fluctuations due to the thermal excitation.

The reactions $^{18}O + ^{72}Ge \rightarrow {}^{90}Zr^*$ at bombarding energies of $E_{proj} = 50MeV$ and $74MeV$ measured at UW and $^{28}Si + ^{64}Ni \rightarrow {}^{92}Mo^*$ at $E_{proj} = 137MeV$ measured at LBL are reported here. The compound nuclei were produced with average final spins and temperatures following GDR γ-decay of $\overline{I} \approx 9\hbar, 22\hbar$ and $33\hbar$ and $\overline{T} \approx 1.6MeV, 1.7MeV$ and $2.0MeV$, respectively. The binned γ-ray spectra are displayed in the first row of fig. 1.4-1 after multiplication by an exponential factor. Two Lorentzians were used to describe the γ-ray strength function in a fit with the statistical model code CASCADE (solid line). On the basis of the extracted GDR parameters with their uncertainties we were unable to extract the shape of the hot nuclei because the two Lorentzians are not resolved. However a strongly increased FWHM of $\approx 8 - -11.5MeV$ was observed as compared to the cold nucleus with the FWHM$\approx 4 - -5.4MeV$. We concluded that the strong width increase can be explained in terms of temperature induced (quadrupole) shape fluctuations about an equilibrium deformation given by the rotating liquid drop model. This is based on strength functions calculated by integrating the GDR over all quadrupole deformations, weighting them by a Boltzmann factor involving the free energy for the shape. Simple parabolic potential energy surfaces were used which closely resemble surfaces calculated with the rotating liquid drop model. The observed FWHM could be reproduced when the phase space element $\beta^4 \mid \sin 3\gamma \mid d\beta d\gamma$ was used, but not when using $\beta d\beta d\gamma$, which yields smaller widths.

The GDR γ-ray angular distribution from a rotating quadrupole deformed nucleus is sensitive to the nuclear deformation. The amount of deformation is reflected in the size of the $a_2(E_\gamma)$ coefficient. The third row in fig. 1.4-1 shows the a_2 coefficient. With increasing spin an increasing a_2-amplitude is observed, indicating that the nuclear deformation is growing with spin. Similar to the interpretation of the spectrum shape, fluctuations must be included for a quantitative assesment. Here we used the liquid drop prediction for the potential energy surface (PES) curvature and the location of the (oblate noncollective) minimum—the latter corresponds to $\beta_0 = 0.015, 0.072,$ and 0.157 for these three cases as a function of increasing spin. The calculated a_2 values are superimposed on the data in fig. 1.4-1.

It was recently shown [1] that shape orientation Euler angles as well as the intrinsic coordinates (β, γ) must be included in the description of the nuclear shape. This allows also to account for shape orientation fluctuations which are important for a quantitative interpretation of the angular distribution. These orientation fluctuations will reduce the angular anisotropy and may bring the calculated a_2-coefficients shown in fig. 1.4-1 into better agreement with the data.

---

*Present address: Institute of Experimental Physics, University of Warsaw, Poland.
†Lawrence Berkeley Laboratory (LBL), Berkeley, CA 94720.

[1] Y. Alhasid, B. Bush, Nucl. Phys. in press; private communication.

In conclusion we have found that while the spectrum shape does not determine the nuclear deformation, the angular distributions provide much more reliable quantitative information.

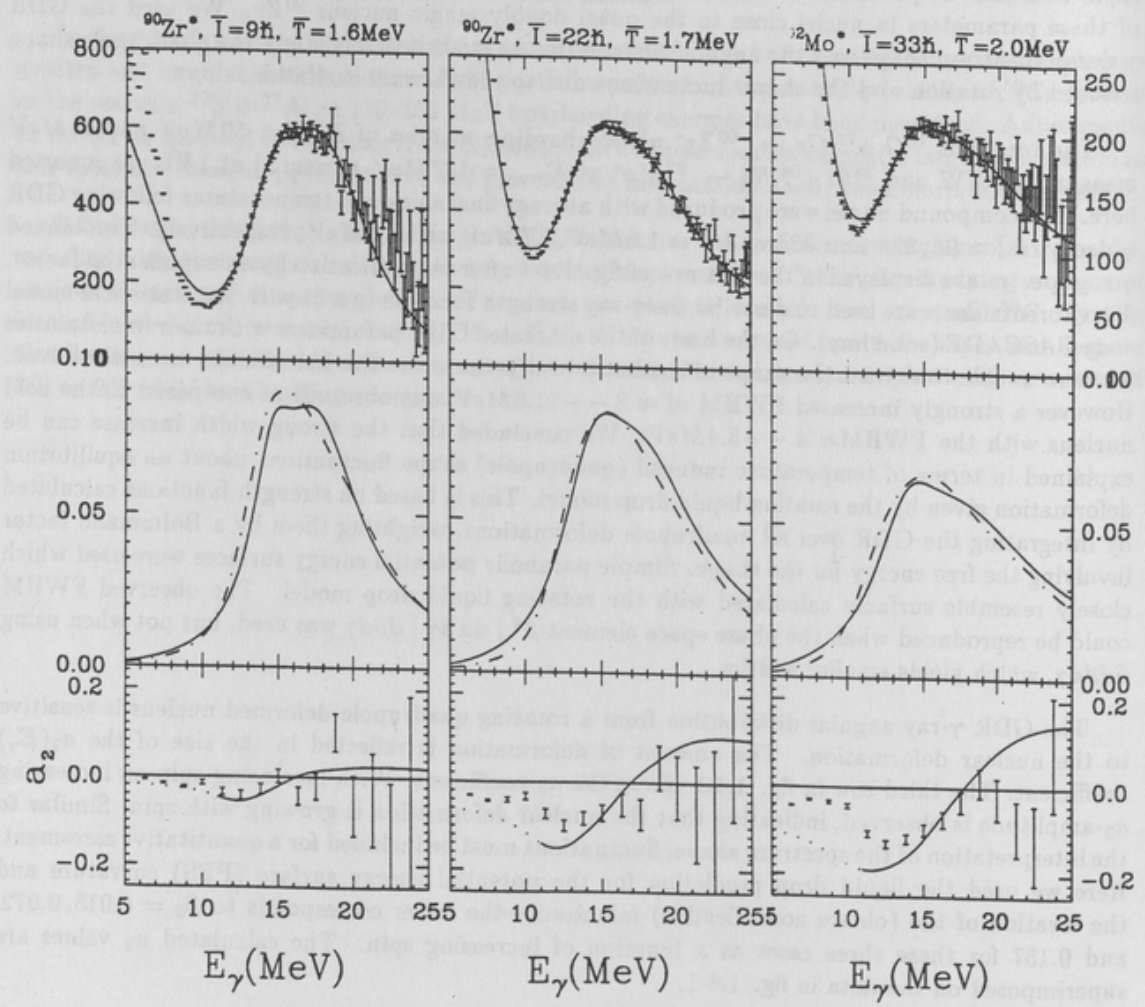

Fig. 1.4-1 Top row: The data and the two Lorentzian CASCADE fit multiplied by an exponential factor. Middle row: The solid line is the two Lorentzian strength function obtained from the fit to the data. The dotdashed line is the calculated strength function including thermal shape fluctuations with the $\beta^4 \mid \sin 3\gamma \mid d\beta d\gamma$ phase space element. Bottom row: Measured and calculated a_2-coefficient of the angular distribution. Thermal shape fluctuations (β, γ plane), but no shape orientation fluctuations are included in the calculations shown in the middle and bottom rows. The a_2 calculation is valid only for $E_\gamma > 11 MeV$.

2 NUCLEUS-NUCLEUS REACTIONS

2.1 The Search for High Energy γ-rays from the Spontaneous Fission of ^{252}Cf

C. A. Gossett, S. J. Luke and R. Vandenbosch

Kasagi, *et al.*[2] reported the emission of very high energy γ-rays from the spontaneous fission of ^{252}Cf. The γ-rays they observed had energies on the order of 100 MeV. They attributed these hard photons to nucleus-nucleus bremsstrahlung arising from the acceleration of the fission fragments. They measured γ-γ coincidences between low energy γ-rays in NE213 liquid scintillator and high energy γ-rays in a seven element BaF_2 array. The justification for this method is that the low energy γ-rays are emitted promptly from the decay of fission fragments, so a coincidence between these γ-rays and the high energy γ-rays should reflect a correlation between the fission fragments and high energy γ-rays.

We performed the measurement in two ways. We essentially reproduced the experiment as Kasagi, *et al.* performed it; we detected a coincidence of γ-rays in a NE213 liquid scintillator detector with photons in the laboratory's 10 in by 15 in NaI spectrometer. The second method we used was by far the most definitive. We measured the coincidence between γ-rays and the fission fragments. To accomplish this we obtained a 50μCi "fission foil" ^{252}Cf source from Isotope Products, Inc. This source allowed us to detect the fission fragments directly and in so doing we were also able to establish correlations between the fission fragment energy and γ-ray energy.

We detected the fission fragments in silicon detectors, with a rate of 2–8 kHz, depending on the size of the detector. Data were collected for roughly two weeks and a total of 2.8 billion fission events were observed. Figure 2.1-1 shows the data, which we collected in the γ-fission fragment coincidence mode. We did not see any events with E_γ greater than 25 MeV, which is distinct from what Kasagi, *et al.* reported. The solid line in figure 2.1-1 is our estimated upper limit of the production of high energy photons from the spontaneous fission of ^{252}Cf. This upper limit was determined by assuming that there was one count between 25 and 180 MeV, the upward slope arises from assuming that the efficiency of NaI decreases exponentially as the energy of the γ-ray increases. The dashed line in this figure is the level of photon yield reported by Kasagi, *et al.* Figure 2.1-2 shows our low energy photon data compared to those of Kasagi, *et al.* and Dietrich, *et al.*[3] Our low energy data agree very well with these data. Our upper limit for high energy γ-ray production, on the other hand, is several orders of magnitude below the yield reported by Kasagi, *et al.* One possible explanation for the higher yield reported by Kasagi, *et al.* is contamination by cosmic ray induced events. For example shower events could be triggered in both the liquid scintillator and their BaF_2 detector. Since our experiment was triggered by coincidences between fission fragments and γ-rays we should not be sensitive to this class of background events.

Our data show that there are medium energy γ-rays (E_γ = 8–20 MeV) emitted from the spontaneous fission of ^{252}Cf, undoubtedly produced from the statistical decay of the highly excited fission fragments. We, however, have not seen any evidence for the emission of higher energy γ-rays

[2]J. Kasagi *et al.*, *Proc. Fifth Int. Conf. Clustering Aspects in Nucl. and Subnucl. Systems*, Kyoto, 1988, J. Phys. Soc. Jpn. 58 (1989) Suppl. p. 620–625.

[3]F. S. Dietrich, J. C. Browne, W. J. O'Connell and M. J. Kay, Phys. Rev C10, 795 (1974).

in the fission fragment-γ coincidence data. We are in the process of analyzing the γ-γ coincidence data to see if we can reproduce the results of Kasagi, *et al.* We are also modeling the emission probability of γ-rays from nucleus-nucleus bremsstrahlung, as the fission fragments are accelerated from scission to infinity.

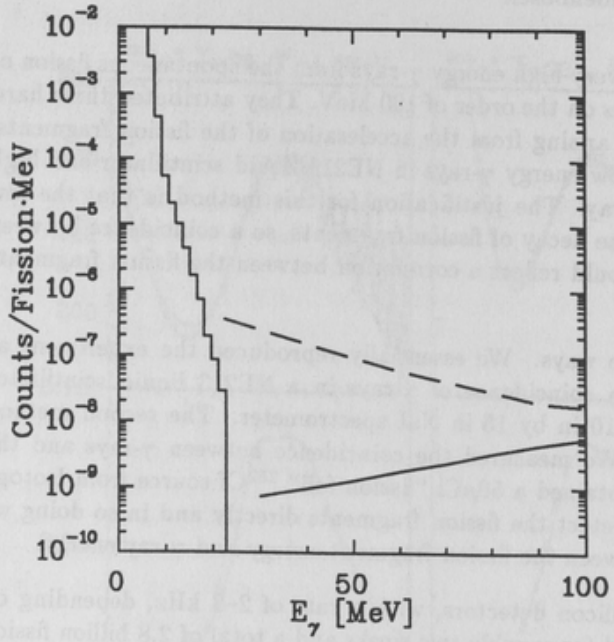

Figure 2.1-1 : The yield for the γ-rays produced from the spontaneous fission of ^{252}Cf, deduced from the fission fragment-γ-ray coincidence data. The solid line represents our calculated upper limit for high energy γ-ray production based upon 2.8 billion fissions. The dashed line is the level at which Kasagi, *et al.* reported high energy photons.

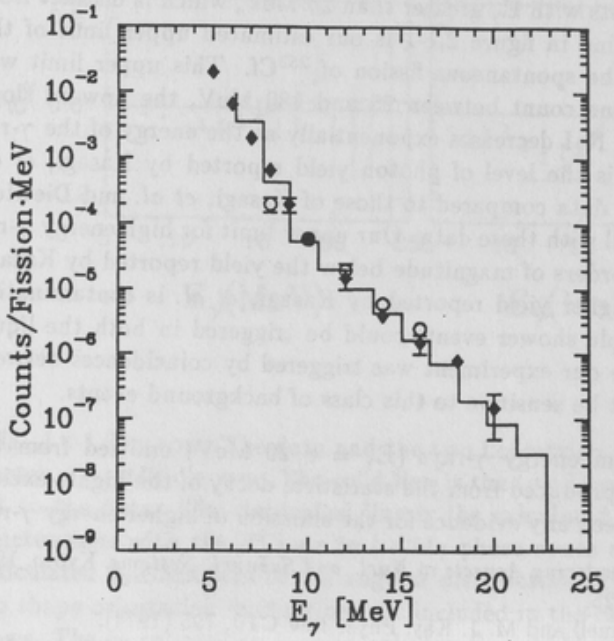

Figure 2.1-2: Low energy photon spectrum compared to Kasagi, *et al.* (diamonds) and Dietrich, *et al.* (circles). The histogram is our measurement.

2.2 Modifications to the Nucleon Exchange Transport Model for the Emission of Energetic Particles at Intermediate Energies

S. J. Luke and R. Vandenbosch

In last year's annual report[1] we reported data for the production of high energy γ-rays from the reaction ^{14}N on ^{nat}Ag at 35 MeV/A. It was our contention that with the hard photon and pre-equilibrium nucleon emission data we would be able to optimize the Randrup and Vandenbosch model[2] for the emission of energetic particles in intermediate energy heavy ion collisions. In the past year we received the pre-equilibrium neutron[3] and proton[4] emission data for the same system. What we have tried to do is understand all of these observables with a single model.

In the model there are basically no adjustable parameters in the traditional sense. The only ingredient in the model which can be varied is the nucleon-nucleon cross-section. The "default" calculation takes this in-medium nucleon-nucleon cross-section to be half its free value. A reasonable assumption is that at high nucleon energies the interaction cross-section in the nucleus might approach its free value. Including this in the calculation yields a factor of two increase at the high energy part of the γ-ray spectrum.

The modification which has had the largest effect is the inclusion of a diffuse momentum distribution for the colliding nuclei, replacing the sharp momentum distribution which exists in the original model. The "diffuseness" parameter for the momentum distributions was determined by reproducing the slope of the empirical momentum distributions.[5] The effect which we observed was dramatic. Figure 2.2-1 shows the effect on photon emission and figures 2.2-2 and 2.2-3 demonstrate the effect for nucleon emission. The solid lines in each case are the calculations using a sharp momentum distribution, while the dashed lines use a diffuse momentum distribution.

There are two major consequences of a diffuse momentum distribution being used in these calculations. First, there are nucleons with higher momentum components, the so called "high momentum tail"; this hardens the spectra in the high energy region. Second, there is an increase in the phase space that the scattered nucleons can explore, decreasing the Pauli Blocking. This is undoubtedly the major reason for the increase in the overall yield of both γ-rays and nucleons at all energy regimes.

We are in the process of considering several other effects that should increase our understanding of the reaction process. The introduction of a variable Fermi momentum as a function of mass[6] may be important in very asymmetric systems. The mocking up of a surface-peaked imaginary potential may be necessary to correct the over-prediction of nucleon yield at backward angles.

---

[1] Nuclear Physics Laboratory Annual Report, University of Washington (1989) pp. 10–11.

[2] Nucl. Phys. **A474**, 218 (1988); Nucl. Phys. A **490**, 418 (1988).

[3] Schelin *et al.*, Phys. Rev. C **C39**, 1827 (1989).

[4] T. Nayak (private communication).

[5] A. Antonov, P. Hodgson and I. Pertov, *Nucleon Momentum and Density Distributions in Nuclei*, (Clarendon Press, Oxford), 1988.

[6] E. J. Moniz *et al.*, Phys. Rev. Lett. **26**, 445 (1971).

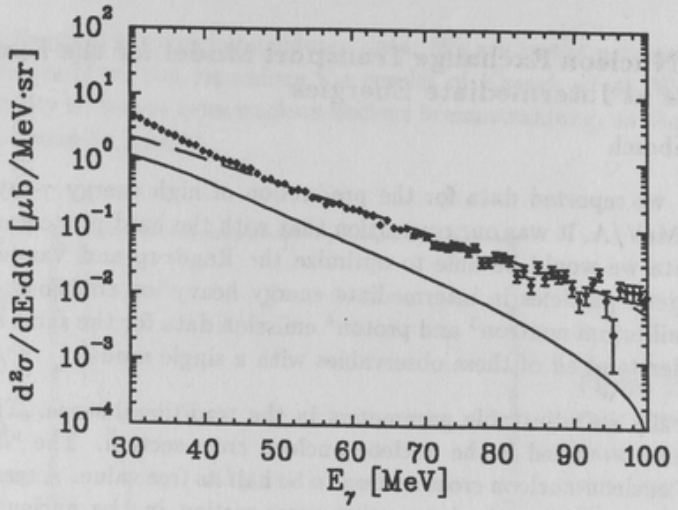

Figure 2.2-1 : The data is our inclusive γ-ray spectrum[1] obtained from ^{14}N + ^{nat}Ag at 35 MeV, at a lab angle of 90°. The calculations are described in the text.

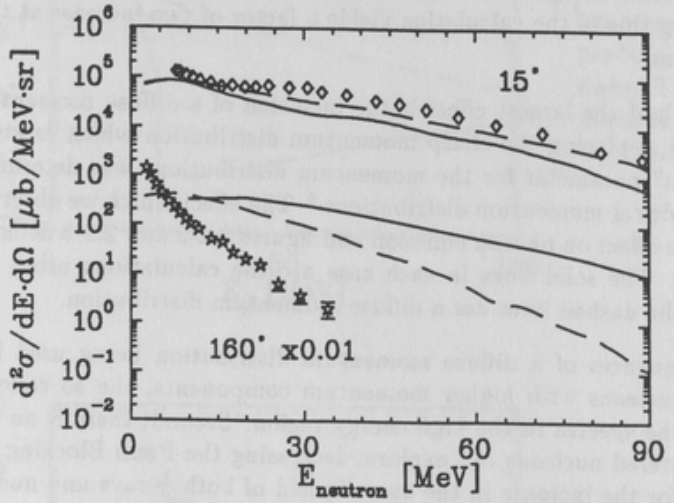

Figure 2.2-2: Inclusive neutron spectrum[3] from ^{14}N + ^{nat}Ag at 35 MeV/A, at lab angles of 15° (diamonds) and 160° (stars).

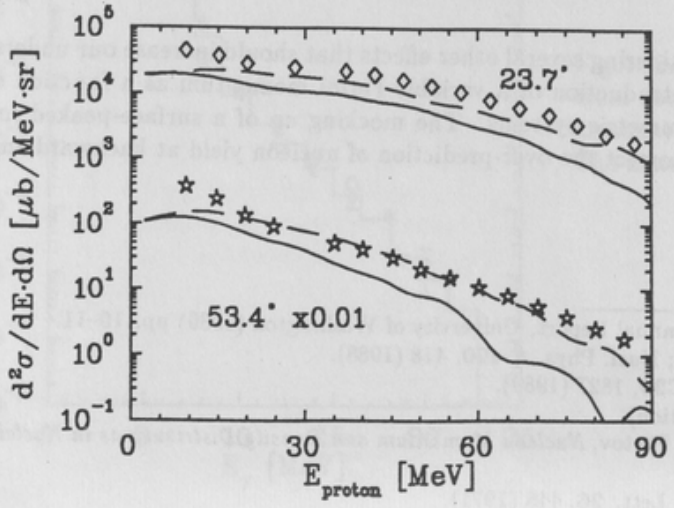

Figure 2.2-3: Inclusive proton spectra[4] from ^{14}N + ^{nat}Ag at 35 MeV/A, at lab angles of 23.7° (diamonds) and 53.4° (stars).

2.3 Light Particle Production in ^{16}O on $^{159}_{65}Tb$, $^{181}_{72}Ta$, $^{192}_{77}Ir$ and $^{197}_{79}Au$

A.W. Charlop, C.E. Hyde-Wright, S. Kailas,* D.J. Prindle, K. Swartz and R. Vandenbosch

In this experiment we measured the light particle (p, d, t and α) multiplicity as a function of impact parameter.[1] Central collisions give rise to evaporation residues (ER) while more peripheral collisions give rise to fission fragments (FF). The four targets we used have similar total cross section, but the boundary between FF and ER moves toward smaller impact parameters as the mass of the compound system increases. Thus tagging the light particles by ER or FF and using a few targets we are able to check the impact parameter dependence of the light particle production.

The FF detector was a silicon surface barrier detector at −145°; there was very little background at this angle. The ER detector was a surface barrier telescope at −20°; ER events stopped in the front detector, whereas elastic ^{16}O punched through to the rear detector and were vetoed. Even after this veto we had to cut on the energy (pulse height) versus Time Of Flight in order to get a clean sample of ER events.

The light particles were detected in coincidence with FF or ER using an array of 11 phoswich detectors.[2] We measured the cross section as a function of angle and energy. The angle was determined by the position of the phoswich counters (covering the range from +7° to +35° in 7° steps). For this analysis we required the energy to be in the range 15 < E < 55MeV for p and 50 < E < 100MeV for α.

We fit the data to a Maxwellian moving source distribution for each particle type;

$$\frac{d^2\sigma}{dEd\Omega} = \frac{M}{2(\pi T)^{3/2}} \sqrt{E'} \; e^{-[E'-2\sqrt{E'E_0}\cos(\theta)+E_0]/T}$$

The fit parameters are the multiplicity, M, the temperature, T, and source velocity, $v = \sqrt{2E_0/m}$. The quantity E' is the measured energy corrected for the Coulomb energy, $E' = E_{measured} - V_c$.

The data samples tagged by FF give good fits to this function. The temperatures are ≈ 4MeV and the source velocities are close to one half the beam velocity. The source velocity and the multiplicity are highly correlated; to determine the multiplicity we fix the source velocity at its average fit value for each of the light ion species. The multiplicities as a function of mean impact parameter are listed in Table 2.3-1. It is somewhat surprising that the multiplicities are roughly independent of impact parameter.

The data samples tagged by ER give very poor fits to the moving source function. It appears that 20° from the beam for the ER detector requires a large enough transverse momentum that the prompt particles are biased toward the other side of the beam. The data suggest that approximately half the transverse momentum of the ER is balanced by the prompt light ions.

We have taken another run in which we varied the angle of the ER detector in order to understand the ER events better. During this run we also covered light particle angles out to 60°; this

*Present address: Nuclear Physics Division, Bhabha Atomic Research Center, Bombay, India.

[1]The motivation for this experiment is also discussed in Nuclear Physics Laboratory Annual Report, University of Washington (1989) p. 15.

[2]Nuclear Physics Laboratory Annual Report, University of Washington (1989) p. 50.

should reduce the correlation between the multiplicity and source velocity. Analysis of these data is in progress.

Table 2.3-1: Light particle multiplicity as function of mean impact parameter.

Impact Parameter (fm)	M_P	M_D	M_T	M_α
8.2	$0.195 \pm .008$	$0.028 \pm .002$	$0.022 \pm .002$	$0.165 \pm .006$
9.2	$0.156 \pm .011$	$0.030 \pm .005$	$0.017 \pm .003$	$0.159 \pm .009$
10.5	$0.176 \pm .006$	$0.030 \pm .002$	$0.021 \pm .002$	$0.139 \pm .005$
11.1	$0.140 \pm .012$	$0.020 \pm .004$	$0.018 \pm .007$	$0.087 \pm .009$

2.4 High Energy Photon Emission in Heavy Ion Collisions at E/A = 9–14 MeV

J.A. Behr, C.A. Gossett, W.T. Hering,* S.J. Luke, B.T. McLain, D.P. Rosenzweig and K.A. Snover

Although there has been extensive experimental and theoretical study of hard photon production in heavy ion collisions for incident energies E/A $\geq$ 20 MeV, very little is known about high energy photon production at energies E/A = 5–20 MeV. Below E/A $\sim$ 5 MeV, the high energy gamma emission process is dominated by the statistical decay of the giant dipole resonance built on excited nuclear states. Above E/A $\sim$ 20 MeV, hard photon production in individual nucleon-nucleon collisions appears to dominate the high energy gamma emission. At intermediate energies, other production mechanisms, such as collective bremsstrahlung, may become important. In order to delineate the production mechanism for E/A = 5–20 MeV, it is crucial to measure not only the photon energy dependence of the cross section, but also the bombarding energy and angular dependences of the high energy photon cross section.

We have studied high energy photon production in $^{12,13}C + {}^{92,100}Mo$ reactions at E/A = 9–14 MeV. The angular distribution, bombarding energy dependence and projectile-target mass dependence of the photon cross section at high energy, $E_\gamma \geq 30$ MeV has been measured. A preliminary report of the results of this work was presented in last year's report.[1] A manuscript of the completed analysis is in preparation.

Our results are generally consistent with high energy photon production via nucleon-nucleon bremsstrahlung,[2] hard photon production in individual nucleon-nucleon collisions in early stages of the heavy ion collision. The cross sections above $E_\gamma = 30$ MeV scale roughly as the number of nucleons in the projectile and target. The angular distributions are strongly forward peaked in the laboratory frame. From fits to the spectra at seven angles in the range 35–145° we find the angular distributions to be characteristic of roughly isotropic emission from a frame moving at one-half of the beam velocity, consistent with photon production in nucleon-nucleon collisions.

---

*Present address: Sektion Physik, Universität München D-8046 Garching, FRG.

[1] Nuclear Physics Laboratory Annual Report, University of Washington (1989) p. 9.

[2] V. Metag, Nucl. Phys. **A488**, 483c (1988).

2.5 Pre-equilibrium Proton Emission in Heavy Ion Collisions

J. Randrup* and R. Vandenbosch

We have recently extended our previously developed nucleon-exchange transport model for pre-equilibrium neutron[1] and hard photon[2] emission to incorporate pre-equilibrium proton emission. This has required the incorporation of the Coulomb barrier retarding proton emission and the kinematics of the acceleration of the protons in the Coulomb field of the emitting nucleus.

We are in the final stage of testing the program and starting to compare with experimental data. Preliminary comparisons with experimental data indicate that the forward yield of protons is somewhat underestimated and that the energy spectrum at forward angles is predicted to be softer than observed. An example of a comparison with experimental data[3] is shown in Fig. 2.5-1. These proton spectra are tagged by fission-fission folding angles as central collisions, suppressing the contamination of the spectra by sequential decay of projectile-like fragments in peripheral collisions. As discussed in section 2.2 of this report, the discrepancies observed may be indicative of the neglect of the tails in the momentum distributions of the projectile and target nuclei. In the present version of the code these are taken to be sharp Fermi spheres when the nuclei are unexcited. We have also incorporated the capability to calculate the parallel component of the momentum carried away by the pre-equilibrium neutrons and protons. This will enable us to calculate the mean velocity of evaporation residues which can then be compared with experiment. We will likely underestimate the momentum loss as our model does not include the emission of complex particles. We do hope however to explore the effects of mass asymmetry in the entrance channel.[4]

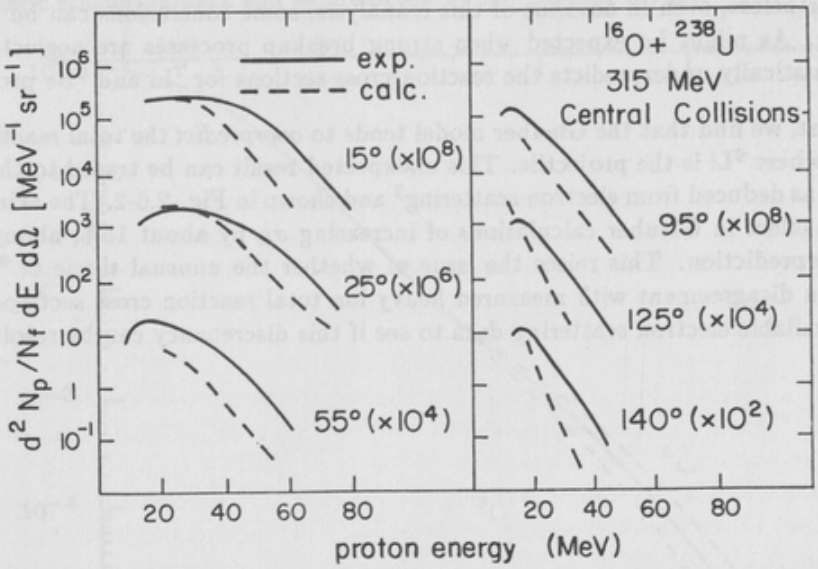

Fig. 2.5-1 Comparison of calculated and experimental proton spectra.

*Lawrence Berkeley Laboratory, Nuclear Science Division, 70A-3307, 1 Cyclotron Rd, Berkeley, CA 94720.

[1]J. Randrup and R. Vandenbosch, Nucl. Phys. **A474**, 219 (1987).
[2]J. Randrup and R. Vandenbosch, Nucl. Phys. **A490**, 418 (1988).
[3]T. C. Awes *et al.*, Phys. Rev. **C24**, 95 (1981).
[4]H. Morgenstern *et al.*, Phys. Rev. Letters 52, 1104 (1984).

2.6 The Glauber Model with Fragile Projectiles

J.G. Cramer and S. Kailas*

Predictions of heavy ion total reaction cross sections using the Glauber model,[1] a theory based on a naively structure-free microscopic description of the colliding nuclei, have proved remarkably accurate for many heavy ion systems over a wide range of energies. In cases where the projectile is "fragile", i.e., breaks up easily in the nuclear and Coulomb fields of a nuclear collision, one might expect the assumptions of the model to fail, leading the Glauber model to under-predict measured total reaction cross sections.

In the present work we have compared Glauber predictions with total reaction cross sections obtained from optical model fits to elastic scattering data taken from the literature, selecting projectiles which are expected to be particularly fragile. The systems examined are ^{6}Li ($Q_{breakup}$=−1.47 MeV) scattered from targets of ^{12}C, ^{40}Ca, and ^{58}Ni, ^{7}Li ($Q_{breakup}$=−2.47 MeV) scattered from ^{12}C, and ^{9}Be ($Q_{breakup}$=−1.57 MeV) scattered from ^{28}Si. The Glauber calculations used are "free", in the sense that they use only nuclear radial form factors taken from electron scattering measurements and nucleon-nucleon total cross sections taken from measured values or, at low energies, from established values of nucleon-nucleon effective range parameters. Fig. 2.6-1 shows an example of such a comparison for ^{9}Be on ^{28}Si.

The measured reaction cross section values used in these comparisons are "noisy" because of normalization errors in some of the elastic scattering measurements and the lack of consistent fitting procedures. We plan to reanalyze all of the elastic scattering data sets to minimize such systematic errors. Nevertheless, even in advance of this reanalysis, some conclusions can be drawn from this investigation. As might be expected when strong breakup processes are neglected, the Glauber model systematically underpredicts the reaction cross sections for ^{7}Li and ^{9}Be projectiles.

In contrast, we find that the Glauber model tends to *overpredict* the total reaction cross section for all cases where ^{6}Li is the projectile. This unexpected result can be traced to the unusual radial shape of ^{6}Li, as deduced from electron scattering[2] and shown in Fig. 2.6-2. The skirt at the 2×10^{-2} level has the effect in Glauber calculations of increasing σ_R by about 15%, about the size of the observed overprediction. This raises the issue of whether the unusual shape of ^{6}Li is real, since it seems be in disagreement with measured heavy ion total reaction cross sections. We intend to re-analyze available electron scattering data to see if this discrepancy can be resolved.

*Present address: Nuclear Physics Division, Bhabha Atomic Research Centre, Bombay, India.

[1] R.M. DeVries and J.C. Peng, Phys. Rev. **C22**, 1055 (1980).

[2] G.C. Li *et al.*, Nucl. Phys. **A162**, 583 (1971).

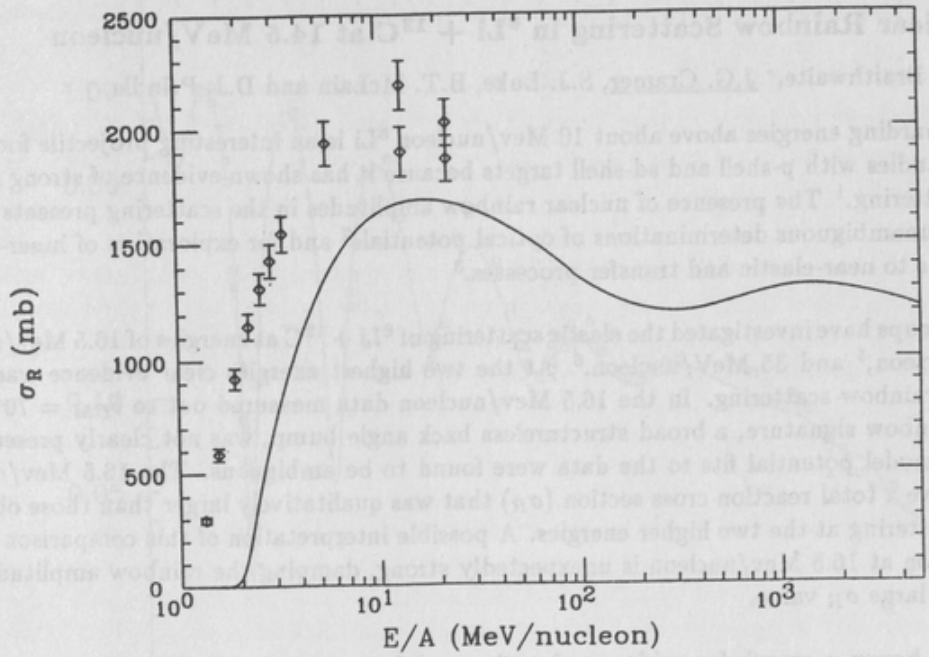

Figure 2.6-1. Comparison of total reaction cross sections for $^{9}Be + ^{28}Si$ as derived from optical model fits to elastic scattering data and as predicted by the Glauber model.

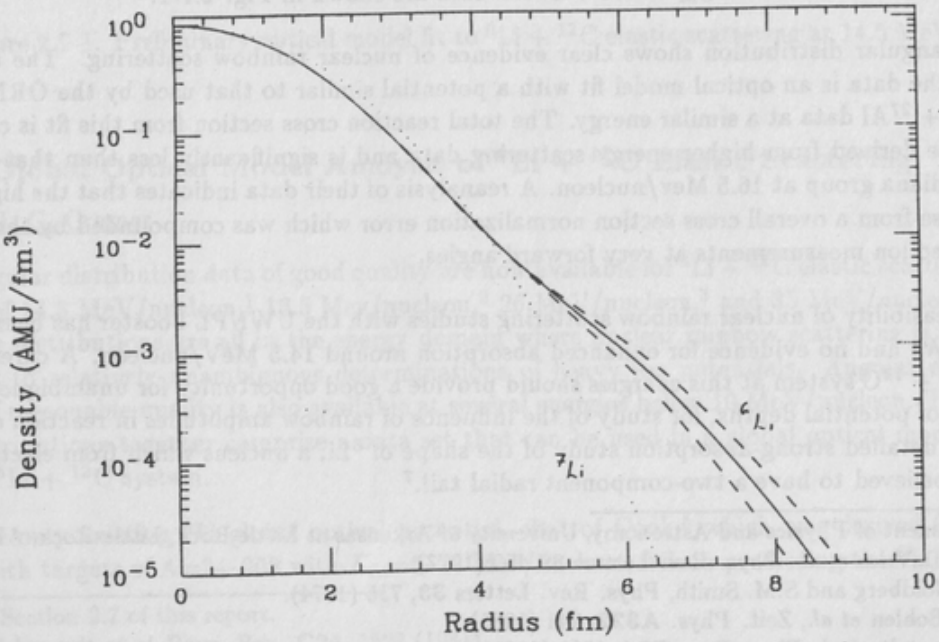

Figure 2.6-2. Comparison of the shapes of ^{6}Li and ^{7}Li as determined by electron scattering. Dashed curves surrounding the ^{6}Li shape indicate $\delta\chi^2$=1 variation boundaries.

2.7 Nuclear Rainbow Scattering in $^{6}Li + ^{12}C$ at 14.5 MeV/nucleon

W.J. Braithwaite,* J.G. Cramer, S.J. Luke, B.T. McLain and D.J. Prindle

At bombarding energies above about 10 Mev/nucleon ^{6}Li is an interesting projectile for elastic scattering studies with p-shell and sd-shell targets because it has shown evidence of strong nuclear rainbow scattering.[1] The presence of nuclear rainbow amplitudes in the scattering presents opportunities for unambiguous determinations of optical potentials[2] and for exploration of inner-surface contributions to near-elastic and transfer processes.[3]

Three groups have investigated the elastic scattering of $^{6}Li + ^{12}C$ at energies of 16.5 Mev/nucleon,[4] 26 MeV/nucleon,[5] and 35 MeV/nucleon.[6] At the two highest energies clear evidence was found for nuclear rainbow scattering. In the 16.5 Mev/nucleon data measured out to $\theta_{CM} = 70°$, however, the rainbow signature, a broad structureless back angle bump, was not clearly present, and the optical model potential fits to the data were found to be ambiguous. The 16.5 Mev/nucleon data also gave a total reaction cross section (σ_R) that was qualitatively larger than those obtained from the scattering at the two higher energies. A possible interpretation of this comparison is that the absorption at 16.5 Mev/nucleon is unexpectedly strong, damping the rainbow amplitudes and leading to a large σ_R value.

We have begun a search for evidence of nuclear rainbow scattering in light ion projectiles at energies available from the UWNPL booster. The first step in this investigation has been the study of the $^{6}Li + ^{12}C$ system at 14.5 MeV/nucleon. Because of the large intensity of lithium beams available from the modified 860 ion source, we have been able to measure differential cross sections with good statistics out to $\theta_{CM} = 100°$. These data are shown in Fig. 2.7-1.

This angular distribution shows clear evidence of nuclear rainbow scattering. The solid line through the data is an optical model fit with a potential similar to that used by the ORNL group to fit $^{6}Li + ^{27}Al$ data at a similar energy. The total reaction cross section from this fit is consistent with those derived from higher energy scattering data and is significantly less than that reported by the Indiana group at 16.5 Mev/nucleon. A reanalysis of their data indicates that the high values of σ_R arose from a overall cross section normalization error which was compounded by the absence of cross section measurements at very forward angles.

The feasibility of nuclear rainbow scattering studies with the UWNPL booster has been demonstrated. We find no evidence for enhanced absorption around 14.5 MeV/nucleon. A careful study of the $^{6}Li + ^{12}C$ system at this energies should provide a good opportunity for unambiguous determination of potential depths, for study of the influence of rainbow amplitudes in reaction channels, and for a detailed strong-absorption study of the shape of ^{6}Li, a nucleus which from electron scattering is believed to have a two-component radial tail.[7]

*Department of Physics and Astronomy, University of Arkansas at Little Rock, Little Rock, AK 72204.

[1] R. M. DeVries *et al.*, Phys. Rev. Letters **39** 450 (1977).
[2] D.A. Goldberg and S.M. Smith, Phys. Rev. Letters **33**, 715 (1974).
[3] H. G. Bohlen *et al.*, Zeit. Phys. **A322**, 241 (1985).
[4] P. Schwandt *et al.*, Phys. Rev. **C24**, 1522 (1981).
[5] J. Cook *et al.*, Nucl. Phys. **A388**, 173 (1988).
[6] A. Nadasen *et al.*, Phys. Rev. **C37**, 132 (1988).
[7] L.R. Suelzle *et al.*, Phys. Rev. **162** 992 (1967).

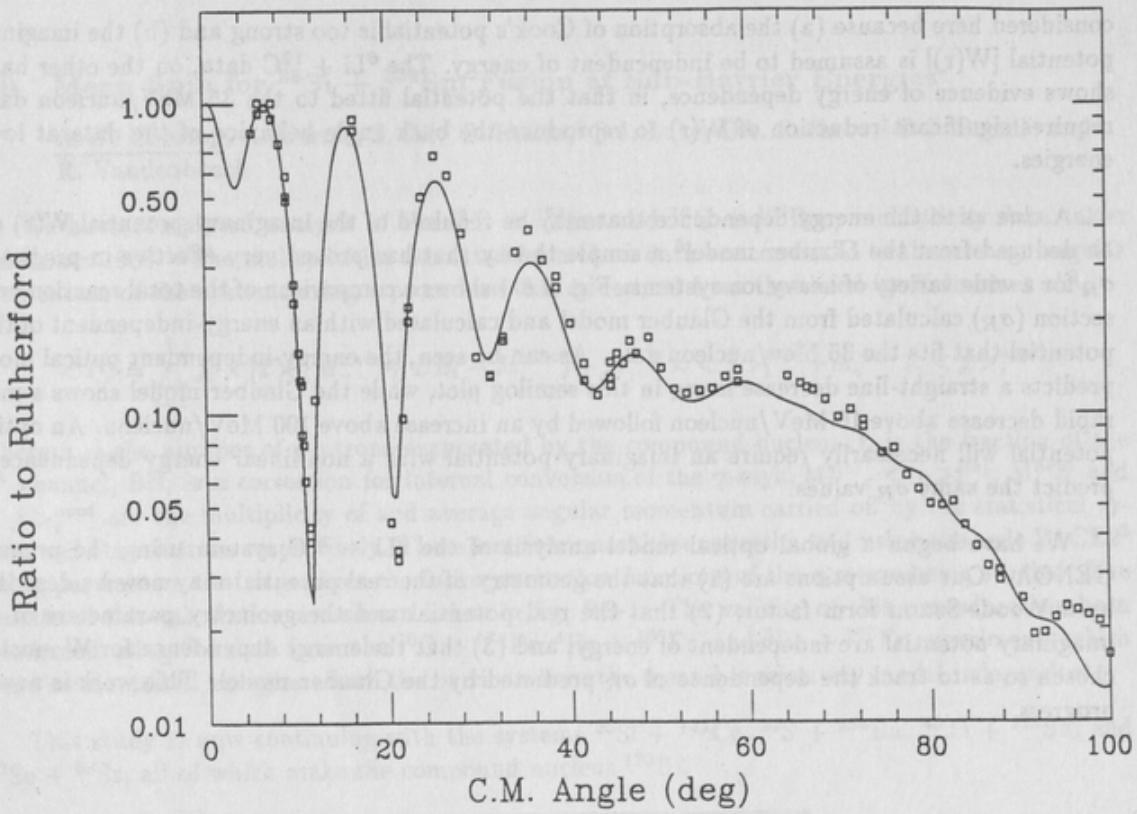

Figure 2.7-1. Preliminary optical model fit to ^{6}Li + ^{12}C elastic scattering at 14.5 MeV/nucleon.

2.8 Global Optical Model Analysis of ^{6}Li + ^{12}C Elastic Scattering

J. G. Cramer

Angular distribution data of good quality are now available for ^{6}Li + ^{12}C elastic scattering at energies of 14.5 MeV/nucleon,[1] 16.5 Mev/nucleon,[2] 26 MeV/nucleon,[3] and 35 MeV/nucleon.[4] These angular distributions are all in the energy domain where nuclear rainbow scattering is significant, leading to relatively unambiguous determinations of heavy ion potentials. Angular distribution data of reasonable quality is also available at several energies below 10 MeV/nucleon. These angular distributions together comprise a data set that can be used in a global optical model analysis of the ^{6}Li + ^{12}C system.

The only existing ^{6}Li global optical potential, that of Cook,[5] which was derived from fits to data with targets of A=24–208 with E_{Li}=6–26 Mev/nucleon, fails in predicting the ^{6}Li + ^{12}C data

[1] see Section 2.7 of this report.
[2] P. Schwandt *et al*, Phys. Rev. **C24**, 1522 (1981).
[3] J. Cook *et al*, Nucl. Phys. **A388**, 173 (1988).
[4] A. Nadasen *et al*, Phys. Rev. **C37**, 132 (1988).
[5] J. Cook, Nucl. Phys. **A388** 153 (1982).

considered here because (a) the absorption of Cook's potential is too strong and (b) the imaginary potential [W(r)] is assumed to be independent of energy. The ^{6}Li + ^{12}C data, on the other hand, shows evidence of energy dependence, in that the potential fitted to the 35 MeV/nucleon data[4] requires significant reduction of W(r) to reproduce the back angle behavior of the data at lower energies.

A clue as to the energy dependence that may be required of the imaginary potential W(r) can be deduced from the Glauber model[6] a simple theory that has proved very effective in predicting σ_R for a wide variety of heavy ion systems. Fig. 2.8-1 shows a comparison of the total reaction cross section (σ_R) calculated from the Glauber model and calculated with an energy-independent optical potential that fits the 35 Mev/nucleon data. As can be seen, the energy-independent optical model predicts a straight-line decrease in σ_R in this semilog plot, while the Glauber model shows a more rapid decrease above 10 MeV/nucleon followed by an increase above 100 MeV/nucleon. An optical potential will necessarily require an imaginary potential with a non-linear energy dependence to predict the same σ_R values.

We have begun a global optical model analysis of the ^{6}Li + ^{12}C system using the program GENOA.[7] Our assumptions are (1) that the geometry of the real potential may now be described by a Woods-Saxon form factor; (2) that the real potential and the geometry parameters of the imaginary potential are independent of energy; and (3) that the energy dependence for W must be chosen so as to track the dependence of σ_R predicted by the Glauber model. This work is now in progress.

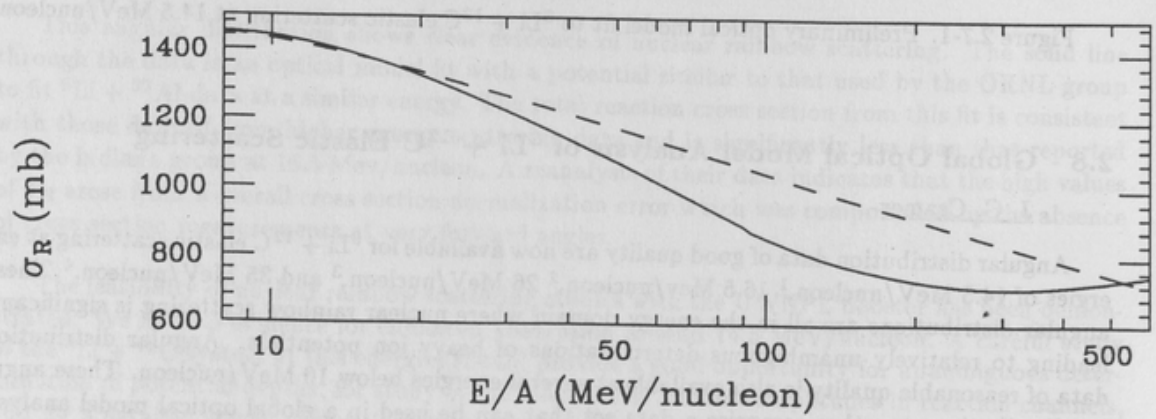

Figure 2.8-1 Comparison of σ_R as predicted by the Glauber model (solid curve) and by an optical model potential with W=29 MeV. An energy-dependent decrease in W will produce a corresponding decrease in σ_R.

[6]R. M. DeVries and J. C. Peng, Phys. Rev. **C22** 1055 (1980).
[7]F. G. Perey, ORNL (unpublished).

2.9 Mean Spin for $^{28}Si + ^{154}Sm$ Fusion at Sub-Barrier Energies*

A.W. Charlop, A. García, S. Gil,† S. Kailas,‡ S.J. Luke, DA. Pacheco,† D.J. Prindle and R. Vandenbosch

We have completed analysis of the $^{28}Si + ^{154}Sm$ and $^{16}O + ^{166}Er$ γ-multiplicity data taken December 1988.[1] The multiplicities extracted from these data are converted to the average angular momentum of the systems using a procedure that is derived from that used by Halbert *et al.*[2],

$$< l >= \sum_{i=1}^{n} f_i \times [2 \times (M_\gamma^{raw} + BB_i - M_i^{stat}) + M_i^{stat} \times < j >_i^{stat} + M_i^{neut} \times < j >_i^{neut}]$$

where n is the number of neutrons evaporated by the compound nucleus, f_i is the fraction of the i^{th} channel, BB_i is a correction for internal conversion of the γ-rays, M_i^{stat}, $< j >_i^{stat}$, M_i^{neut} and $< j >_i^{neut}$ are the multiplicity of and average angular momentum carried off by the statistical γ-rays and the neutrons respectively. These last four quantities are estimated using the code PACE2[3] using parameters that reproduce the fusion excitation functions of the systems being studied. The results of this calculation are shown below in fig. 2.9-1. The validity of this procedure has been confirmed using the data from the $^{16}O + ^{166}Er$, $^{4}He + ^{166}Er$, and $^{3}He + ^{167}Er$ experiments which were conducted at energies above the barrier where the mean l is relatively model independent.

This study is now continuing with the systems $^{28}Si + ^{142}Ce$, $^{32}S + ^{138}Ba$, $^{48}Ti + ^{122}Sn$, and $^{82}Se + ^{88}Sr$, all of which make the compound nucleus ^{170}Hf.

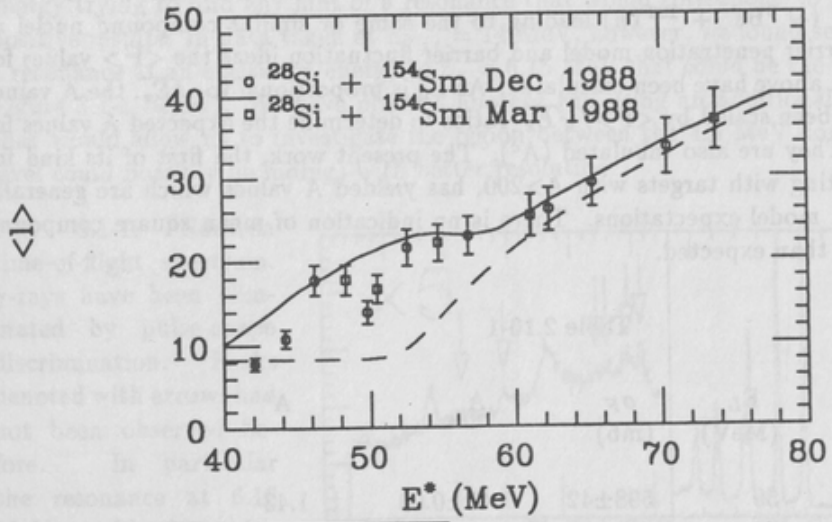

Figure 2.9-1. Average angular momentum as a function of the excitation energy of the system. The solid and dashed curves are the Wong model results, with and without inclusion of deformation effects respectively, using parameters that reproduce the fusion cross section excitation function.

*This research supported in part by the NSF and the Argentinian National Research Council under the auspices of the U.S. - Argentina Cooperative Science Program.

†Present address: TANDAR, Departamento de Física, Comisión Nacional de Energía Atómica, Buenos Aires, Argentina.

‡Present address: Nuclear Physics Division, Bhabha Atomic Research Center, Bombay, India.

[1] Nuclear Physics Laboratory Annual Report, University of Washington (1989) p. 14.

[2] M.L. Halbert *et al.*, Phys. Rev. **C40**, 2558 (1989).

[3] A. Gavron, Phys. Rev. **C21**, 230 (1980).

2.10 Fission Angular Distributions for $^{9}Be + {}^{232}Th, {}^{235}U$

A.W. Charlop, S. Kailas,* S.J. Luke, D.J. Prindle, V.S. Ramamurthy,* R. Vandenbosch and S.P. Van Verst

As a part of a program to investigate the effect of entrance channel asymmetry on fission anisotropy,[1] the angular distributions of fission fragments for the systems $^{9}Be + {}^{235}U$, ^{232}Th have been determined.

The measurements were carried out at ^{9}Be energies of 50 and 53 MeV. Enriched ^{235}U (97.5%) and natural ^{232}Th targets of thicknesses 200 and 424$\mu g/cm^2$ respectively on Ni backing (thickness 0.5–1mg/cm^2) were employed for the measurements. Six silicon detectors ranging in thickness from 20 to 60 microns were positioned suitably to cover the angular range of 80° to 170°. Relative solid angle calibration of the detectors was obtained using a ^{252}Cf source placed at target site. In general the relative solid angles computed from geometry agreed with the ones determined using Cf source and the two were normalized for the detector placed at $\theta \sim 130°$. A monitor detector was positioned at θ=26.5° to detect the elastically scattered ^{9}Be . Absolute cross sections were obtained by assuming the measured elastic cross section to be Rutherford.

The c.m. angular distributions were fitted using Legendre polynomials and then integrated to obtain total fission cross sections. The experimental values of σ_F and anisotropy $A = \sigma(180°)/\sigma(90°)$ are listed in Table 2.10-1.

The quantity A is usually represented as $A = 1 + \langle I^2 \rangle / 4K_0^2$ where $\langle I^2 \rangle$ and K_0^2 have the usual meaning.[2] The A values have previously been measured[3] for the systems $^{4}He + {}^{240}Pu$ ($^{9}Be + {}^{235}U$) and $^{4}He + {}^{238}U$ ($\sim {}^{9}Be + {}^{232}Th$) leading to the same or similar compound nuclei at E=43 MeV. Using the barrier penetration model and barrier fluctuation ideas the $\langle I^2 \rangle$ values for all the systems mentioned above have been calculated. As K_0^2 is proportional to $\sqrt{E_x}$, the A values measured using ^{4}He have been scaled by $\langle I^2 \rangle / \sqrt{E_x}$ ratios to determine the expected A values for ^{9}Be + target systems. They are also tabulated (A^c). The present work, the first of its kind for ^{9}Be as projectile interacting with targets with A>200, has yielded A values which are generally consistent with statistical model expectations. There is no indication of mean square compound nuclear spin values larger than expected.

Table 2.10-1

A_T	E_L (MeV)	σ_F (mb)	A	A^c
^{232}Th	50	598±42	1.45±0.04	1.43
^{232}Th	53	789±55	1.49±0.04	1.56
^{235}U	50	602±42	1.26±0.04	1.34
^{235}U	53	802±56	1.30±0.04	1.42

*Present address: Nuclear Physics Division, Bhabha Atomic Research Center, Bombay, India.

[1]V.S. Ramamurthy and S.S. Kapoor, Intl. Conf. on Fifty Years with Fission, Gaithersburg, Apr. 1989.
[2]R. Vandenbosch and J.R. Huizenga, Nuclear Fission, Academic, New York, 1973.
[3]R.F. Reising, G.L. Bate, and J.R. Huizenga, Phys. Rev. 141, 1161 (1968).

3 NUCLEAR ASTROPHYSICS

3.1 'Missing' levels in ^{18}Ne and breakout from the hot CNO cycle

E.G.Adelberger, A. García, K.I. Hahn,* P.V. Magnus,* D.M. Markoff M.S. Smith* and K.B. Swartz

Information about the nuclear structure of ^{18}Ne is essential to determine the rate of two reactions of considerable astrophysical interest: ^{17}F(p,γ) and ^{14}O(α,p). The first reaction determines the ^{17}O/^{18}O abundance produced in explosive hydrogen burning and could be the clue to understanding the puzzling overabundance of ^{22}Ne observed in meteorites and the apparent presence of $\sim$ 4 solar masses of ^{26}Al in the center of the Galaxy.[1] The second, on the other hand, is one of two most probable ways of producing Z $\geq$ 10 nuclei in explosive hydrogen burning which determines the onset of the r(apid)p(roton)-process.[2]

Using information available for ^{18}F and ^{18}O, Wiescher and collaborators showed that there should be a $J^\pi = 3^+$ level at E_x = 4.33 MeV[1] which would dominate the rate of ^{17}F(p,γ) and a $J^\pi = 1^-$ level at E_x = 6.12 MeV[3] that mostly determines the rate of ^{14}O(α,p). However, since the reaction rates depend exponentially on the excitation energies, measurements of widths and positions of these levels is essential for understanding their influence on the rates.

We have conducted an experimental search for the 3^+ and 1^- 'missing' levels in ^{18}Ne by means of the reaction ^{16}O(^{3}He,n) using the pulsed-beam time-of-flight spectrometer at the University of Washington tandem accelerator with which we were able to get a time resolution of 1 nsec. We took data at ^{3}He beam energies of 9.6, 9.8, 10.0, 10.2, 10.5 and 11 MeV for about 10 hours at each energy trying to find any hint of a resonance that would correspond to the $J^\pi = 3^+$ level with no positive results. In data taken at $E_{^3He}$ = 14 MeV, however, we found several new levels including a resonance at an excitation energy of E_x = 6.15 MeV that could be the missing $J^\pi = 1^-$ level (see Figure 3.1-1 below). We have planned another run using an additional thinner neutron detector that would allow us to investigate the region between the 4.5 MeV doublet (where the $J^\pi = 3^+$ level could possibly be hiding) with better resolution.

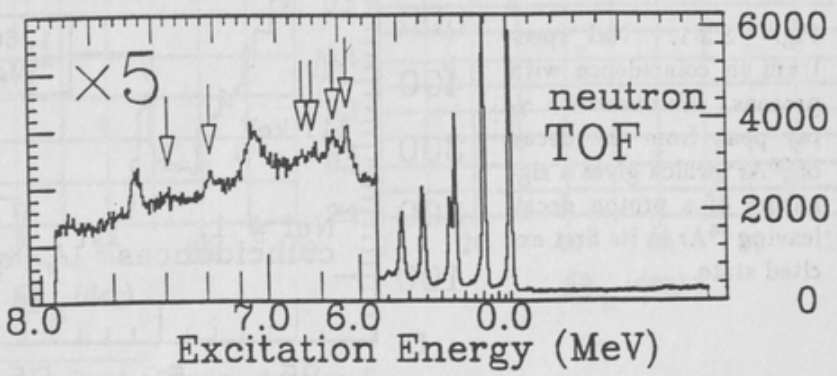

Fig. 3.1-1. Neutron time-of-flight spectrum. γ-rays have been eliminated by pulse-shape discrimination. Peaks denoted with arrows had not been observed before. In particular the resonance at 6.15 MeV could determine the ^{14}O(α,p) reaction rate.

*Yale University, A.W. Wright Nuclear Structure Laboratory, New Haven, CT.

[1]M. Wiescher *et al.*, Astrophys. J. **326**, 384 (1988).
[2]R.K. Wallace and S.E. Woosley, Astrophys. J. Suppl. **45**, 389 (1981).
[3]M. Wiescher *et al.*, Astrophys. J. **316**, 162 (1987).

3.2 ^{37}Ca β-decay: A Status Report

E.G. Adelberger, A. García, T.F. Lang,* D.M. Moltz* and H.E. Swanson

There is a qualitative disagreement between the Gamow-Teller strength function extracted from the β-delayed proton decay of ^{37}Ca and that estimated using the ^{37}Cl (p,n) reaction. Adelberger and Haxton[1] have shown that this could be explained taking into account that proton decays of high energy states in ^{37}K have a strong tendency to leave ^{36}Ar in its first excited state. It was then clear that a β-delayed proton measurement, in coincidence with γ-rays that would give a signature of a decay leaving ^{36}Ar in its first excited state, was necessary. An experiment was performed using the 88-Inch cyclotron at Lawrence Berkeley Laboratory to produce a ^{3}He beam with an energy of 60 MeV. The 2 μA beam impinged on a ^{nat}Ca target producing ^{37}Ca($\tau_{1/2}$ = 173 msec) which recoiled into a He atmosphere and was sent to the counting station by a He-jet system. The radioactivity was deposited on a tape in front of a ΔE-E telescope where protons from the decay of ^{37}Ca where identified. Two 12.7 x 15.2 cm NaI detectors where used to count γ-rays. The tape was moved every 4 seconds to avoid background from long-lived radioactivity. Figure 3.2-1 shows a γ-ray spectrum in coincidence with protons in the telescope. Even when the whole set-up was designed to minimize background on the NaI detectors, the counting rate was fairly high ($\sim$ 100 kHz) and the NaI spectra show signs of pulse pile-up.

Although the number of protons in coincidence with γ-rays of 1.97 MeV is not enough to estimate intensities for individual transitions, we can calculate the total fraction of decays that feed the first excited state in ^{36}Ar and make a comparison with the shell model prediction[2]. The observed fraction of 2.0 $\pm$ 0.5 % agrees well with the predicted value of 1.8 $\pm$ 0.2 %.

In order to measure individual transitions we need to be able to count ^{37}Ca decays 10 times faster and reduce the counting rate in the NaI detectors at the same time. A proposal has been accepted to use the ISOLDE facility at CERN where about 50 atoms/sec of ^{37}Ca could be produced. Our detectors and beamline are going to be designed and tested at the NPL and brought overseas for the experiment which could take place before the end of the year.

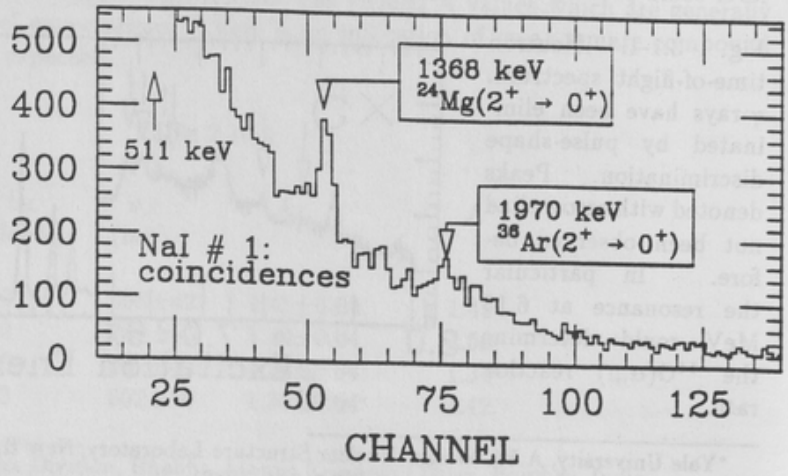

Fig. 3.2-1. NaI spectrum in coincidence with protons. We observe a γ-ray peak from the decay of ^{36}Ar* which gives a signature of a proton decay leaving ^{36}Ar in its first excited state.

*Lawrence Berkeley Laboratory, 1 Cyclotron Road, Berkeley, CA.

[1]E.G. Adelberger and W.C. Haxton Phys. Rev. C36, 879 (1987).

3.3 Angular Distributions of ^{14}N(p,n) and the Width of the First Excited State in ^{14}O

E.G. Adelberger, P.B. Fernández,* A. García, D.M. Markoff, M.S. Smith† and K.B. Swartz

The γ-width of the first excited state in ^{14}O has received a lot of attention from nuclear physicists because its absolute value determines the onset of the Hot CNO cycle. There have been a number of theoretical predictions and recently the first experimental results have been published.[1,2] A third experiment[3] was recently performed at ANL which could help resolve a discrepancy of a factor of 2 between the first two experiments. ^{14}O was produced by the reaction ^{1}H(^{14}N,^{14}O) at 175 MeV bombarding energy. A spectrometer was used to measure the ratio of $^{14}O_1$ recoils undergoing γ-decay to $^{14}O_0$ recoils. In order to obtain the gamma width, however, a measurement of the production cross-section ratio σ_{n0}/σ_{n1} is necessary.

We have used the pulsed-beam time-of-flight spectrometer at the University of Washington to measure the absolute differential cross-section for the reaction ^{14}N(p,n) at E_p = 12.5 MeV for neutrons leaving ^{14}O in its ground (n_0) and first excited (n_1) state. Targets were prepared evaporating melamine ($C_3H_6N_6$) on carbon foils. We calibrated the efficiencies of our neutron liquid scintillator detectors using the well known differential cross-section for ^{7}Li(p,n) which we measured using the same technique and targets of lithium fluoride evaporated on tantalum.

The Figures below show preliminary results for the absolute differential cross-sections. Data analysis of the experiment at ANL is still on progress and a number for the γ-width should soon be published.

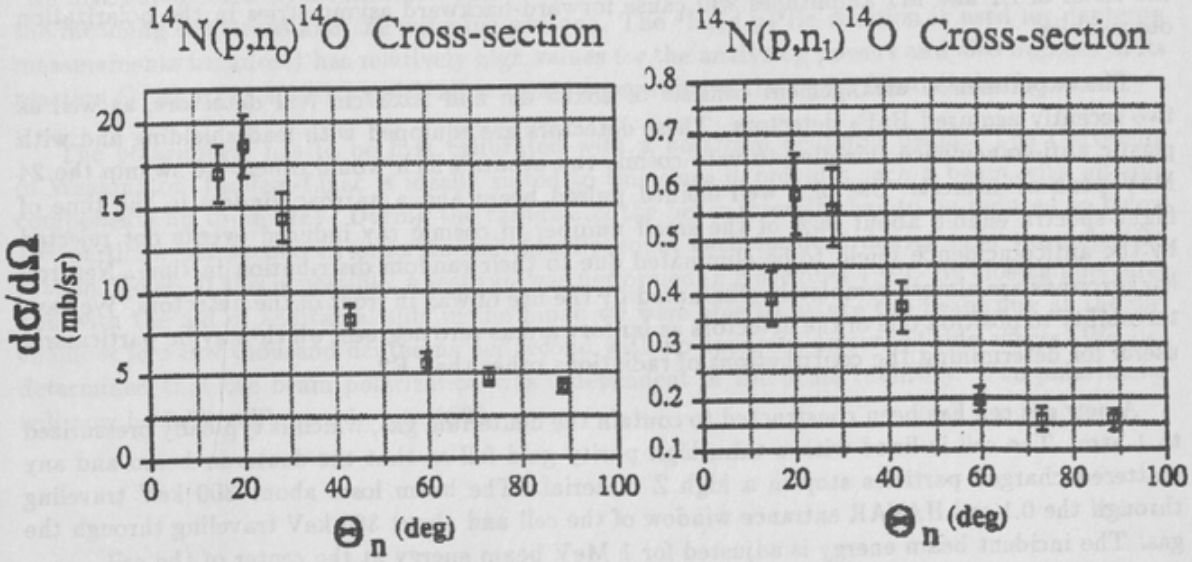

*Argonne National Laboratory, Physics Division, Argonne, Il.
†Yale University, A.W. Wright Nuclear Structure Laboratory, New Haven, CT.

[1]P.B. Fernández *et al.*, Phys. Rev. C40, 1887 (1989).
[2]P. Auger *et al.* in *Proc. Int. Sym. Heavy Ion Physics and Nuclear Astrophysical Problems*, edited by S. Kubono, M. Ishihara, T. Nomura, (World Scientific, Singapore 1989).
[3]M.S. Smith, to be presented at the Spring Meeting of APS, Washington (1990).

4 POLARIZATION

4.1 Polarized Radiative Capture in ^{2}H($\vec{d},\gamma$)^{4}He at Low Energies

C.A. Gossett, M.S. Kaplan, S.J. Luke and S.P. Van Verst

Recent measurements[1] of the cross section and angular distribution of the $^2H(d,\gamma)^4He$ reaction at very low energies have been reported. On the basis of their work, the authors of Ref. 1 suggest that the astrophysical S factor at zero energy is approximately 32 times larger than previously expected and that this enhancement results from E2 capture into the D-state of ^{4}He. In reaching this conclusion the authors have assumed only E2 capture amplitudes are involved, although at higher energies analyzing power measurements[2] clearly demonstrate that other multipolarities, including isospin forbidden E1 and isospin inhibited M1, significantly contribute. The data of Ref. 1 are insufficient to rule out contributions of amplitudes other than E2 and moreover, at low energy due to penetrability effects, the amplitude of E1 relative to the dominant E2 may become even more significant than observed in Ref. 2.

We are presently conducting experiments to measure angular distributions of the cross section and four analyzing powers for $^2H(\vec{d},\gamma)^4He$ at E_d = 1 MeV. Completion of these measurements will provide sufficient observables to determine all the E1, M1, E2, M2 amplitudes and phases allowed in the reaction. Measurement of the vector analyzing power is particularly sensitive to the contribution of E1 and M1 amplitudes since the vector analyzing power should be small, and should be identically zero at 90 degrees if only E2 amplitudes contribute. For E2 capture only, the cross section and analyzing powers must be symmetric or antisymmetric about 90 degrees, while the effect of E1 and M1 amplitudes will cause forward-backward asymmetries in the polarization observables.

The experimental arrangement consists of 25x25 cm and 25x37cm NaI detectors, as well as two recently acquired BaF_2 detectors. These detectors are equipped with lead shielding and with plastic anti-coincidence shielding to veto cosmic ray events which would otherwise swamp the 24 MeV peak of interest. Use of a well defined pulsed beam and a narrow window in the time of flight spectra enable about 90% of the small number of cosmic ray induced events not rejected by the anticoincidence shield to be eliminated due to their random distribution in time. Neutron backgrounds are almost completely eliminated by the use of wax in front of the detectors. We have the ability to position one of the detectors as far forward as zero degrees, which may be particularly useful for determining the contributions of radiations other than E2.

A new gas cell has been constructed to contain the deuterium gas, which is typically pressurized to 1 atm. The cell is lined with a thin, high purity gold foil so that the deuteron beam and any scattered charged particles stop in a high Z material. The beam loses about 300 keV traveling through the 0.1 mil HAVAR entrance window of the cell and about 300 keV traveling through the gas. The incident beam energy is adjusted for 1 MeV beam energy at the center of the cell.

Preliminary experiments have been carried out to test the suitability of the new BaF_2 detectors and to measure the vector analyzing power, $i\,T_{11}$. We have also measured the angular distribution of the cross section. The resolution of the BaF_2's was found to be 7% and the cosmic rejection

[1] C.A. Barnes *et al.*, Phys. Lett. **B197**, 315 (1987).
[2] S. Mellema *et al.*, Phys. Rev. **C34**, 2043 (1986).

efficiency is about 95%. Although this performance is not as good as the NaI, this resolution is more than adequate to separate the 24 MeV peak from the lower energy background.

Our preliminary data suggest that the vector analyzing power is different from zero. This would indicate that radiations other than E2 contribute to the reaction. Presently, we are working on optimizing detector resolution and cosmic rejection, as well as improving beam output from the polarized source.

4.2 Calibration of a Tensor Polarimeter

C.A. Gossett, Y.M. Shin* and N.R. Stevenson*

$\pi - d$ elastic scattering is one of the most extensively studied processes in intermediate energy physics. Measurements of cross-sections, analyzing powers, and polarizations[1,2] have been made up to T_π=300 MeV. Nevertheless, several outstanding problems yet remain to be resolved such as the contribution of the relatively small P_{11} πN intermediate amplitude which plays an important role in the complementary absorption process.

A complete set of measurements in this system is a vital step in gaining a thorough understanding of this interaction and other reactions that couple to it. A complete description of this system requires the measurement of several spin-transfer observables[1] which in turn require the use of a polarized target and a deuteron (tensor) polarimeter. A tensor polarimeter has been constructed at TRIUMF[3,4] based on the ^{3}He(d,p)^{4}He analyzing reaction. It consists of a liquid ^{3}He disk surrounded by scintillation counters, solid-state detectors, and wire chambers to detect the incoming deuterons and the outgoing protons. The ^{3}He(d,p)^{4}He reaction is used for deuteron measurements because it has relatively high values for the analyzing powers and also because of its reaction Q-value (18.4 MeV) which allows good separation of the signal from the background.

The polarimeter has to be first calibrated with a polarized deuteron beam. The University of Washington Tandem-Linac is ideally suited to this since it provides such a beam with all spin components up to 36 MeV. During the calibration the beam intensity has to be reduced to below 10^6 particles per second in order to individually count each incident deuteron in the detection system. To see if this is possible, a test run was performed in November 1989. By closing apertures and with the aid of additional slits in the Linac we were able to reduce the beam flux at the 60" chamber to a few thousand deuterons per second with no apparent unwanted side-effects. We also determined that the beam polarization was independent of the beam intensity. The polarimeter will now be fully calibrated in late 1990.

*Physics Department, University of Saskatchewan, Saskatoon, Sask. Canada S7N 0W0.

[1]N.R. Stevenson and Y.M. Shin, Phys. Rev. **C36**, 1221 (1987), and references cited therin.
[2]N.R. Stevenson *et al.*, Phys. Rev. **C36**, 1221 (1987), and references cited therin.
[3]Y.M. Shin *et al.*, Nucl. Instrum. Meth. A274, 227 (1989), and references cited therin.
[4]N.R. Stevenson, AIP Conf. Proc. 187, Ed. K.J. Heller (1988), p. 1381.

4.3 Production of Polarized Beta-emitters

K. Coulter,* J.K. Eisenberg, P.B. Fernández,* S.J. Freedman,* C.A. Gossett, M.S. Kaplan, D. Krakauer,* M. Leskovar, D.M. Markoff and K. Swartz

The β-decay vector coupling constant, G_β^V, has been determined for a number of $0^+ \rightarrow 0^+$ allowed transitions. In these decays, the Gamow-Teller matrix element vanishes, allowing the determination of G_β^V from the Fermi matrix element and measurement of the $ft_{1/2}$ value. However, these transitions represent only a fraction of all β decays. There is interest in precise measurements of G_β^V in $T = 1/2$ mirror pair transitions, which have been studied only in the cases n$\rightarrow$p, ^{19}Ne $\rightarrow ^{19}$F, and ^{35}Ar $\rightarrow ^{35}$Cl. A less precise measurement has been made for ^{29}P $\rightarrow ^{29}$Si. To determine G_β^V in these mixed Fermi and Gamow-Teller transitions, one needs an observable in addition to $ft_{1/2}$ in order to separate the two matrix elements. We plan to use the β-decay asymmetry parameter of polarized nuclei.

Aligned β-emitters are produced in reactions in which a polarized beam is incident on a suitable target. Collaborators at Argonne National Laboratory are developing a scattering chamber and detector array for use in the final experiment. Two plastic scintillator telescopes will be used for β detection. To determine the polarization of the β-emitter, the asymmetry of pure Gamow-Teller excited state branches will be measured by detecting βs in coincidence with γs from decays of the excited states using NaI detectors. Since the excited state asymmetry is readily calculated, the polarization can be extracted from the measured asymmetry.

At present we are exploring which β-emitters, target materials and conditions (e.g. temperature and magnetic field) will be best for the experiment by optimizing the observed value of the product of the nuclear polarization and the asymmetry parameter, PA. For this purpose we have built a small scattering chamber which is placed between the poles of an NMR-type magnet capable of generating up to 3.5 Kilogauss fields. Silicon charged particle detector telescopes are placed on the left and right. For the reaction ^{28}Si$(\vec{d},p)^{29}$P, 3 MeV, vector-polarized deuterons with spin oriented left-right have been used. The targets are 130 mg/cm^2 thick, natural abundance, high-purity silicon wafers. They are placed in a strong magnetic field in order to decouple the nuclear magnetic moment from the magnetic field of the atomic electrons and thus increase the relaxation time. Data are collected by cycling the beam on target for four seconds and then counting the βs for 8 seconds (about two half-lives of the ^{29}P). This process is repeated with alternate cycles reversing the sign of the incident beam polarization. By this method, the asymmetry can be found in terms of a "four-way" ratio of the counts in the left and right detectors for spin left and right deuterons so that the relative efficiencies of the left and right detectors cancel.

We have had two runs thus far. In the first, the chamber, beamline, and electronics setup were tested. The second run suffered from detector noise, making analysis difficult. We have determined that the effect of the magnetic field saturates at about 1.5 Kgauss. The highest average PA was $(2.0 \pm 0.1) \times 10^{-2}$with typical values of 1.5×10^{-2}. Having isolated the noise problem, we expect to collect clean data with better statistics in our next run. In the near future we will use a Si target cooled to liquid nitrogen temperature, which is expected to lengthen the relaxation time by reducing thermal depolarization. Also planned are investigations of the systems ^{27}Si using the reaction ^{27}Al$(\vec{p},n)^{27}$Si, and ^{31}S using the reaction ^{31}P$(\vec{p},n)^{31}$S.

*Argonne National Lab, Physics Division, Bldg. 203, Argonne, IL. 60439.

4.4 Polarized Protons from the ^{59}Co(^{3}He, $\vec{p}$) Reaction

M. Frodyma, S. Kailas,* W.G. Weitkamp and D.I. Will

We are continuing the measurements of the polarization of protons from the ^{59}Co(^{3}He,$\vec{p}$) reaction initiated by 27 MeV ^{3}He described in last year's Annual Report.[1] These measurements, which use a ^{4}He gas polarimeter at the final focus of the magnetic momentum filter/spectrograph to measure the proton polarization, have given a somewhat surprising result: the protons show a fairly constant, non-zero polarization of about 0.2 to 0.3 in the region of proton energy and angle bounded by 20 and 31 MeV and 12 and 42 degrees. That this result is surprising was accentuated by a recent publication of a measurement of the proton polarization resulting from the (d,p) reaction.[2] In this reaction, which has a spin structure analogous to the (^{3}He,p) reaction, the proton polarization is essentially zero at all energies and angles measured.

During the past year, we have improved the accuracy of our polarimeter calibration and added new measurements to our cross section and polarization data set.

We calibrate the polarimeter using protons of known polarization from the elastic scattering of protons on carbon.[3] Our previous calibration did not include corrections for the effects of oxygen contaminants in the target and was based on only three points. We measured the oxygen content of our target (2.8%) and made appropriate corrections using published data for the scattering of protons from oxygen. We measured the analyzing power of the polarimeter for 7 points with widely varying values of proton polarization and cross section to obtain a calibration which has an accuracy of about 2%, a value much less than the statistical uncertainties in our (^{3}He,$\vec{p}$) polarization data. The new calibration is, however, in reasonable agreement with our earlier calibration.

We have added to our cross section data. We repeated some of the measurements reported in last year's Annual Report to check the absolute value of the cross section and the shapes of the spectra. The new data agree satisfactorily with the old.

The values of the proton polarization from the (^{3}He,$\vec{p}$) reaction we measured previously suggest that the polarization approaches zero at energies below 20 MeV. One would expect this because the probability of proton evaporation and ^{3}He breakup increase at lower proton energies. Both of these processes should lead to small polarizations; evaporation because the spin orientation of protons evaporated by the compound nucleus is generally random in direction, and breakup because the two protons in ^{3}He have antiparallel spins so breakup results in as many spin-up protons as spin-down protons. We measured the polarization at a proton energy of 10.5 MeV, near the peak of the breakup spectrum and find (preliminary) values of 0.06 $\pm$ 0.04 at 12 degrees, 0.11 $\pm$ 0.04 at 18 degrees and 0.11 $\pm$ 0.05 at 24 degrees.

In the future, we expect to complete our data set and improve the precision of the measurements, both by reducing statistical uncertainties and examining possible systematic effects. We are also looking for a reaction mechanism that can lead to the positive, constant polarization we observe.

---

*Present address: Nuclear Physics Division, Bhabha Atomic Research Centre, Bombay, India.

[1] Nuclear Physics Laboratory Annual Report, University of Washington (1988) p. 32.

[2] M. Ieiri *et al.*, Nucl. Phys. **A504**, 477 (1989).

[3] H.O. Meyer, W.G. Weitkamp, D.S. Dunham, T.A. Trainor and M.P. Baker, Nucl. Phys. **A269**, 269 (1976).

5 FUNDAMENTAL SYMMETRIES AND INTERACTIONS

5.1 New Limits on Exotic Macroscopic Interactions

E.G. Adelberger, B.R. Heckel, * C.W. Stubbs,† Y. Su, H.E. Swanson, G. Smith and W.F. Rogers‡

We have continued to improve the sensitivity of our torsion-balance search for new macroscopic forces produced by the exchange of exotic ultra-low-mass vector or scalar bosons. In order to have sensitivity to interactions with ranges λ between infinity and 1 m, corresponding to boson masses less than 0.2 μeV, we study the differential acceleration of three different materials (Be, Al and Cu) in the field of the earth. The most precise previous tests of the weak equivalence principle studied differential acceleration of test bodies toward the *sun*, in order to avoid potentially severe systematic problems that affect measurements using the *earth* as a source:

1. disturbing the delicate balance while rotating it about the vertical axis
2. perturbations of the balance by terrestrial magnetic fields
3. perturbations of the balance by ambient gravity gradients.

Over the last 2 years we have developed an instrument that reduces these problems to a negligible level. The reader is referred to our most recent publication[1] for details. Our recent null result sets a limit on infinite range interactions coupled to Baryon number which is roughly an order of magnitude better than that set by the celebrated experiment by Dicke *et al.*[2] For most of the region 1 m $\leq \lambda \leq 10^{11}$ m, our constraints are at least one order of magnitude better than those of the best previous $1/r^2$ or equivalence principle results.

Our work was undertaken in response to Fischbach *et al.*'s[3] report of an anomaly in the von Eötvös data. We show below the reanalyzed von Eötvös data along with our recent results using Be/Cu and Be/Al test bodies. "One picture is worth a thousand words."[4]

*Physics Department, University of Washington, Seattle, WA 98195.
†Present address: Center for Particle Astrophysics, 301 Lecont Hall, UC Berkeley, Berkeley, CA 94720.
‡Present address: SUNY at Geneseo, Geneseo, NY 14454.

[1] B.R. Heckel *et al.*, Phys. Rev. Lett. 63 2705 (1989).
[2] J.E. Moody and E. Wilczek, Phys. Rev. D30, 130 (1984).
[3] E. Fischbach *et al.*, Phys. Rev. Lett. 56, 3 (1986).
[4] Confucius.

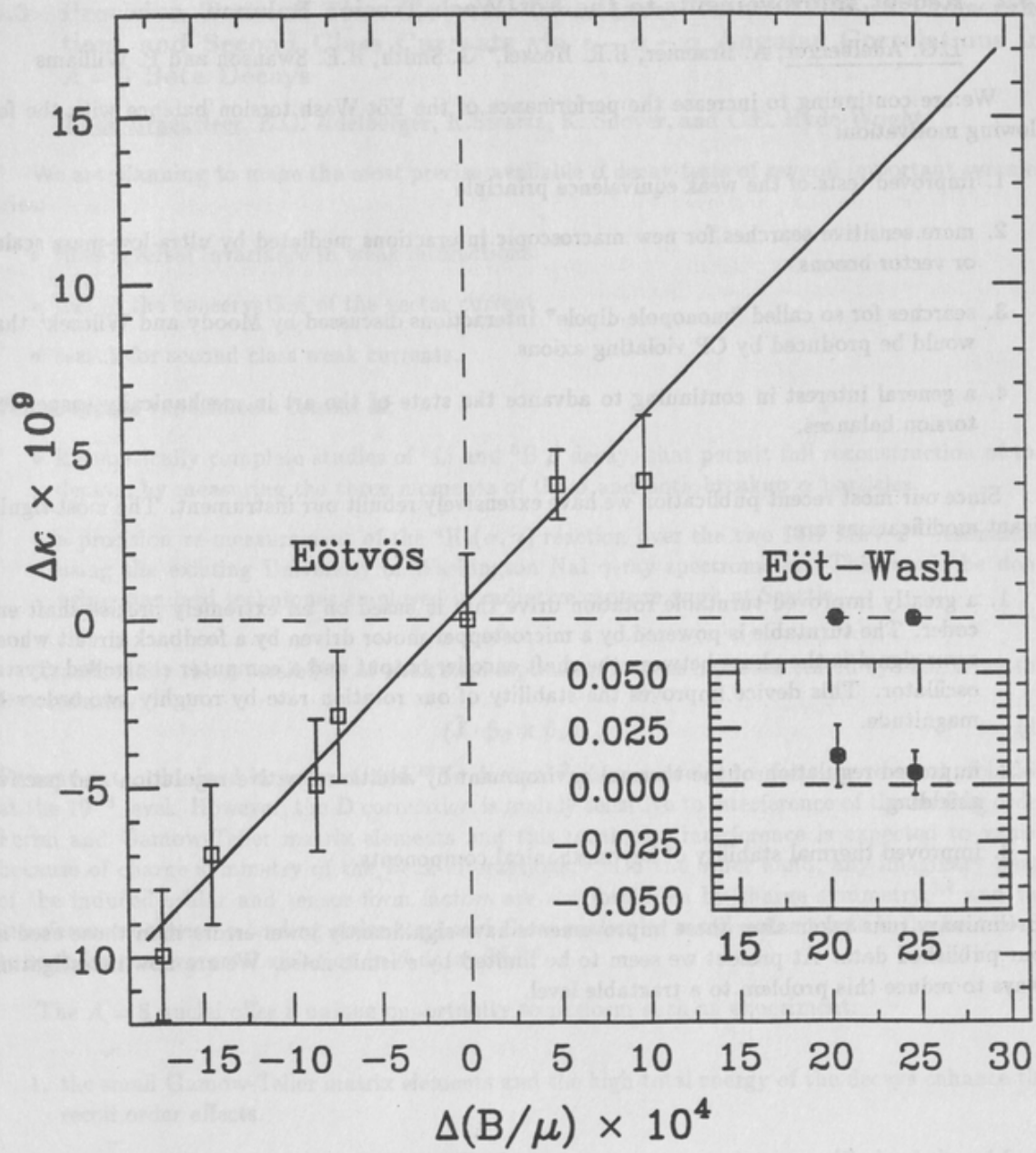

Figure 5.1-1. Differential horizontal acceleration of test body pairs as a function of their differential Baryon number to mass ratio. The open squares are the von Eötvös data as reanalyzed by Fischbach *et al.* The solid points are the Eöt-Wash data of ref. 1.

5.2 Recent Improvements to the Eöt-Wash Torsion Balance

E.G. Adelberger, A. Braemer, B.R. Heckel,* G. Smith, H.E. Swanson and P. Williams

We are continuing to increase the performance of the Eöt-Wash torsion balance with the following motivation:

1. improved tests of the weak equivalence principle
2. more sensitive searches for new macroscopic interactions mediated by ultra-low-mass scalar or vector bosons
3. searches for so called "monopole-dipole" interactions discussed by Moody and Wilczek[1] that would be produced by CP violating axions
4. a general interest in continuing to advance the state of the art in mechanically suspended torsion balances.

Since our most recent publication we have extensively rebuilt our instrument. The most significant modifications are:

1. a greatly improved turntable rotation drive that is based on an extremely precise shaft encoder. The turntable is powered by a microstepper motor driven by a feedback circuit whose error signal is the phase between the shaft encoder output and a computer controlled crystal oscillator. This device improves the stability of our rotation rate by roughly two orders of magnitude.
2. improved regulation of the thermal environment by additional active regulation and passive shielding.
3. improved thermal stability of key mechanical components.

Preliminary runs taken after these improvements have significantly lower errors than those used in our published data. At present we seem to be limited by seismic noise. We are now investigating ways to reduce this problem to a tractable level.

*Physics Department, University of Washington, Seattle, WA 98195.

[1]J.E. Moody and E. Wilczek, Phys. Rev. **D30**, 130 (1984).

5.3 Precision Tests of Time-Reversal Invariance, Vector Current Conservation, and Second Class Currents via $e - \alpha - \alpha$ Angular Correlations in $A = 8$ Beta Decays

L. de Braekeleer, E.G. Adelberger, K.Swartz, K. Snover, and C.E. Hyde-Wright

We are planning to make the most precise available β decay tests of several important symmetries:

- time-reversal invariance in weak interactions
- test of the conservation of the vector current
- search for second class weak currents.

The proposed experiments consist of:

- kinematically complete studies of ^{8}Li and ^{8}B β decays that permit full reconstruction of the decays, by measuring the three momenta of the β and both breakup α particles.
- a precision re-measurement of the ^{4}He(α,γ) reaction over the two 16.7 MeV 2^+ resonances using the existing University of Washington NaI γ-ray spectrometer. This would be done using standard techniques employed in radiative capture work at Seattle.

Traditionally the reversibility of weak semi-leptonic processes has been tested by measuring the D correlation:

$$(\hat{\mathbf{J}} \cdot \hat{\mathbf{p}}_\beta \times \hat{\mathbf{p}}_\nu) \ . \tag{1}$$

Present data, obtained in neutron and ^{19}Ne decays[1,2] show no evidence for time reversal violation at the 10^{-3} level. However, the D correlation is mainly sensitive to interference of the leading order Fermi and Gamow-Teller matrix elements and this particular interference is expected to vanish because of charge symmetry of the weak interactions.[3,4] On the other hand, any imaginary parts of the induced scalar and tensor form factors are not forbidden by charge symmetry,[3,4] and the interference between a leading order term and these particular recoil order terms is the best place to look for time reversal violation in β-decay.[3,5,6,7]

The $A = 8$ nuclei offer a unique opportunity to perform such an experiment:

1. the small Gamow-Teller matrix elements and the high total energy of the decays enhance the recoil order effects.
2. the neutrino momentum (usually a difficult quantity to measure) can readily be deduced from the measurement of momenta of the two α's in the final state.

[1] B.G. Erosolimsky *et al.*, Sov. J. Nucl. Phys., **28**, 48 (1978).
[2] A.L. Hallin *et al.*, Phys. Rev. Lett., **52**, 337 (1984).
[3] R.J. Blin Stoyle, *Fundamental Interactions and the Nucleus*, North Holland Publishing Co. p. 98 (1973).
[4] E.D. Commins and P. Bucksbaum, *Leptons and Quarks*.
[5] T.D. Lee, C.S. Wu, Ann. Rev. Nucl. Sci. **15**, 381 (1965).
[6] N. Cabbibo, Phys. Lett. **12**, 137 (1964).
[7] L. Maiani, Phys. Lett. **26 B**, 538 (1968).

3. the alignment of the final nucleus is determined automatically by the α momenta. Thus correlations with spin can be made without orienting the initial state.

4. time reversal unhindered by charge symmetry can be probed by two different correlations:

$$(\hat{\mathbf{p}}_\beta \cdot \hat{\mathbf{p}}_\alpha)(\hat{\mathbf{p}}_\alpha \cdot \hat{\mathbf{p}}_\beta \times \hat{\mathbf{p}}_\nu) \tag{2}$$

$$(\hat{\mathbf{p}}_\nu \cdot \hat{\mathbf{p}}_\alpha)(\hat{\mathbf{p}}_\alpha \cdot \hat{\mathbf{p}}_\beta \times \hat{\mathbf{p}}_\nu) \tag{3}$$

5. in these correlations the simulation of a TRV effect by final state interactions is negligible.

The $A = 8$ decays also offer unique opportunities to test two other important symmetries involving induced weak form factors as well:

- the conservation of the vector current (CVC)[8]
- the absence of second class currents (SCC)[9]

The CVC and SSC symmetries can be investigated directly and separately in the $A = 8$ decays, by measuring the energy dependence of the $\beta - \nu$ angular correlation.[10] Space limitations prevent us from discussing them further in this report.

Here is a brief description of the proposed apparatus. The isotopes will be produced by the reactions:

$$d + {}^7Li \rightarrow {}^8Li + p \quad (E_d = 0.8MeV) \tag{4}$$

$${}^3He + {}^6Li \rightarrow {}^8B + n \quad (E_{{}^3He} = 3.MeV) \tag{5}$$

The beam impinges on a rapidly rotating target to take advantage of the high currents ($\approx 10\mu$A) available from the UW tandem accelerator. The ^{8}Li or ^{8}B activity recoils into a thin catcher foil. The catcher foil is mounted on an arm which is rapidly ($t \approx 0.1$ s), precisely and repetitively moved by a high speed stepping motor into the center of a counting chamber. The α 's are detected in four gas position sensitive counters situated above, below, right and left of the chamber center. Five β telescopes are placed in the perpendicular plane at 30, 60, 90, 120, 150 degrees with respect to the axis defined by the left and right detectors. Triple coincidences are recorded, allowing us to measure different correlations simultaneously.

[8] R.P. Feynman and M. Gell-Mann, Phys. Rev.**109**, 193 (1958).
[9] S. Weinberg, Phys. Rev.**112**, 1375 (1958).
[10] B.R. Holstein, Phys. Rev. **C5**, 1529 (1972).

5.4 Experiment to Measure the PNC Spin Rotation of Transmitted Cold Neutrons

E.G. Adelberger, B.R. Heckel,* S.K. Lamoreaux,* D.M. Markoff and S. Saha*

Design work has continued on an apparatus to measure the parity non-conserving (PNC) spin-rotation of transversely polarized neutrons. Initially, we explored using a liquid parahydrogen target to probe neutron-proton scattering, specifically the dominant isovector pion exchange amplitude, F_π.[1] The strong interaction absorption and scattering cross sections for low energy neutrons on parahydrogen are not negligible. Scattering can indirectly produce a false PNC signal by altering the amount of time a transversely polarized neutron spends in any stray axial magnetic fields. The size of this effect is dependent upon whether the material is in the near or far target chamber.

In order to understand the effects of scattering in the neutron-hydrogen experiment, a Monte Carlo computer simulation has been developed. Absorption losses in 20cm of parahydrogen remove approximately 40% of the beam, with scattering removing an additional 35–40%. When losses from beam divergence are included, only 14% of the beam is transmitted to the detector. The number of neutrons that scatter and are detected constitute approximately 7% and 35% of the total number of detected neutrons, for material in the first and second target chambers respectively. We are currently adding more realistic refinements to the computer simulation in order to determine if the resulting false PNC signal is prohibitively large.

We have decided to use liquid helium as the target material for our initial spin rotation experiment. The spin rotation in liquid helium is predicted to be about eight times smaller than that in parahydrogen.[2,3] The spin rotation in helium is sensitive to almost all of the n-p scattering amplitudes, specifically, the pion exchange amplitude can be obtained from the indirect exchange term.

There are two major experimental advantages of a helium target. Because there is no bound state in the n-α system, the absorption cross section is essentially zero, and the scattering is reduced. Thus, longer target chambers with corresponding larger signals are possible. Calculations show that 38% of the initial beam is transmitted, with 2% and 9% of the detected particles from scattering events in the first and second target chambers respectively. The other main advantage of working with helium is the absence of stringent safety requirements, easing the design demands on the cryogenic apparatus.

The apparatus developed to transfer the parahydrogen between two target regions will also function with liquid helium. Minor modifications to the existing design for the parahydrogen target system have been made to accommodate the cryogenic requirements for helium.

*Department of Physics, University of Washington, Seattle, WA 98195.

[1] Nuclear Physics Laboratory Annual Report, University of Washington (1987) p. 27; (1989) p. 18.

[2] Y. Avishai and P. Grange, J. Phys. G. Nucl. Phys. 10 (1984).

[3] V.F. Dmitriev *et al.*, Phys. Lett. 125, 1 (1983).

5.5 Precision Measurement of the Antiproton Mass—First Results

X. Fei,* G. Gabrielse,* J.Haas,† H. Kalinowsky,† W. Kells,‡ L.A. Orozco,* R.L. Tjoelker* and T.A. Trainor.

A preliminary comparison of proton and antiproton masses was achieved in May, 1989. The inertial masses are found to be equal to 2 parts in 10^6. Measurements were made with $\bar{p}$ clouds from 100 to 5000 particles cooled to temperatures at or below 100 K.

In the past year progress in this program has been made in three areas. 1.) The x-y PPAC beam profiling system[1] was calibrated in the ion chamber mode to yield absolute numbers of $\bar{p}$ entering the trap system. 2.) Electron cooling techniques were substantially developed. 3.) A preliminary mass measurement was made using cooled clouds of $\sim 1000\bar{p}$ and detection via $\bar{p}$ and e^- axial motion.

Calibration of the PPAC beam monitor for ion chamber use is detailed in Section (calibration of LEAR PPACs of this report). Absolute calibration of this system provides independent information on how many $\bar{p}$ should appear in the trap. Departures from expectations indicate poor beam pulse quality or a trap malfunction. This information simplifies the number of systematics to keep track of, especially in the early stages of this experiment.

Antiprotons are delivered from the LEAR ring at CERN on demand in single pulses of $10^8 - -10^9$ $\bar{p}$ in a 200–300 ns pulse. The estimated trapping efficiency is $\sim 2 \times 10^{-4}$ into the 3 kV anharmonic (cylinder) trap (Fig. 5.5-1). Antiprotons in the trap at this stage have an energy spectrum as shown in Fig. 5.5-2. This spectrum is obtained by ramping down the trap potential linearly in time (3 kV $\rightarrow$ 0 kV) while counting pions produced in annihilation of escaped $\bar{p}$.

The $\bar{p}$ must be cooled below 1 eV before a mass measurement can be attempted. The cooling is done with electrons introduced into the trap prior to the $\bar{p}$ load which themselves cool to $\sim$4 K via synchrotron radiation in $\sim$0.1 sec. Initial attempts at cooling in which the electrons shared the long anharmonic trap with the $\bar{p}$ resulted in inconsistent behavior and catastrophic loss of the $\bar{p}$ cloud in some cases. This behavior was traced to known instabilities in single-charge plasma columns.[2]

By suitable adjustment of potentials on certain trap cylinder segments a harmonic trap for electrons can be produced near the center of the anharmonic trap. Such a harmonic or quadrupole trap is known to be quite stable for single-charge plasmas. The "hot" $\bar{p}$ moving axially in the 3 kV anharmonic trap pass repeatedly then through the cold electron cloud and are slowed, much as if they made multiple passes through a degrader foil. As their energies are reduced below the top of the harmonic trap they are captured in this trap and approach thermal equilibrium with the electron cloud. This process takes about 10 sec. A spectrum of such a $\bar{p}$ population cooled below 1 eV is shown in Fig. 5.5-3. The degree of cooling is masked by the coulomb energy of the cloud of $\sim 10^7 e^-$ in the harmonic trap. If the e^- are resonantly ejected from the trap after thermal equilibrium

*Department of Physics, Harvard University, Cambridge, MA 02138.
†Institut für Physik, Universität Mainz, BRD.
‡Institute for Boson Studies, Pasadena, CA.

[1]Nuclear Physics Laboratory Annual Report, University of Washington, p.54 (1989).

[2]C.F. Driscoll, J.H. Malmberg, K.S. Fine, R.A. Smith, X.P. Huang and R.W. Gould "Growth and Decay of Turbulent Vortex Structures in pure Electron Plasmas", publ. in *Plasma Physics and Controlled Nuclear Fusion Research*, Vol.3, Vienna, International Atomic Energy Agency, p.507–514 (1989).

a narrower spectrum is produced (Fig. 5.5-4a). If the harmonic well depth is slowly reduced so that hotter $\bar{p}$ evaporate out of the well and thereby further cool the remaining population, then a spectrum consistent with 100K is obtained as in Fig. 5.5-4b. Much of this remaining 9 meV width may be due to coulomb effects, TOF variations and other electronic contributions. The $\bar{p}$ represented by this spectrum may well be very near the ambient 4.2K of the trap.

In order to make the preliminary mass measurement cyclotron frequencies $\nu_c'(\bar{p})$ and $\nu_c'(e)$ for the $\bar{p}$ and electrons are measured. In either case a drive oscillator coupled to the harmonic trap is swept through the region of the cyclotron frequency. Power is coupled into the cyclotron motion of the $\bar{p}$ or e^- cloud and then, with various characteristic times this power is shared among various degrees of freedom of the two particle types. The temperature of the system is monitored by the noise amplitude in the axial motions of the $\bar{p}$ or e^- cloud via tuned circuits. A temperature rise and fall is observed as the cyclotron drive oscillator passes through the cyclotron frequency for one of the particles. Fig. 5.5-5 shows scans through $\nu_c'(\bar{p})$ monitored by axial temperatures $T_z(e^-)$ and $T_z(\bar{p})$.

Various corrections to ν_c' for either particle must be made to compensate for magnetron motion, magnetism of trap materials, slow drift of the B field between measurements, external fields, effects of magnetic shims, etc. The results as of June, 1989 are

$$\nu_c(\bar{p}) = 89.152{,}718(164) \text{ MHz}$$
$$\nu_c(e^-) = 163.698{,}062(10) \text{ GHz}$$

using $M(p)/M(e^-) = 1836.152701(37)$ yields

$$M(p)/M(\bar{p}) - 1 = 0.4(1.9) \times 10^{-6}$$

Further refinements of this measurement require reduction of the number of $\bar{p}$ to near unity, resonant detection of $\bar{p}$ cyclotron motion, optimum cooling of axial and magnetron motion and direct measurement of $\nu_c(p)$ and $\nu_c(\bar{p})$ in the same trap.

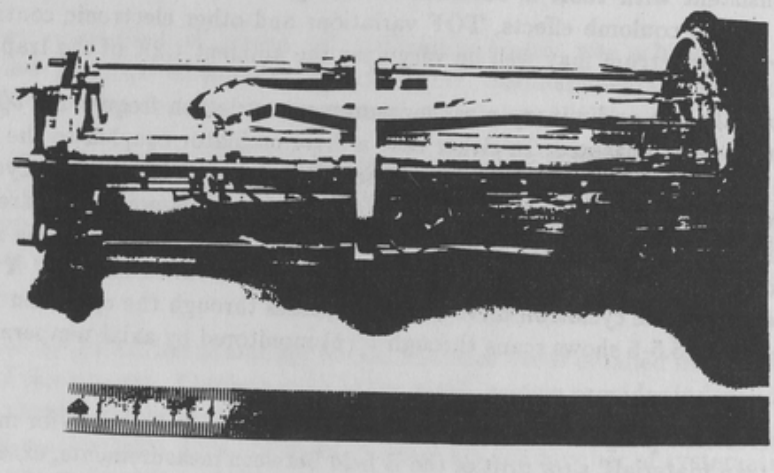

Figure 5.5-1 Cylindrical Trap Assembly. Small harmonic trap section is to left of center at ends of flat conductors.

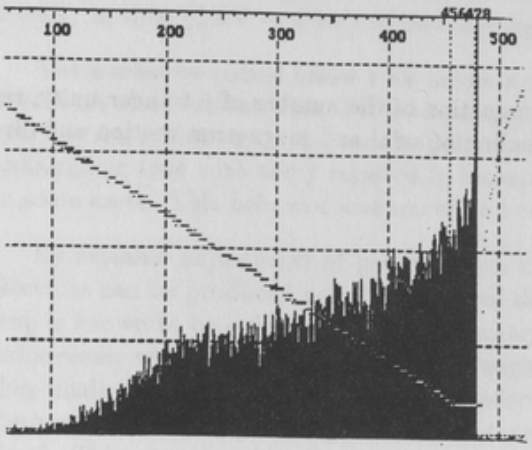

Figure 5.5-2 Spectrum of uncooled $\bar{p}$. 3kV span.

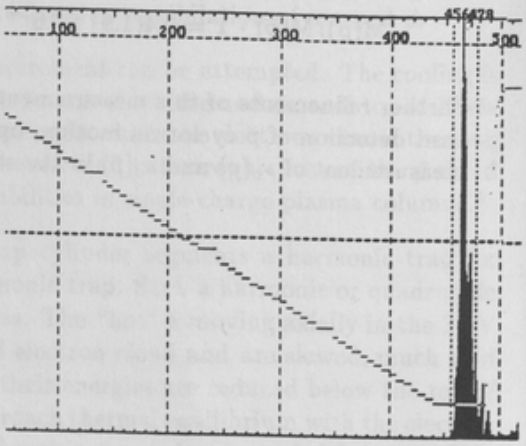

Figure 5.5-3 Spectrum of electron cooled $\bar{p}$. 50V span

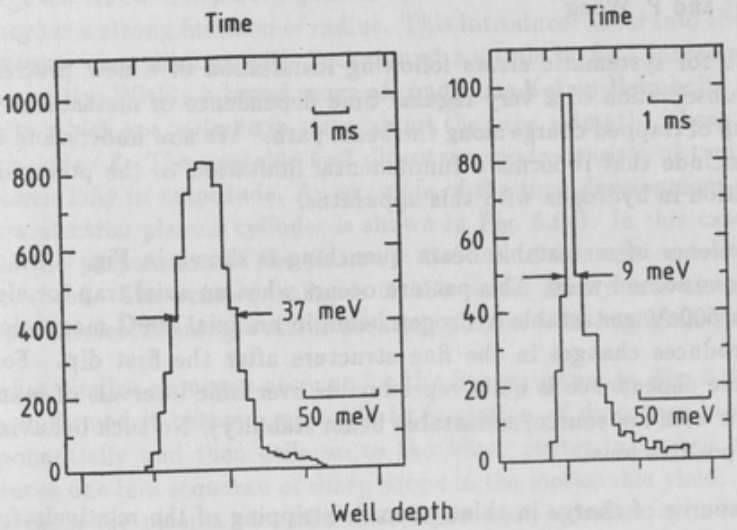

Figure 5.5-4 Spectrum of electron-cooled $\bar{p}$ after resonant removal of electrons from trap (a) and after further evaporation of warm $\bar{p}$ from shallow trap (b).

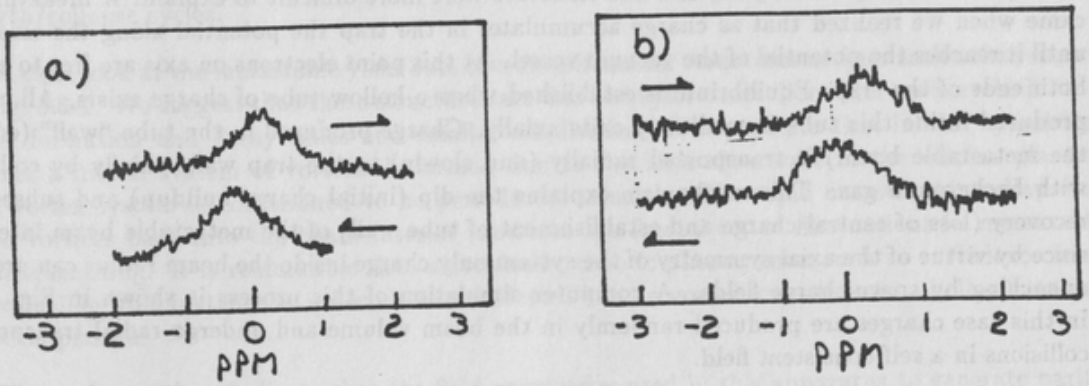

Figure 5.5-5 Scans of $\bar{p}$ cyclotron drive oscillator frequency through $\nu_c'(\bar{p})$ while monitoring a) electron axial temperature or b) $\bar{p}$ axial temperature.

5.6 Hydrogen Atom Experiment: Chaos and Fractals in a Cylindrical Electron Plasma

T.A. Trainor and P. Wong

During a search for systematic errors following installation of a new precision solenoid last year, we reported observation of a very regular time dependence of metastable beam quenching produced by buildup of trapped charge along the beam path.[1] We now understand this phenomenon completely and conclude that it forms a fundamental limitation to the possibility of measuring parity nonconservation in hydrogen with this apparatus.

The time dependence of metastable beam quenching is shown in Fig. 5.6-1. The first, large minimum is about one second wide. This pattern occurs when an axial trap for electrons is formed along the path of a 500eV metastable hydrogen beam in an axial 600G magnetic field. Variation in beam tuning produces changes in the fine structure after the first dip. For a given set of adjustments the time dependence is quite reproducible over time intervals of many minutes to an hour (i.e., consistent with ion source/metastable beam stability). No such behavior is observed for a trap polarity for positive ions.

The dominant source of charge in this system is stripping of the relatively fragile metastable atoms on background gas (mainly hydrogen). The positive ions (protons) carry away most of the beam energy essentially undeviated from the atomic beam. The electrons carry away less than 1eV and are easily stopped in an axial trap of modest depth (50–100 Volts).

While initial estimates of electron production indicated that sufficient space charge could build up in the axial trap to produce fields able to quench the beam in a fraction of a second, the subsequent recovery of the yield and fine structure were more difficult to explain. A breakthrough came when we realized that as charge accumulates in the trap the potential along the axis rises until it reaches the potential of the vacuum vessel. At this point electrons on axis are free to exit at both ends of the trap. Equilibrium is established when a hollow tube of charge exists. All charge produced inside this tube immediately exits axially. Charge produced in the tube "wall" (edge of the metastable beam) is transported radially (and slowly) to the trap walls chiefly by collisions with background gas. This mechanism explains the dip (initial charge buildup) and subsequent recovery (loss of central charge and establishment of tube wall) of the metastable beam intensity, since by virtue of the axial symmetry of the system only charge inside the beam radius can produce quenching by space-charge fields. A computer simulation of this process is shown in Fig. 5.6-2. In this case charges are produced randomly in the beam volume and undergo radial transport by collisions in a self-consistent field.

The remaining phenomenon to be explained, the fine structure following the dip, is associated with instabilities in the hollow electron plasma cylinder. These instabilities became known to us in a different context, the antiproton mass measurement at CERN (c.f. sec. 5.5) in which an electron plasma in a cylinder trap (for $\bar{p}$ cooling) exhibited erratic behavior. The problem of instabilities on a hollow cylindrical electron plasma has recently been examined.[2] An electron plasma in a

[1] Nuclear Physics Laboratory Annual Report, University of Washington, (1989) p. 23.

[2] C.F. Driscoll, J.H. Malmberg, K.S. Fine, R.A. Smith, X.P. Huang and R.W. Gould, "Growth and Decay of Turbulent Vortex Structures in pure Electron Plasmas", publ. in *Plasma Physics and Controlled Nuclear Fusion Research*, Vol.3, Vienna, International Atomic Energy Agency, p.507–514 (1989).

cylindrical Penning trap should, for a simple monotone-decreasing-in-r radial charge distribution, rotate uniformly about the symmetry axis at a magnetron frequency independent of radius. The hollow tube charge distribution departs significantly from this case, and the magnetron frequency (E x B drift frequency) is a strong function of radius. This introduces shear into the plasma, and radial transport of electrons via collisions with background neutrals or field inhomogeneities provides a mechanism for viscosity. Within a broad range of conditions Kelvin-Helmholtz instabilities arise on the plasma density which are periodic in space about the tube azimuth. These are called diocotron instabilities, with index ℓ. The unstable ℓ=2 diocotron mode consists of two vortices 180° apart which grow exponentially in amplitude. An example of the time development of an ℓ=2 diocotron mode on a hollow electron plasma cylinder is shown in Fig. 5.6-3. In this case the ℓ=2 mode has been "seeded" in the preparation of the plasma.[2] Growth of the vortices continues until most of the plasma is involved. The vortices collapse to the center finally in a time short compared to collisional transport times, forming a stable rotating plasma with negligible shear.

We believe that similar processes account for the fine structure in Fig. 5.6-1. Once the hollow electron plasma is formed it becomes unstable to formation of diocotron instabilities (ℓ=2,3,...) which grow exponentially and then collapse to the beam center in a time of order 100's of μs. This event produces one in a sequence of sharp drops in the metastable yield. Electron production by stripping increases the plasma potential once again until a hollow cylinder is reformed. This process continues to repeat, but the trap volume is meanwhile filling out to the wall with charge by radial collisional transport. Thus, the charge density on the hollow cylinder is less each time and takes longer to grow the diocotron instability. Equilibrium is achieved when a great majority of the charge required to fill the trap is external to the beam (in radius) and radial transport out to the walls of the trap is just equal to charge production at the surface of the beam. At this point the charge density in the hollow cylinder wall is too low to produce observable diocotron growth/collapse cycles.

A close look at the metastable yield data reveals self-similar structures at finer scales than shown in Fig. 5.6-1. We suggest that these structures are due to higher order diocotron modes which have faster formation and decay times and smaller amplitudes. We speculate that in this cylindrical plasma a fractal system of vortices is formed due to the high shear rate in the viscous plasma. The vortex system is constrained to be periodic in azimuth. The rapid catastrophic collapse of these vortices back into the beam interior produces the fractal set of fluctuations in metastable beam quenching. It is remarkable that a nominally chaotic phenomenon such as turbulence is so reproducible from instance to instance, as manifested here in vortex formation on a hollow rotating electron plasma.

These observations indicate that the field geometries used in this apparatus to generate parity conserving amplitudes for the $\alpha \rightarrow \beta$ transition, which also form charge traps, are unlikely to permit a significant improvement in the determination of C_2p. The copious production of charge by metastable atom stripping is unavoidable when the atomic beam is fast (500eV). The present field geometries would be optimal for a thermal metastable beam for which the stripping cross section would be negligible.

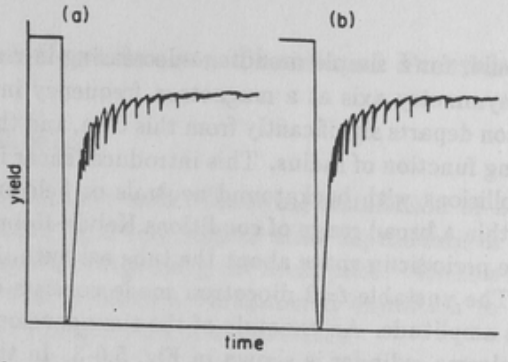

Figure 5.6-1 Observed metastable atom transmission through Penning trap.

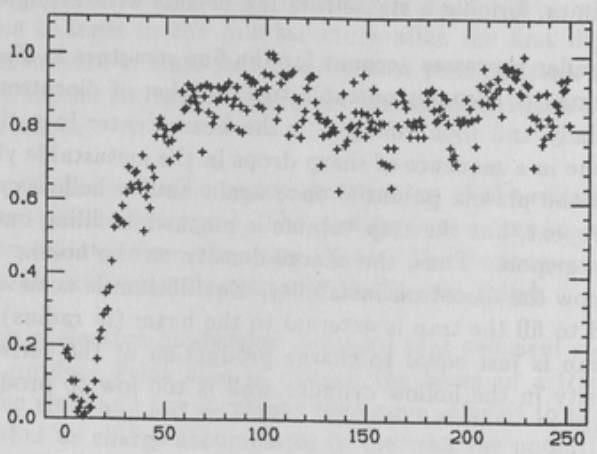

Figure 5.6-2 Calculated metastable transmission vs. time.

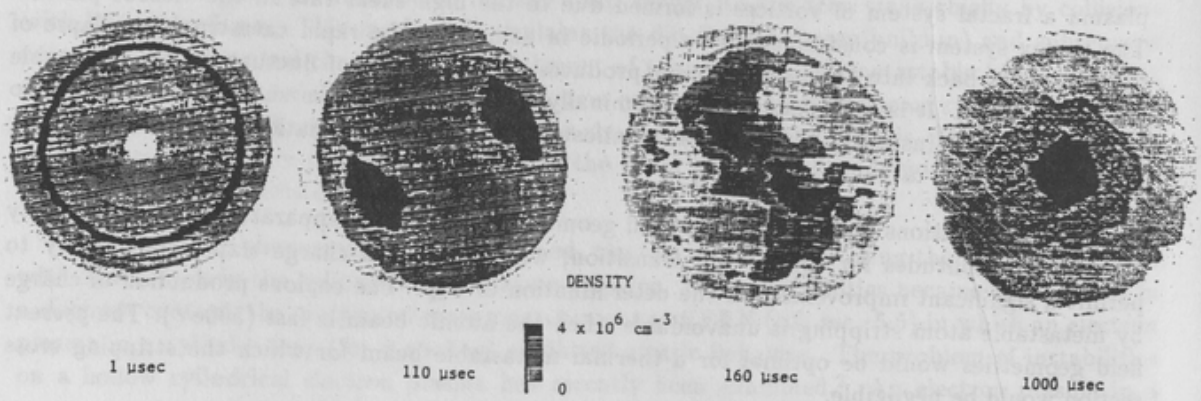

Figure 5.6-3 Observed formation and collapse of ℓ=2 diocotron mode on hollow plasma cylinder (Ref. 2).

5.7 APEX: Argonne Positron Experiment

T.A. Trainor *et al.**

This collaboration has been formed to carry out a new and improved set of experiments to further elucidate and perhaps solve the puzzle of positron peaks and correlated e^+-e^- pairs produced in heavy ion collisions as first observed at GSI ten years ago. A new electron spectrometer of the solenoid type based on the EPOS design at GSI is under construction. Assembly of the apparatus at Argonne is expected to go on late this year, and data acquisition should commence during Spring, 1991.

Correlated e^+-e^- pairs have been observed in a number of collision systems with united Z in the range 163–188. Based on data obtained by the ORANGE and EPOS collaborations over nearly ten years, a number of interesting characteristics have been observed. Particles in a pair appear to emerge from the collision nearly back to back in most cases. The energy spectra of emitted particles are discrete, with energy equally shared between members of a pair. The spectra appear to be essentially independent of the heavy ion collision system and consist of three major lines at total kinetic energies of 620 keV, 760 keV and 810 keV. The pairs seem to be emitted from the center-of-mass system and not from either of the heavy ion collision partners. Pairs appear to be created at specific CM energies and angles corresponding to "contact" of the collision partners.

Even before the discovery of correlated e^+-e^- pairs, the properties of the narrow positron peaks alone suggested that a neutral particle precursor might be involved. The observation of correlated pairs seemed to add weight to this theory. However, the introduction of a new elementary particle, with a decay channel to e^+-e^- is inconsistent with an array of precision tests of QED. And, direct searches for such a particle have subsequently ruled out its existence under almost all possible circumstances.

A more recent theory preserves the neutral particle hypothesis by suggesting that the large, time-dependent electric and magnetic fields generated in these heavy ion collisions may cause a phase transition of the QED vacuum to a metastable strong coupling state.[1] In this phase electrons take on a much larger effective mass and can form "positronium" with a mass spectrum as observed in the GSI experiments. Some time after the heavy ion collision partners have separated the vacuum decays and an e^+-e^- pair is emitted.

What is needed to test this or any other hypothesis regarding the production of correlated e^+-e^- pairs is high-quality invariant mass spectra for the pairs, good data regarding the heavy ion kinematics associated with pair production under carefully controlled beam energy and target conditions, and information on the angular correlations of pair production.

APEX should achieve a twenty-fold increase in data rate over EPOS based on the 100% duty cycle of ATLAS (vs. 20% for the GSI UNILAC) and a roughly four-fold increase in spectrometer efficiency. The APEX spectrometer shown in Figs. 5.7-1 and 5.7-2 is an end-for-end symmetric 300G solenoid. Heavy ion PPAC detectors feature full coverage in azimuth (ϕ) and in the angle range ($20° \leq \theta \leq 70°$). Electrons follow helix trajectories out to segmented cylindrical (3 cm ϕ) silicon detectors in the range (120 cm <z<156 cm) from the target. Surrounding these silicon arrays outside the vacuum vessel are NaI detector barrels segmented in azimuth. Each NaI segment is

[1] D.G. Caldi, Comments Nucl. Part. Phys. **19**, 137 (1989).

capable of axial position determination with a resolution of about 2 cm. Two γ-ray hits on a barrel indicate a positron hit on the silicon detector. Interpolation of the γ-ray hit positions locates the positron hit on the silicon array.

The time-of-flight of the electrons combined with their energies and hit positions as determined by the silicon arrays serve to determine their emission energies and angles (E,θ,ϕ). From this information the invariant mass and angular correlations can be inferred.

The University of Washington contribution to the collaboration to date is development of a silicon detector kapton shroud and gas cooling system (Sect. 9.10), high resolution ion chambers for beam position and target monitoring, alignment criteria for the solenoid and silicon detector arrays (Sect. 9.9) and various other monitoring and calibration systems.

*The APEX collaborators: I. Ahmaa,[‡] S. Austin,[§] R. Betts,[†] F.P. Calaprice,[¶] P. Chowdhury,[‖] R. Dunford,[†] J.D. Fox,[**] S. Freedman,[†] J.S. Greenberg,[‖] A.L. Hallin,[§] T. Hopp,[†] E. Kashy,[‡] W. Kutschera,[†] J. Last,[†] K. Lister,[¶] M. Maier,[‡] D. Mikolas,[‡] J.P. Schiffer,[†] T.A. Trainor, J. Winfield,[‡] F. Wolfs[†] and J. Yurkon[‡]

[‡]Argonne National Laboratory, Argonne, IL 60439.
[§]Michigan State University, East Lansing, MI 48824.
[¶]Princeton University, Princeton, NJ 08543.
[‖]Yale University, New Haven, CT 06520.
[**]Florida State University, Tallahassee FL 32306.

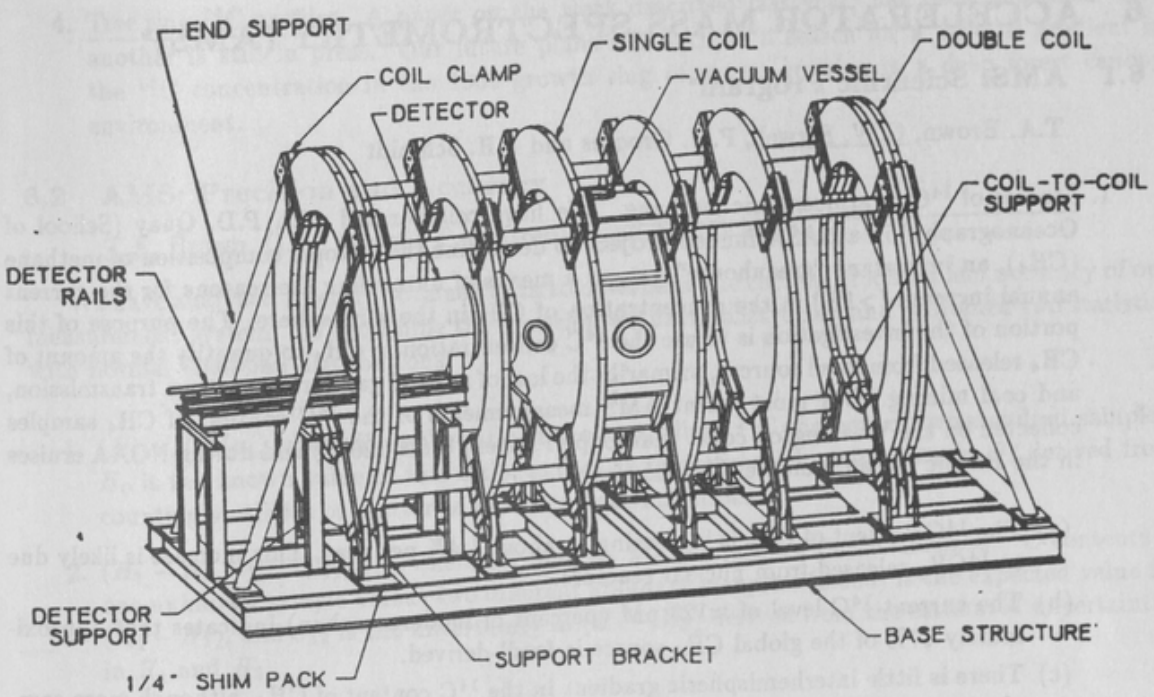

Figure 5.7-1 APEX Mechanical Structure.

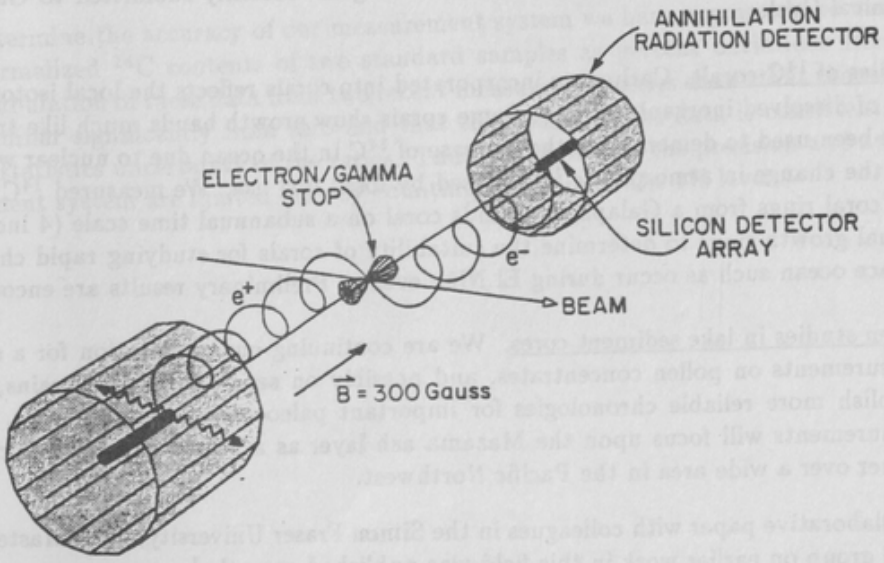

Figure 5.7-2 APEX Schematic Design.

6 ACCELERATOR MASS SPECTROMETRY (AMS)*

6.1 AMS: Scientific Program*

T.A. Brown, G.W. Farwell, P.M. Grootes and F.H. Schmidt

1. Studies of ^{14}C in atmospheric methane. We have collaborated with P.D. Quay (School of Oceanography) in a NASA-funded project to determine the isotopic composition of methane (CH_4), an important "greenhouse" gas, as a means of unraveling the reasons for the current annual increase (>1%) in the concentration of CH_4 in the atmosphere. The purpose of this portion of the investigation is to use the ^{14}C concentration in CH_4 to quantify the amount of CH_4 released from fossil sources, primarily the loss of natural gas during venting, transmission, and coal mining. Our most recent AMS measurements of the ^{14}C content of CH_4 samples collected on the Washington coast near Cape Flattery (46N 126W) and during NOAA cruises in the Pacific Ocean indicate the following:

   (a) The ^{14}C content of CH_4 is increasing at about 1.4% per year. This increase is likely due to $^{14}CH_4$ released from nuclear reactors.
   (b) The current ^{14}C level of $\approx$123 pM (percent of modern carbon) indicates that approximately 17% of the global CH_4 source is fossil-derived.
   (c) There is little interhemispheric gradient in the ^{14}C content of CH_4, although more samples are needed to verify this preliminary observation.

   These results are discussed in a paper entitled "Carbon Isotopic Composition of Atmospheric CH_4: Fossil and Biomass Burning Source Strengths" recently submitted to Global Biogeochemical Cycles.

2. Studies of ^{14}C corals. Carbonate incorporated into corals reflects the local isotopic composition of dissolved inorganic carbon. Some corals show growth bands much like tree rings and have been used to demonstrate the increase of ^{14}C in the ocean due to nuclear weapons tests and the change in atmospheric ^{13}C caused by fossil fuel use. We measured ^{14}C fluctuations in 4 coral rings from a Galapagos Islands coral on a subannual time scale (4 increments per annual growth ring) to determine the suitability of corals for studying rapid changes in the surface ocean such as occur during El Niño events. Preliminary results are encouraging.

3. Pollen studies in lake sediment cores. We are continuing our preparation for a series of ^{14}C measurements on pollen concentrates, and possibly on separated pollen grains, in order to establish more reliable chronologies for important paleoenvironmental events. The initial measurements will focus upon the Mazama ash layer as a potentially reliable chronological marker over a wide area in the Pacific Northwest.

   A collaborative paper with colleagues in the Simon Fraser University — McMaster University AMS group on earlier work in this field was published recently.[1]

*Our work was supported in part by NSF (Grant EAR-8115994, Environmental Geosciences Program) and by NASA (Grant NAGW-844).

[1]Thomas A. Brown, D. Erle Nelson, Rolf W. Matthewes, John S. Vogel, and John R. Southon, Quaternary Research **32**, 205 (1989).

4. Tree ring ^{14}C profiles. A paper on the work described last year[2] has been published[3] and another is still in press. Our future plans still include a search for a vertical gradient in the ^{14}C concentration in the 1963 growth ring of a tree growing in a deep forest canopy environment.

6.2 AMS: Precision and Accuracy

T.A. Brown, G.W. Farwell, P.M. Grootes and F.H. Schmidt

We have analyzed recently obtained data to determine the current precision and accuracy of our measurement system. To determine the precision we have constructed and combined two statistics with normal Gaussian distributions:

1. $(H_1 - H_0)/\sigma_1$, where H_1 is the ratio of the normalized ^{14}C contents of two standard samples, H_0 is the known value of this ratio, and σ_1 is the estimated uncertainty in H_1 derived from counting statistics or scatter of repeated determinations.

2. $(H_1 - H_2 - (0.000))/\sigma_{12}$, where H_1 and H_2 are the ratio of the normalized ^{14}C contents of one unknown sample versus two different standard samples, (0.000) is the expected value for $(H_1 - H_2)$, and σ_{12} is the uncertainty in $(H_1 - H_2)$ derived from the estimated uncertainties in H_1 and H_2.

Minimum χ^2 fitting of the distributions obtained from these statistics shows that our counting-statistics-based estimate of the uncertainties in the data accurately represents the precision of our measurements.

To determine the accuracy of our measurement system we have expressed the measured ratios of the normalized ^{14}C contents of two standard samples as percent deviations from the known values. Tabulation of these data from two recent measurement series shows that the mean deviation does not differ significantly from zero and that the scatter of the data is consistent with the 1% counting statistics uncertainty of the ratios. Thus, we show that the precision and accuracy of our measurement system are limited only by counting statistics at the 1% level.

[2]Nuclear Physics Laboratory Annual Report, University of Washington (1989), p. 34.
[3]P.M. Grootes, G.W. Farwell, F.H. Schmidt, D.D. Leach, and M. Stuiver, Tellus **41B**, 134 (1989).

6.3 AMS: Technical Highlights

T.A. Brown, G.W. Farwell, P.M. Grootes and F.H. Schmidt

A. A new rotor for the Generating Voltmeter (GVM) was constructed. After some initial troubles (see Section 10.10) it performed very well. The terminal potential is now held constant to within ±1 K.V. at 7 M.V. The improved regulation has brought about considerable improvement to AMS measurements.

B. In last year's Annual Report we discussed our new sample preparation equipment which reduced our sample size from 0.093 inch diameter (~2mg C) to 0.028 inch diameter (~400 μg C). The system has been improved considerably; hundreds of samples have now been fabricated with a rate of failure (i.e., giving a poor beam) of less than 2%. It takes about one hour to fabricate a graphitized sample from the powdered graphite stage to a sintered form ready to install in the source. Such samples produce large (50–60 μA) carbon beams, and are well worth the additional work.

C. A totally unexpected dividend has come from the small diameter (0.028 inch) samples. We have found that by defocussing the cesium beam (by a shift of ~10% in the optimum reflection potential) so as to irradiate most of the surface of the sample with cesium, the efficiency of carbon utilization is increased, while the emittance of the source is not impaired. The negative carbon beam is slightly reduced (~15%) because of less efficient use of the cesium, but this loss of (cheap) cesium atoms is unimportant compared with the gain in utilization of (expensive) carbon atoms.

   The 0.028 inch diameter sample produces an image following the inflection magnet which matches (to within 10%) the diameter (0.156 inch) of the aperture in the beam line. This aperture is the exit aperture of the ion source mass spectrometer, and in turn it matches the entrance pupil of the Tandem stripper aperture.

   There is evidence that this reflection potential defocussing scheme has been responsible for a portion of our considerably improved performance, probably because of reduced criticality to the effects of sample cratering.

D. The combined benefits due to A and C above and to other factors have brought us close to the ideal measurement accuracy, *viz.*, that depending only upon counting statistics (see above). It is interesting that a search for the cause of the difference between counting statistical accuracy and the standard deviation of a set of measurements led us to discover the trouble with the GVM. In a sense this is a 12-year triumph.

7 MEDIUM ENERGY

7.1 Inclusive Photoproduction of π^+ on a Variety of Nuclei

M. Doss,* J.K. Eisenberg, K. Fissum,* I. Halpern, D.P. Rosenzweig and D.W. Storm

We have been studying inclusive pion scattering at energies on the low side of the (3,3) resonance.[1] Inclusive photoproduction of pions in nuclei provides additional information about the interaction of pions with the nuclear medium, as was described in last year's Annual Report.[2]

We plan to use the tagger in conjunction with the new pulse stretcher ring at Saskatchewan Accelerator Laboratory (SAL) to provide monochromatic photons with energies from 200 to above 250 MeV. We have assembled a 30-cm long by 15-cm diameter plastic (BC 408) scintillation counter which we will use to measure the π^+ spectra. This counter will stop pions of approximately 100 MeV. The scheme for identifying π^+ by observing the decay muons was outlined in our previous report.[2] We plan to use four of these counters simultaneously, provided the present one proves to be satisfactory.

During the previous year we have tested the counter both at TRIUMF and at SAL. At TRIUMF we were able to test the counter as parasites, using 120-MeV positive pions which were scattered from a target and which were then degraded in energy by slabs of material placed in front of our counter. Although this was far from an optimum geometry for obtaining a clean beam, we measured an energy resolution of 5% for 95-MeV pions. As thicker degraders were used to provide lower energies, the resolution became steadily worse due to straggling. We did not have an opportunity at TRIUMF to set up the electronics required to identify decay muons.

At SAL we were able to test the counter with a 293-MeV bremsstrahlung beam and a liquid hydrogen target, again as parasites. To identify π^+ we used a set of gated ADC's to digitize the main pulse and a series of six sequential 20-nsec bites starting 25 nsec after the main pulse. We expect the 4-MeV muons from stopped-pion decays occurring during these bites to produce an excess pulse height.

We placed a 6-mm thick plastic counter, Δ, in front of the large counter, E, in order to identify particle masses by relating the Δ and E pulse heights. The large flux of electrons masks the pions when no additional selection criteria are applied. If we only consider events with an extra few MeV in one of the delayed gates, then electrons, pions, and protons are somewhat separated by the Δ – E comparison. If we consider the subset of these events with total energy in excess of 20 MeV, the separation is quite good. See Fig. 7.1-1. By observing the relative rate of decay muon signal in the various 20-nsec bites, we see pions (having the correct lifetime). When we exclude events with total energy less than 20 MeV, there is very little contamination, as shown in Fig. 7.1-2. The number of pions that we identify is roughly 20% of the number expected from the hydrogen target. As only 40% are expected to survive more than 25 nsec, this result is encouraging.

We are looking forward to the opportunity to continue the tests with the tagged photon beam and a hydrogen target. (We will use a plastic target and will do a carbon subtraction.) The pions

*University of Saskatchewan, Saskatoon, S7N 0W0, Canada.

[1] K.A. Aniol *et al.*, Phys. Rev. C33, 208 (1986); D.P. Rosenzweig *et al.*, Bull. Am. Phys. Soc. **34**, 1204 (1989); M.A. Khandaker *et al.*, to be published.

[2] M. Doss *et al.*, Nuclear Physics Laboratory Annual Report, University of Washington, p.28 (1989).

from hydrogen are monoenergetic, and we expect to have much lower backgrounds. Because the phototube pulse will go over a much shorter cable, we expect to be able to decrease the 25 nsec between the main pulse and the delayed samples. We are also exploring the possibility of testing the counter directly in a low intensity pion beam at TRIUMF.

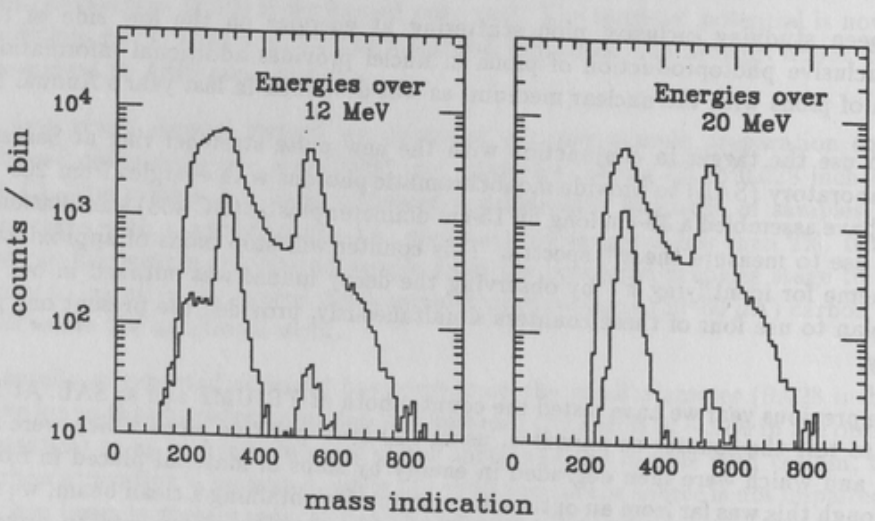

Figure 7.1-1: The events are histogramed against the relative mass determined from the Δ and E pulse heights. On the left, all events triggering the apparatus are histogrammed, while on the right only events with energy above 20 MeV are included. There was a 12 MeV threshold in the trigger. In each case, the upper histogram is of all the events for which both Δ and E signals were present, while the lower one is of events that exhibit an excess pulse height in one of the delayed gates. Protons form the group around channel 540, pions form the group around channel 300, and electrons are in the lower channels.

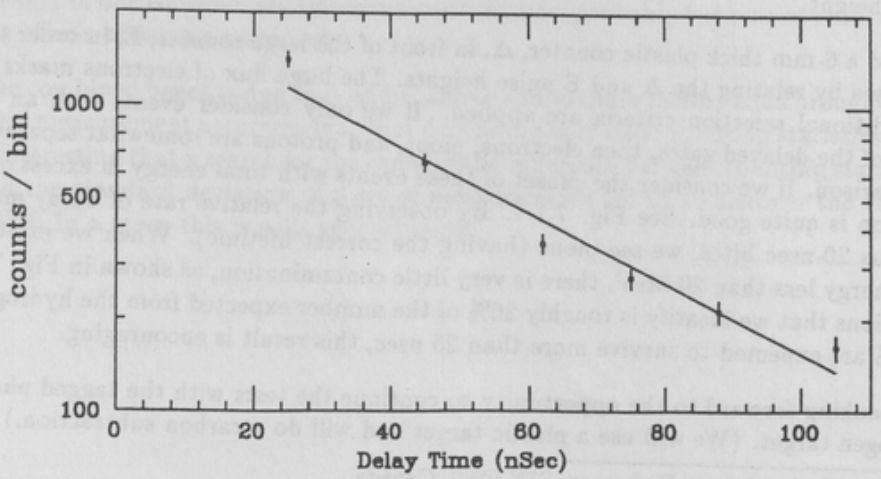

Figure 7.1-2: The events identified as pions are histogrammed against the mean time for the bite in which the $\pi^+ - \mu^+$ decay occurred. The curve is a fit of a time independent background plus an exponential decay with the pion lifetime.

7.2 Inclusive Spectra for Scattering 100MeV $\pi^{\pm}$ from a Variety of Nuclei

J.F. Amann,* R.L. Boudrie,* K.G.R. Doss,† D. Drake,* I. Halpern, J. Nelson,‡
M. Khandaker,§ D.P. Rosenzweig, D.W. Storm, D.R. Tieger‡ and S.A. Wood¶

The results of our measurement of the inclusive inelastic scattering spectra of pions from ^{12}C, ^{40}Ca, ^{120}Sn, and ^{208}Pb were reported last year.[1] We have continued to investigate and improve certain aspects of the data analysis, allowing us to achieve lower background contamination and to reduce our systematic uncertainties. While the back angle differential cross-sections are not substantially changed by the additional work, it appears as though the 50° data set has become usable; previously the forward angle data was swamped by a high background of muons. The 50° data set is helpful in performing the extrapolation used to obtain the total inelastic scattering cross section.

The improved background suppression is made possible by an optimization of the trajectory reconstruction software, especially that part which determinines the position and angle of the trajectories at the target. Utilizing the strong correlation between these two quantities we are able to eliminate those events not originating from the beam spot. These include events from muons in the beam halo and from pions which decay to muons after they scatter. Muon scattering is forward peaked, and the muon contamination increases drastically between 75° and 50°. The increased signal-to-noise ratio has also allowed us to determine better the focal plane efficiency function of the spectrometer, because the calibration data set (π-p elastic yields) shows much less scatter.

Still unresolved, however, are discrepencies between transmission and reflection target geometries, as well as fluctuations in the spectrometer's acceptance as a function of spectrometer angle. We suspect these are both related to target misallignment, and hope to understand them further. At this point they are the main cause of systematic error. The discrepencies are typically 5%, but range to 15%. Shown below are the total inelastic cross-sections deduced from our angular distribution measurements. In last year's report reasons were given as to why one expects the N=Z nuclei to have similar inelastic cross-section for π^- and π^+, and why the π^- cross section should be about a factor of 2 larger than the π^+ cross-section for the case of Pb.

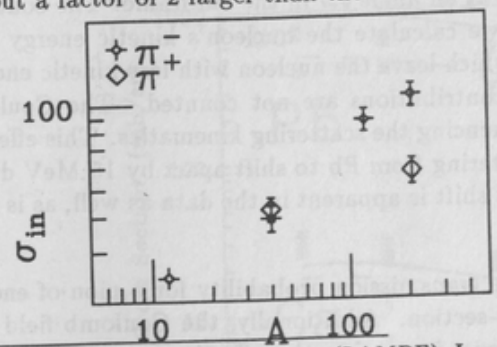

Figure 7.2-1. Total inelastic cross-sections for $\pi^{\pm}$ scattering from C, Ca, Sn and Pb.

*Los Alamos National Laboratory (LAMPF), Los Alamos, NM 87545.
†University of Saskatchewan, Saskatoon, S7N OWO Canada.
‡Massachusetts Institute of Technology, Cambridge, MA 02139.
§University of Maryland, College Park, MD 20742.
¶University of Illinois, Champaign, IL 61820.

[1] Nuclear Physics Laboratory Annual Report, University of Washington (1989) p. 31.

7.3 Modeling Inclusive Inelastic $\pi^{\pm}$ Scattering

I. Halpern, D.P. Rosenzweig and D.W. Storm

In connection with the measurement of the inelastic scattering spectra reported in the previous section,[1] we have been investigating the applicability of a semi-classical model to account for our data. We are encouraged by the model's ability to reproduce both the spectral shape and the overall magnitude of the inelastic cross-section.

The model involves two simplifying approximations: 1) the nucleon momentum distribution is uniform throughout the nucleus, and 2) the pion-nucleon interaction is assumed to be described by the free πN cross-section for the appropriate kinematics. For each outgoing pion angle and energy a calculation is made of the effective volume of the nucleus which is able to scatter that pion and have it escape. This function is folded together with a spectrum calculated for that angle by assuming the pions impinge on nucleons which have a momentum distribution that is taken to be Wood-Saxon in shape.

Each point of the nuclear volume can be assigned a probability of having a pion arrive at it, scatter at the detector angle, and traverse back out of the nucleus. The attenuation is energy dependent, so this probability is a function of not only the scattering angle, but also of the initial and final pion energy. The $\pi^{\pm}$ energy in the nucleus is modified by Coulomb and nuclear field effects, such that $E_{\pi Nuc} = E_{\pi beam} \mp V_C + U_N$. We use a value for the nuclear potential of $U_N \approx 20$ MeV in order to account for the kinematic effects. The transmission probability $T(\vec{r}, \theta_{\pi'}, E_{\pi}, E_{\pi'})$ is determined by integrating the pion attenuation along straight line paths to the point $\vec{r}$. The attenuation is calculated using the free π-nucleon cross section modified by Pauli blocking in the nucleus, and a Wood-Saxon parameterization of the density. For high energy pions the attenuation is strong, and only the volume near the surface can emit a scattered pion. Integration of T over $d\vec{r}$ gives us a factor describing the emitting volume.

The double differential cross-section for pion scattering from the moving nucleons is determined as follows. Contributions from each portion of the momentum distribution are weighted by the elementary differential cross-section evaluated at the center-of-mass angle chosen such that the pion scattered from the moving nucleon will appear at an angle $\theta_{\pi'}$ in the lab frame. The contributions are compiled into a histogram. In addition, we calculate the nucleon's kinetic energy from the momentum, and assume that those collisions which leave the nucleon with less kinetic energy than the Fermi energy are Pauli blocked. Their contributions are not counted. The Coulomb and nuclear fields shift the initial pions energy, influencing the scattering kinematics. This effect causes the centroids in the spectra of π^- and π^+ scattering from Pb to shift apart by 15 MeV due to the strong Coulomb potential ($V_C = 18$ MV). This shift is apparent in the data as well, as is shown in Fig. 7.3-1.

The spectrum obtained is multiplied by the transmission probability for a pion of energy $E_{\pi'}$, producing the desired double differential cross-section. Additionally, the Coulomb field modifies the pion trajectory as it approaches the nucleus, increasing the effective π^- cross-section (and decreasing that for π^+) by a factor of $1 \mp V_C/T$ for $\pi^{\pm}$.

The results of these calculations are shown in the following figures. Typical spectra are shown

[1] Nuclear Physics Laboratory Annual Report, University of Washington (1990), Section 7.2.

in Fig. 7.3-1, for the case of the Pb target and scattering angle of 100°. The histograms are the measured data, extending to the cutoff at E_{ex} = 75MeV. Fig. 7.3-2 compares the angular distributions with those measured for the Pb and Ca targets. There are no free parameters besides the nucleon potential U_N, and one can see that overall magnitudes are reasonably well reproduced.

We are attempting to use an extension of the model described here to account for data taken at a similar energy using targets of A $\leq$ 4, and are encouraged by the preliminary results. These nuclei differ from the heavy nuclei, because all nucleons are in the same energy eigenstate and their momenta are distributed in a Gaussian. In this case the Pauli blocking is treated differently; the pion energy transfer must exceed the nucleon's binding energy.

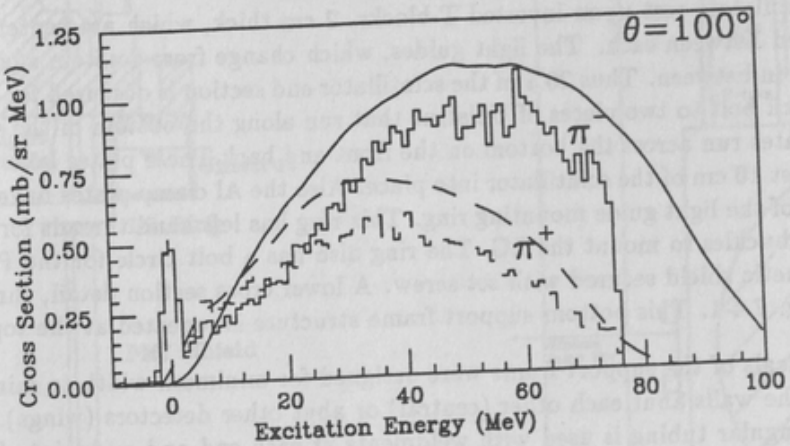

Figure 7.3-1. Double diffential energy spectra for inelastic pion scattering for Pb target at θ = 100°. The histograms are our data, and the smooth curves are the model calculation. The solid curve is for π^- and the dashed curve is for π^+.

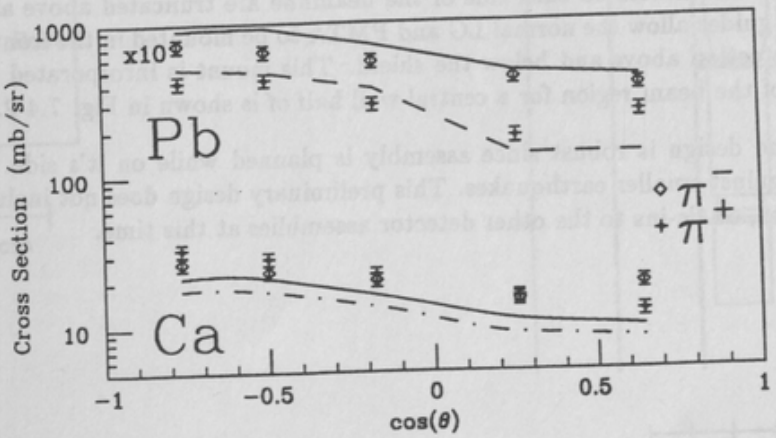

Figure 7.3-2. The angular distribution for inelastic pion scattering, comparing the data with our model calculation. The solid curve is for π^- and the dashed curve is for π^+.

7.4 Mechanical Design for the PEGASYS T.O.F. Wall

J.F. Amsbaugh and C.E. Hyde-Wright

The preliminary mechanical design for the time of flight wall of PEGASYS has a central wall, in two halves, and two wing walls. Each wall is a number of plastic scintillators placed side by side with a light guide (LG) and photomultiplier tube assembly (PMTA) on the top and bottom of each bar. The scintillator cross section is 10 × 5 cm, and two lengths are used, 500 cm in the central wall and 430 cm in the wings. These long scintillator bars are made by glueing two shorter pieces of equal length together. A central wall half has 28 detectors for a total weight of 810 kg for the detectors and a wing wall has 22 for a weight of 530 kg.

The scintillators rest upon inverted T-blocks, 2 cm thick, which are centered along the 5 cm edge centered between each. The light guides, which change from 8×5 cm square section to 5cm diameter, fit in between. Thus 20% of the scintillator end section is obscured for support. The arms of the T-block bolt to two pieces of Unistrut that run along the bottom of the wall.[1] Two padded Al clamp plates run across the bottom on the front and back These plates bolt to the T-block and clamp the last 10 cm of the scintillator into place. Also the Al clamp plates have threaded holes for the tie rods of the light guide mounting ring. This ring has left hand threads for the tie rods which act like turnbuckles to mount the LG. The ring also has a bolt circle for the PMT base, a recess for the magnetic shield secured with set screw. A lower cross section detail, through a T-block, is shown in Fig. 7.4-1. This bottom support frame structure is repeated at the top.

The verticals of the support frame were designed for minimum width to minimize the inactive area where the walls abut each other (central) or abut other detectors (wings). Thick wall 2.5 × 7.5 cm rectangular tubing is used with weldments at each end and midpoint. The end weldment has tangs for connecting to the Unistrut, and bolts into the end T-blocks. The midpoint weldment is for a connecting midplane clamp. This padded clamp plate is made of 5 cm square SST tubing and prevents the scintillators from buckling at the midplane glue joint.

The interior midpoint weldments of the central halves are designed for a 12inch O.D. beamline to pass through. It also provides the space and mounting for 16 radiation lengths of Pb shielding. The first two scintillators on each side of the beamline are truncated above and below the shield. U-turn light guides allow the normal LG and PMTA to be mounted in the front or back of the wall, providing detection above and below the shield. This mount is incorporated in the weldment. A detail view of the beam region for a central wall half of is shown in Fig. 7.4-2.

The frame design is robust since assembly is planned while on it's side. This also provides protection against smaller earthquakes. This preliminary design does not include floor mountings, lifting fixtures, or tie-ins to the other detector assemblies at this time.

[1] Unistrut is a registered trade mark of the Unistrut Corporation, Wayne, Michigan.

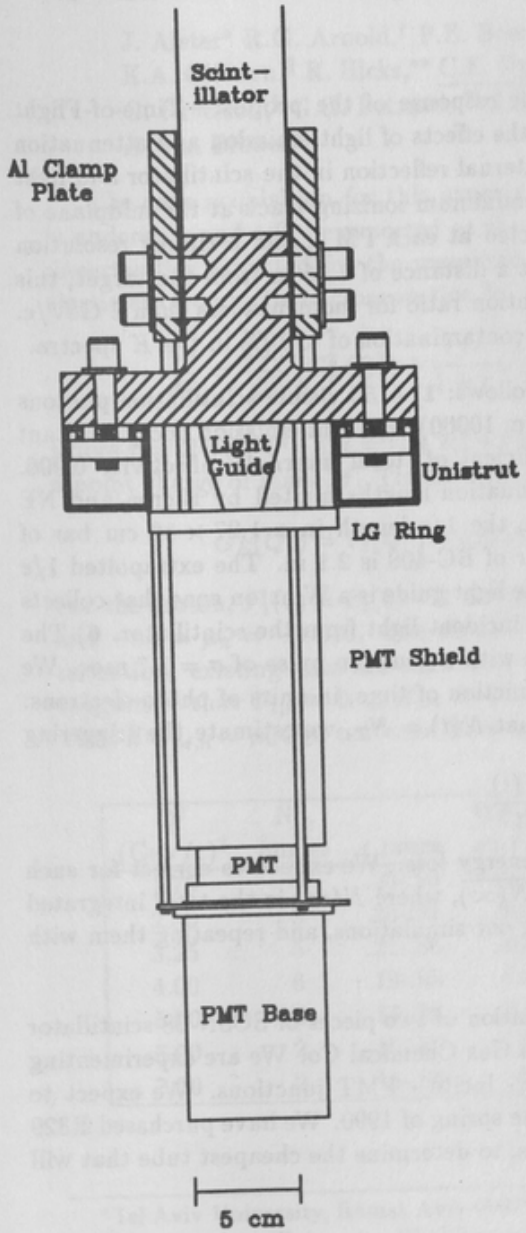

Figure 7.4-1 : Section through T-Block.

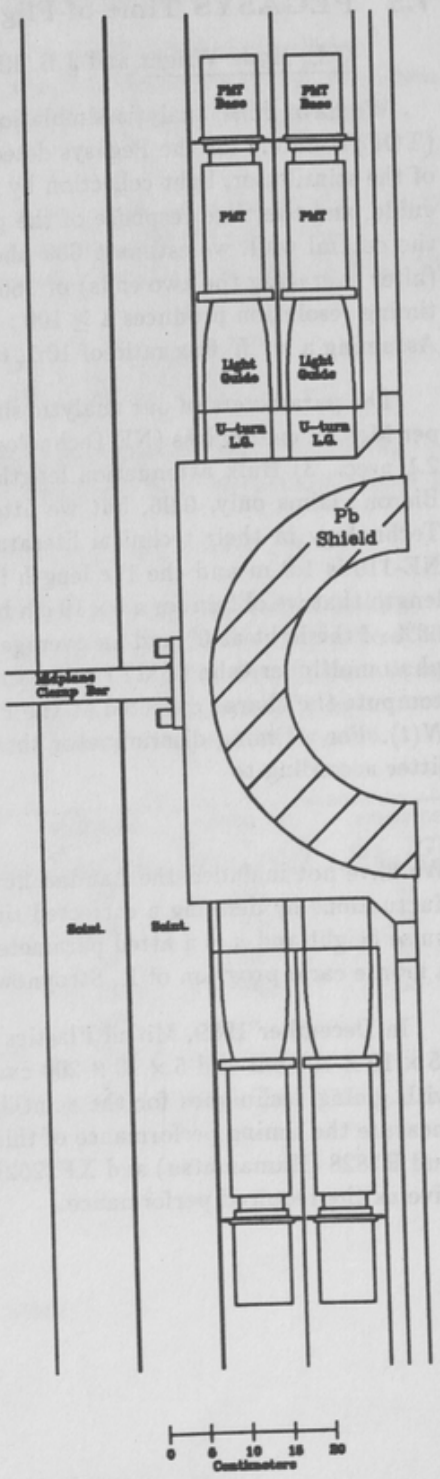

Figure 7.4-2 : View of the Beamline Area.

7.5 PEGASYS Time-of-Flight Resolution

C.E. Hyde-Wright and J.B. Ritter

We have done analytic simulations of the the time response of the proposed Time-of-Flight (TOF) counters for the Pegasys detector. We include the effects of light emission and attenuation of the scintillator, light collection by imperfect total internal reflection in the scintillator and light guide, and the time response of the phototube. For a minimum ionizing track at the midplane of the central wall, we estimate 330 photoelectrons collected at each PMT, and a timing resolution (after averaging the two ends) of 160 psec (sigma). At a distance of 7.75 m from the target, this timing resolution produces a $\geq 100:1$ $\pi:K$ discrimination ratio for momenta less than 2 GeV/c. Assuming a $\pi:K$ flux ratio of 10:1, this results in a π contamination of $< 10\%$ in the K spectra.

The parameters of our analytic simulations are as follows: 1) 4150 visible scintillation photons per MeV of energy loss (NE Technology and Bicron claim 10000). 2) Light emission decay constant 2.1 nsec. 3) Bulk attenuation length 3.8 m. 4) Coefficient of (total internal) reflectivity 0.996. Bicron claims only, 0.96, but we fitted 0.996 to atttenuation lengths quoted by Bicron and NE Technology in their technical literature. For example, the $1/e$ length in a 1.27×10 cm bar of NE-110 is 1.9 m and the $1/e$ length in a 1×12 cm bar of BC-408 is 2.1 m. The extrapolted $1/e$ length that we obtain for a 5×10 cm bar is 2.4 m. 5) The light guide is a Winston cone that collects 66% of the light at 0° and an average of 40% of all the incident light from the scintillator. 6) The photomultiplier tube (PMT) quantum efficiency is 25% with a gaussian pulse of $\sigma = 1.7$ nsec. We compute the charge collected at the PMT anode as a function of time, in units of photo-electrons: $N(t)$. For a timing discriminator threshold N_T such that $N(t) = N_T$, we estimate the triggering jitter according to

$$\sigma_t = \sqrt{N_T} \Big/ \frac{dN(t)}{dt}$$

We have not included the Landau fluctuations in the energy loss. We expect to correct for such fluctuations by defining a corrected time[1] $t' = t + \kappa/\sqrt{N(\infty)}$, where $N(\infty)$ is the total integrated pulse height and κ is a fitted parameter. We are refining our simulations, and repeating them with a monte carlo program of R. Stroynowski.

In December 1989, Mitsui Plastics arranged the donation of two pieces of SCSN-38 scintillator ($5 \times 10 \times 100$ cm and $5 \times 10 \times 200$ cm) from the Kyowa Gas Chemical Co. We are experimenting with gluing techniques for the scintillator - scintillator - lucite - PMT junctions. We expect to measure the timing performance of this 3 m sample in the spring of 1990. We have purchased R329 and R1828 (Hamamatsu) and XP2262B (Phillips) PMTs, to determine the cheapest tube that will give us the required performance.

[1] T. Sugitate *et al.*, Nucl Inst Meth **A249** 354 (1986).

7.6 Electron Scattering from the Proton and the Deuteron

J. Alster* R.G. Arnold,† P.E. Bosted,* C.C. Chang,‡ F.S. Dietrich,§ R.A. Gearhart,¶ K.A. Giffioen,‖ R. Hicks,** C.E. Hyde-Wright, S.E. Kuhn,†† J. Lichtenstadt,‡‡ R. Miskimen,§ G. Peterson,§ G.G. Petratos,‡‡ S.E. Rock,* S.H. Rokni,§ K. Swartz, Z. Szalata* and K. van Bibber†

The data acquisition for this experiment was reported in last years annual report[1]. Analysis is underway, and will be reported at the PANIC conference in June 1990 (P. Bosted, *et al.*). The uncertainties expected for the measured nucleon form factors are listed in the table below. The elastic electron nucleon cross section is:

$$\frac{d\sigma}{d\Omega} = \frac{d\sigma_0}{d\Omega}\left[G_E^2(Q^2) + \frac{\tau/\epsilon}{1+\tau}G_M^2(Q^2)\right], \qquad \frac{d\sigma_0}{d\Omega} = \frac{\alpha^2\cos^2(\theta/2)}{4E^2\sin^4(\theta/2)}\frac{E'}{E}\frac{1}{1+\tau},$$

where $\tau = Q^2/(4M^2)$, $1/\epsilon = [1+2(1+\tau)\tan^2(\theta/2)]$, and $d\sigma_0$ is the cross section for scattering from a point charge of mass M. The Sachs (G), Dirac (F_1), and Pauli (F_2) form factors are related by

$$G_E(Q^2) = F_1(Q^2) - \kappa\tau F_2(Q^2), \qquad G_M(Q^2) = F_1(Q^2) + \kappa F_2(Q^2).$$

For the proton, $F_1(0) = F_2(0) = 1$ and $1 - \kappa_p = \mu_p = 2.793$. For the neutron, $F_1(0) = 0$, $F_2(0) = 1$ and $-\kappa_n = \mu_n = -1.913$. The dipole form factor $G_D = [1 + Q^2/\Lambda^2]^{-2}$ is a convenient parameterization: existing data are consistent with $G_{M,n}/\mu_n \approx G_{M,p}/\mu_p \approx G_{E,p} \approx G_D$. It has has been suggested[2] that $F_{1,n} \approx 0 \ll G_D$. In this case, $G_{E,n} = -\tau G_{M,n}$. At our highest Q^2 point $\tau \approx 1.0$. Thus if $G_{M,n} \approx \mu_n G_D$, our error bars will easily distinguish between $G_{E,n} = 0$ or $F_{1,n} = 0$.

Q^2 $(GeV/c)^2$	No. angles	ϵ range	typ. error on $d\sigma/d\Omega$	error on $G_{Mp}/\mu_p G_D$	error on G_{Ep}/G_D	error on $G_{Mn}/\mu_n G_D$	error on G_{En}^2/G_D^2
1.75	4	.25-.95	0.5%	.015	.07	.08	.27
2.50	6	.23-.91	0.5%	.015	.09	.08	.34
3.25	5	.21-.86	0.8%	.015	.12	.08	.45
4.00	6	.19-.95	0.8%	.015	.14	.08	.55
5.00	5	.17-.92	0.8%	.015	.17	–	–
6.00	2	.16-.89	1%	.015	.21	–	–
7.00	2	.15-.86	3%	.022	.30	–	–

*Tel Aviv University, Ramat Aviv 69978 Israel.
†The American University, Washington DC 20016.
‡University of Maryland, College Park MD 20742.
§Lawrence Livermore National Laboratory, Livermore, CA 94550.
¶Stanford Linear Accelerator Center, Stanford, CA 94305.
‖University of Pennsylvania, Philadelphia, PA 19104.
**University of Massaschusetts, Amherst MA 01003.
††Stanford University, Stanford CA 94305.
‡‡University of Rochester, Rochester, NY 14627.

[1] Nuclear Physics Laboratory Annual Report, University of Washington (1989) p. 29
[2] M. Gari and W. Krümpelmann, Z. Phys., **A322** 689 (1985).

7.7 Virtual Compton Scattering with PEGASYS

C.E. Hyde-Wright

The figure on the following page summarizes our studies of the virtual compton reaction $N(e,e'\gamma)$ for the Pegasys proposal. In deep inelastic kinematics (large energy and momentum transfer) this reaction is predicted to scale[1] as a function of the Compton x-variable $x_C = Q^2_C/[2M(\nu - k)]$, where k is the detected photon momentum, ν, Q^2 are the energy and invariant momentum squared transfer by the electron, and $Q^2_C = -(p - p' - k)^2$. The contributions to the $(e,e'\gamma)$ reaction are illustrated at the bottom of this page. The compton and bethe-heitler (or radiative tail) amplitudes lead to indistinguishable final states: consequently there is an interference amplitude as well. Photons from the decay of hadrons (mostly $\pi^0 \rightarrow \gamma\gamma$ decays) lead to distinguishable final states. These photons form a statistical background to the measurement of the bethe-heitler, compton, and interference cross sections.

The top panels on the following page illustrate the particle decay background, and compare this to the compton part of $(e,e'\gamma)$. The cross section (in units of μb) is integrated by monte-carlo techniques over the Pegasys acceptance, and plotted in bins of $k^2_\perp$, the component of the photon momentum perpendicular to the virtual photon direction.

In all figures, the cross section is integrated over the kinematic domain 1 $(\mathrm{GeV/c})^2 \leq Q^2 \leq 4.0$ $(\mathrm{GeV/c})^2$, 4 GeV $\leq \nu \leq$ 10 GeV, $k \geq \nu/2$, and 1 $(\mathrm{GeV/c})^2 \leq Q^2_C$. In the right hand column, an additional constraint is imposed that the residual mass of the final state $W^2_f = (p + P - p' - k)^2 \geq 4$ GeV^2. In the bottom panels, the constraint $k^2_\perp \geq 1.0$ $(\mathrm{GeV/c})^2$ is also included.

In the top panels, the dot-dashed curves represent the total photon production from hadron decays, as simulated by the LUND monte carlo. The dash curves (roughly 2/3) represent those photons which are reconstructed to a π^0, and can be eliminated on an event-by-event basis. The residual dotted line is the difference of these two: this is the statistical background of photons. The constraint $k \geq \nu/2$ reduces the combinatorial background from multiple π^0 events. In both the left and the right samples, the background is well below the compton signal for $k^2_\perp \geq 1.0$ $(\mathrm{Gev/c})^2$.

The bottom panels illustrate the three deep inelastic processes: compton, bethe-heitler, and their interference, in bins of x_C. In the bottom right hand panel, it is seen that the three processes are roughly equal. The main purpose of this proposed experiment is to test the scaling law prediction for these cross sections. At fixed x_C, the cross section is exactly predicted (as a function of the 5 other kinematic variables) with just three empirical constants, normalizing the three terms in the lower panels.[2] The onset of this scaling, as a function of Q^2_C is an important indicator of the transition from hadronic to quark degrees of freedom.

Figure 7.7-1. Feynman diagrams for the $(e,e'\gamma)$ reaction.

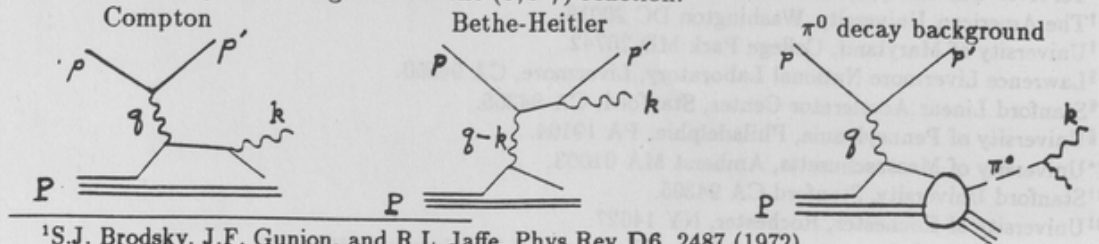

[1] S.J. Brodsky, J.F. Gunion, and R.L. Jaffe, Phys Rev D6, 2487 (1972).

[2] Nuclear Physics Laboratory Annual Report, University of Washington (1989) p. 29.

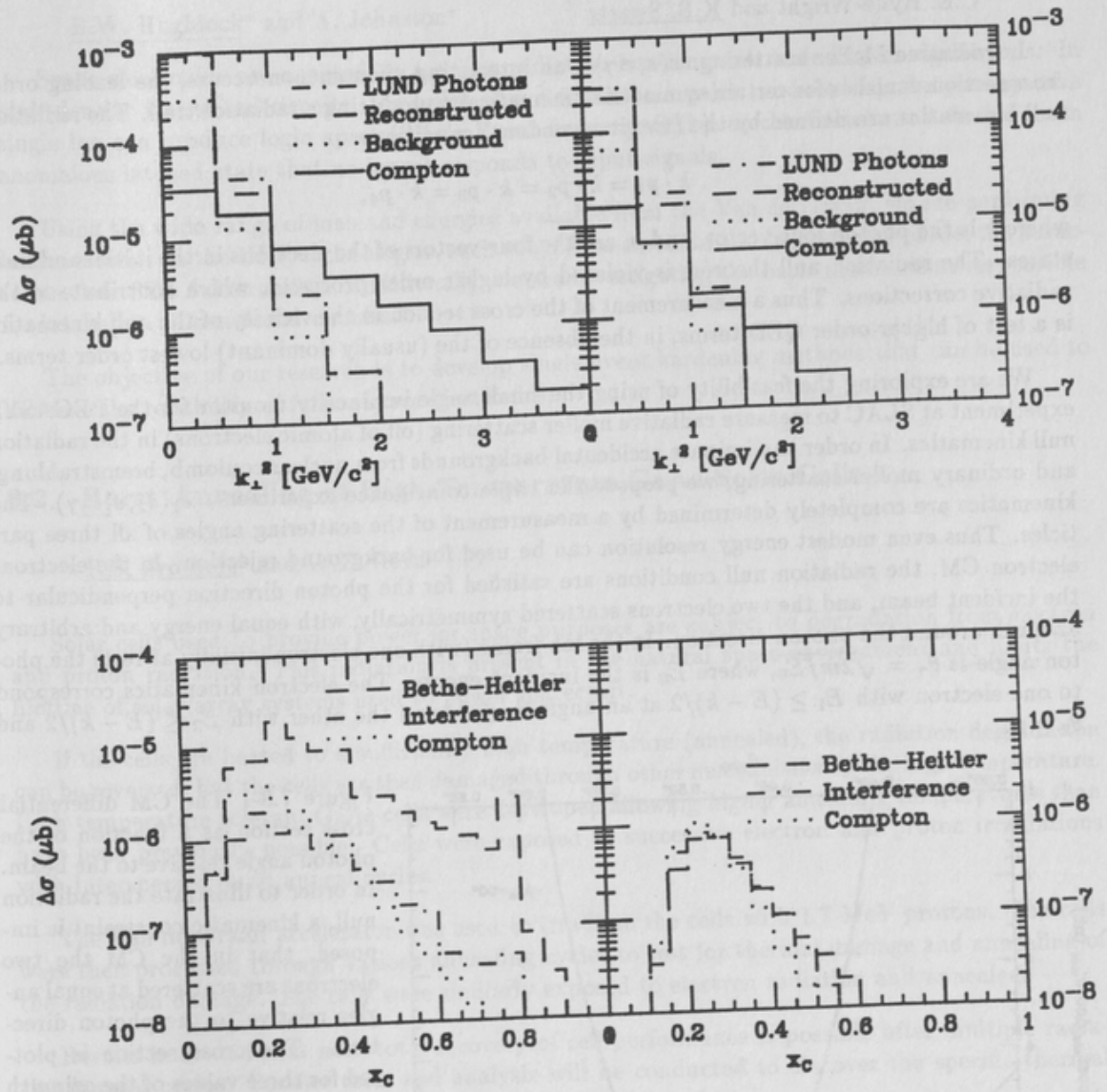

Figure 7.7-2. Integrated inclusive $p(e, e\prime\gamma)x$ Top: Background from hadron decays in μb. Bottom: Integrated $p(e, e\prime\gamma)x$ signal in μb for $k_\perp^2 \geq 1.0$ (Gev/c)^2.

7.8 Radiative Møller Scattering

C.E. Hyde-Wright and K.B. Swartz

In radiative Møller scattering: $e(e, e'\gamma)e$, an interesting phenomenon occurs, the leading order cross section vanishes for certain symmetric kinematics[1,2] producing a radiation null. The radiation null kinematics are defined by the (two independent) conditions:

$$k \cdot p_1 = k \cdot p_2 = k \cdot p_3 = k \cdot p_4,$$

where k is the photon four-vector, and p_i are the four-vectors of the electrons in the initial and final states. The radiation null theorem is violated by higher order processes, which contribute to the radiative corrections. Thus a measurement of the cross section in the vicinity of the null kinematics is a test of higher order QED terms, in the absence of the (usually dominant) lowest order terms.

We are exploring the feasibility of using the small angle luminosity monitor for the PEGASYS experiment at SLAC to measure radiative moller scattering (off of atomic electrons) in the radiation null kinematics. In order to eliminate accidental backgrounds from nuclear coulomb, bremstrahlung, and ordinary moller scattering, we propose the triple coincidence experiment: $e_1(e_2, e_1' e_2' \gamma)$. The kinematics are completely determined by a measurement of the scattering angles of all three particles. Thus even modest energy resolution can be used for background rejection. In the electron-electron CM, the radiation null conditions are satisfied for the photon direction perpendicular to the incident beam, and the two electrons scattered symmetrically, with equal energy and arbitrary azimuth around the photon direction. In the lab frame (with one electron initially at rest) the photon angle is $\theta_\gamma = \sqrt{2m/E_0}$, where E_0 is the incident energy. The electron kinematics correspond to one electron with $E_1 \geq (E-k)/2$ at an angle $\theta_1 \leq \theta_\gamma$ and the other with $E_2 \leq (E-k)/2$ and $\theta_2 \geq \theta_\gamma$.

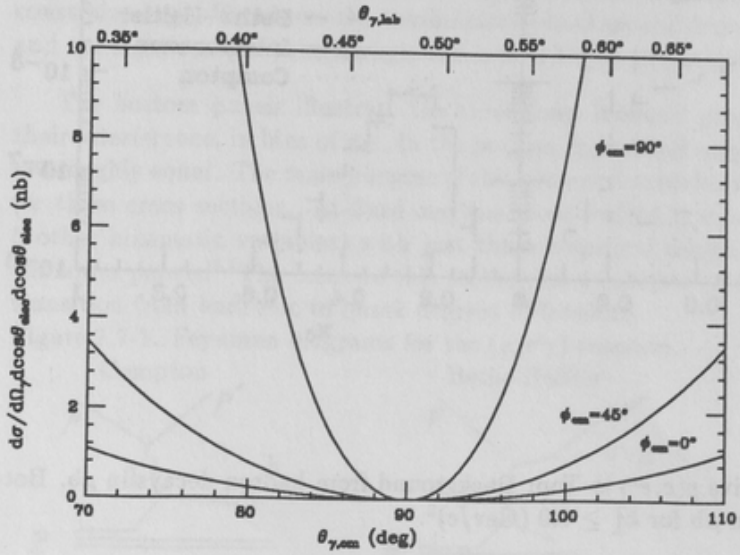

Figure 7.8-1 The CM differential cross section as a function of the photon angle relative to the beam. In order to illustrate the radiation null, a kinematic constraint is imposed, that in the CM the two electrons are scattered at equal angles relative to the photon direction. The cross section is plotted for three values of the azimuth of the electrons around the photon direction. For $\phi_{CM} = 0$, the entire event lies in a plane. For $\phi_{CM} = 90$, the two electrons are equal energy and equal angle relative to the beam, in the lab.

[1] Brodsky, S.J. and Brown, R.W. Phys Rev Lett. 49 (1982) 966.
[2] Brown *et al.* Phys Rev **D28**, 624 (1983).

8 EXTERNAL USERS

8.1 Single Event Phenomenology by Heavy Ions

B.W. Hughlock* and A. Johnston*

Space electronics are exposed to a severe radiation environment, including energetic ions. In high density integrated circuits, the track of a electron-hole pairs produced by the passage of a single ion can produce logic upset (Single Event Latchup, SEL), or can transform a device to an anomalous latched state that no longer responds to input signals.

Using the wide range of ions and energies available from the Van de Graaff, we are performing basic research on the III-V technologies, such as gallium-arsenide and indium-phosphide, to characterize their SEL vulnerability. Additionally, we are investigating the basic mechanisms responsible for latchup in silicon based circuits.

The objective of our research is to develop single event hardening methods that can be used to increase the reliability of future space electronics.

8.2 Burst Annealing of High Temperature GaAs Solar Cells

P.B. Brothers† and W.E. Horne†

Solar cells used to provide power for space purposes are subject to degradation from electron and proton radiation. This radiation is present in the natural space environment and limits the lifetime of solar array systems used to power spacecraft.

If the cells are heated to a sufficiently high temperature (annealed), the radiation degradation can be reversed, but the cells are then damaged through other mechanisms by the high temperature. High temperature tolerant GaAs cells were developed allowing higher annealing temperatures than have been previously possible. Cells were exposed to successive electron and proton irradiations with interspersed burst anneal cycles.

The Van de Graaff accelerator was used to irradiate the cells with 1.7 MeV protons. The cells were then processed through various annealing cycles to test for thermal damage and annealing of the radiation damage. The cells were similarly exposed to electron radiation and annealed.

Results indicated that near total recovery of cell performance is possible after multiple radiation/anneal cycles. Further tests and analysis will be conducted to discover the specific thermal damage mechanisms and the effects of many radiation/anneal cycles.

*Boeing Aerospace & Electronics, Seattle, WA 98124-2499.
†Boeing Defense & Space Group, Seattle, WA 98124-2499.

8.3 Lightweight Tandem Solar Cell Module Qualification Testing

P.A. Dillard* and L.T. Nirider*

The purpose of this testing program was to obtain test data which characterizes the electrical performance of each of a set of sub-cells in a tandem solar cell module over a range of environmental conditions likely to be encountered in space. A part of this testing program consisted of exposure of the tandem cells to particle radiation fluences equivalent to those accumulated in a typical space "lifetime" for the space mission.

The type of radiation of concern for space missions in the near-earth environment consists of energetic charged or massive neutral particles (i.e., electrons, protons, heavy ions, or neutrons). These particles interact with the solar cell materials in various ways including:

1. Elastic collisions with atomic nuclei.
2. Inelastic collisions with bound electrons.
3. Inelastic collisions with atomic nuclei.

All of these processes induce damage in the solar cell causing a degradation of electrical performance. The values of the relative damage constants for omnidirectional proton fluences on shielded solar cells allow a space proton environment to be reduced to an equivalent fluence of normally incident 10 MeV protons on unshielded solar cells.[1] Our experiments consisted of exposure of unshielded solar cells to normally incident 10 MeV protons to total fluences of from 1.0×10^{10} protons/cm^2 to 1.0×10^{12} protons/cm^2. The electrical characteristics of each of the test cells were carefully measured in a Xenon-arc solar simulator both prior to and immediately after exposure to the 10 MeV protons.

Measured levels of damage induced in the tandem cells as a result of these exposures agreed well with previously calculated models of damage coefficients. Development of the Tandem Solar Cell Module is continuing.

8.4 Stability of Fused Silica Under Proton Irradiation

W.G. Bartholet,* L.B. Fogdall,* L.D. Milliman,* L.T. Nirider,* D.A. Russell* and J.L. Wert*

Fused silica covers are useful for absorbing ionizing radiation that would otherwise damage spacecraft solar cells. It is among the most stable spacecraft materials for this application and transmits more than 90 percent of incident solar energy to the underlying cells. In these studies we sought data on the performance/stability of uncoated fused silica after irradiation by 1 MeV, 5 MeV, and 10 MeV protons to fluences as great as 1×10^{15} p/cm^2. Normal spectral transmittance was measured in air before and after irradiation. Between 250 and 2500 nm the measured changes were less than one percent both spectrally and weighted by the solar radiance spectrum, verifying the utility of fused silica for the intended purpose. In addition, there were no visually apparent changes such as tracking or dielectric breakdown due to testing at accelerated rates.

---

*Boeing Defense & Space Group, Seattle, WA 98124-2499.

[1] "Solar Cell Radiation Handbook", H.Y. Tada *et al.* National Aeronautics and Space Administration, Nov. 1982.

8.5 Isotope Wear Analysis for Turbopump Bearings

P.T. Coleman,* H.B. Knowles,* R.S. Nelson* and M.R. Randall*

Rocketdyne has been developing a wide variety of technologies to provide direct information about the health of critical rocket engine components. One of these technologies, Isotope Wear Analysis (IWA), can quantify component mass loss (caused by rubbing, eroding, ablating, dissolving, etc.) without engine disassembly: low levels of radioactive isotopes are generated within a limited area of the component by bombardment with a high-energy particle beam. Gamma emissions from the isotopes penetrate through the engine housing, where they can be measured using a scintillation detector. As the component degrades, some of the activated material is removed, proportional to the total amount of mass loss. The corresponding reduction in emissions received by the scintillation detector can be analyzed to determine the amount of degradation.

Monitoring the condition of the bearings in the Space Shuttle Main Engine liquid oxygen and liquid hydrogen turbopumps is of particular interest to Rocketdyne: tremendous forces are exerted on these bearings, as the pumps can generate more than 77,000 horsepower at speeds greater than 37,000 rpm. It is desirable to monitor adjacent bearings or different components on the same bearing (e.g. inner race vs. outer race). Therefore, methods to generate unique, long-lived, gamma-emitting isotopes are being explored.

It is not possible to change the bearing composition at this time, so unique isotopes or isotope combinations must be created in other ways. Bearing material samples were sent to the University of Washington for irradiation as the first step in experimentally determining radioisotope yield as a function of particle type of energy. The unique information obtained by analyzing the activated samples showed that it is possible to create several distinct isotope ratio "signatures", allowing degradation to be measured on adjacent bearings or bearing components.

*Rockwell International, Rocketdyne Division, Canoga Park, CA 91303.

9 INSTRUMENTATION

9.1 BGO Compton Suppressed Ge Detectors

D.J. Prindle and R. Vandenbosch

As part of an upgrade of our γ-ray detectors we are in the process of acquiring three Compton-suppressed, intrinsic Germanium detectors. These will complement the recently acquired BaF_2 detectors, which are discussed in section 9.4 of this report. The Ge detectors will be useful for measuring discrete γ lines ranging in energy from $\approx$ 100keV to $\approx$ 10MeV. In order to keep the Compton tail of higher energy γ-rays from swamping the lower energy γ lines the Ge detectors are surrounded by BGO Compton suppression shields.

The specifications of the Ge detectors are listed in Table 1. The material is intrinsic germanium. This means we will be able to repair neutron damage at our laboratory. Also, there is no evidence that temperature cycling of an intrinsic Ge detector causes a degradation of energy resolution.

The Compton suppression shields are made of BGO, allowing a compact construction. The Ge detectors will be about 7 inches from the target and we will be able to place three of them on one side of the beam in one plane. For maximum suppression of the low energy part of the Compton tail the Compton suppressor is asymmetric; there is BGO material directly behind the Ge. This means the Ge detector comes in from the side and presents a square face to the target. The design is very similar to the Compton suppressors of the Argonne-Notre Dame Ge array.

The three Ge detectors are on order. We expect delivery of the first two in April with the third to follow soon after. Two of the BGO suppressors are on order. Delivery of the first is expected in April, with the second to be delivered in May. All the necessary electronics have been ordered. This includes the signal processing electronics to determine energy of the Ge signal and Ge-BGO coincidence as well as electronics for a liquid nitrogen auto-fill system and a neutron damage repair system. The current support plan will place them on the BaF_2 table (or an extension of it). Construction of this table will begin soon and should be completed by summer. We will have to construct a smaller scattering chamber in order to place the Ge within 7 inches of the target. Plans for this chamber are at an early stage.

Table 9.1-1: Ge detector specifications.

Resolution	at 122 keV	$\leq 950eV$
	at 1.3 MeV	$\leq 2.2keV$
FWTM/FWHM*	at 122 keV	≤ 2.00
FWFM/FWHM*	at 1.3 MeV	≤ 3.00
Peak/Compton	for 1.3 MeV line	$\geq 60/1$
Efficiency	for 1.3 MeV line	$\geq$ 55% relative to 3" x 3" NaI
Timing	at 500 keV	$\leq$ $7ns$ FWHM*
		$\leq 20ns$ FWTM*
	at 150 keV	$\leq 12ns$ FWHM*

*FWHM = Full Width Half Max: FWTM = Full Width Tenth Max: FWFM = Full Width Fiftieth Max

9.2 Calibration of The Plastic Wall Phoswich Array

A.W. Charlop, C.E. Hyde-Wright, S. Kailas,* D.J. Prindle, K.B. Swartz and R. Vandenbosch

The Plastic Wall phoswich array was designed to measure energy and direction of light particles (p, d, t and α) over a large solid angle. The details of the array are given in last years annual report.[1] Briefly, a phoswich counter consists of a thin fast plastic acting as a δE counter in front of a thick slow plastic acting as an E counter. This article describes how the electronic signals are calibrated for particle identification and energy measurement.

For each counter we measure three things; the 'fast charge' during the prompt part of the signal, the 'slow charge' during a delayed part of the signal, and the Time Of Flight (TOF). Plotting fast versus slow it is easy to distinguish between $Z = 1$ and $Z = 2$ but difficult to separate the $Z = 1$ isotopes. The calibration serves two primary purposes; first it allows a separation of $Z = 1$ from $Z = 2$ using an algorithm as opposed to drawing banana gates. More importantly it allows a determination of the energy using the 'slow'.

The timing calibration is straight forward. Using a mylar target we trigger on 'elastic' protons; the energy, and hence TOF, is determined by angle. Selecting elastic protons with a gate in 'fast' versus 'slow', we plot $\mathrm{TDC_{measured}} - \mathrm{TOF}$ which is the TDC offset. The peak has a FWHM of $\approx 300ps$.

The charge calibration is a little more complicated. First of all there are the ADC pedestals and the contribution of the slow plastic to the prompt signal. We assume

$$\begin{aligned} \mathrm{Fast^{meas}} &= \mathrm{Fast} + \mathrm{Ped_{Fast}} + \mathrm{A} * \mathrm{Slow} \\ \mathrm{Slow^{meas}} &= \mathrm{Slow} + \mathrm{Ped_{Slow}} + \mathrm{B} * \mathrm{Fast} \end{aligned}$$

$\mathrm{Ped_{Fast}}$, $\mathrm{Ped_{Slow}}$ A, and B are determined by fitting straight lines to the edges of the 'fast' versus 'slow' plot. We expected to find B = 0; we find B small but nonzero.

For the energy calibration we start with Fast and Slow. Samples of protons and αs are obtained by banana gates on Fast versus Slow and the energy is derived from the TOF. The light output of plastic scintillator is not linear with the input energy, primarily because of a saturation at large $\frac{dE}{dx}$ which is described by Birks' formula;

$$\bar{\mathrm{C}}_{\mathrm{Slow}} = \mathrm{G_S} \int_0^{\mathrm{E_s}} \frac{\mathrm{dE}}{1 + \mathrm{S}\frac{\mathrm{dE}}{\mathrm{dx}}}.$$

$\mathrm{G_S}$ is related to the gain of the photo-tube and S describes the saturation at high dE/dx. The integration limits are the energies at which the particle entered and left the plastic. $\bar{\mathrm{C}}_{\mathrm{Fast}}$ is calculated in a similar way using the appropriate limits of integration and replacing $\mathrm{G_S}$ with $\mathrm{G_F}$. We determine $\mathrm{G_S}$, $\mathrm{G_F}$ and S by doing a simultaneous least squared fit to $\mathrm{Fast_p}$, $\mathrm{Slow_p}$, $\mathrm{Fast_\alpha}$ and $\mathrm{Slow_\alpha}$. We find $\mathrm{Slow_p}$, $\mathrm{Slow_\alpha}$ and $\mathrm{Fast_\alpha}$ are well described by Birks' formula.

Unfortunately $\mathrm{Fast_p}$ is poorly described by this parameterization, which is difficult to understand. Possibly the pedestals have been subtracted incorrectly. Until we understand better how to

*Present address: Bhabha Atomic Research Center, Bombay, India.

[1]See Nuclear Physics Laboratory Annual Report, University of Washington (1989) p. 50 for more details of the phoswich array.

describe Fast_p we can not use it to separate the $Z = 1$ isotopes. We can do a reasonable job by plotting $\text{TOF}_{\text{measured}} - \text{TOF(Slow)}$ where we assume all $Z = 1$ events are protons. We find peaks due to p, d and t that are separated by about 3σ.

9.3 A Beam Polarization Monitor

J.K. Eisenberg, C.A. Gossett and K.B. Swartz

The polarized ion source has produced polarized beam reliably, but to measure the beam polarization, to date, a separate scattering chamber has had to be setup and calibrated. A permanent setup to measure and monitor beam polarization is sorely needed. It would be more convenient because only a one time investment in calibrating and understanding the apparatus would be needed. Such a device has been designed and most parts of it have been built. It should be avaliable for use in a couple of months.

A polarimeter that could measure proton vector and deuteron vector and tensor polarization up to a energy of approximately 36 MeV is desirable. However as a quick first step a polarimeter that can measure only vector polarization in the limited energy range 3 to 10 MeV has been designed. It should be straightforward to upgrade it to measure a larger energy range and to include the possibility of measuring tensor polarization. The reactions that will be used to measure polarization are: proton or deuteron elastic scattering from ^{4}He for vector moments, and eventually ^{3}He(d,p)^{4}He for deuteron tensor moments.

The polarimeter is designed to be used on more than one beam line, since it is desirable that the beam polarization be measured as close to the experiment as possible. The polarimeter consists of a 12 inch diameter scattering chamber with all the components mounted on the lid. The lid is easily removable and replaceable by a blank when not in use. The convenience of the design is that to install the polarimeter on another beam line, only another chamber has to be built. The polarimeter has a gas target which will typically contain ^{4}He and, possibly in the future, ^{3}He. There are two telescopes consisting of delta E and E silicon surface barrier detectors each with an active area of 50mm^2. The angle of the telescopes can be varied from 20 to 65 degrees in steps of 5 degrees.

For the future the possibility of using a CsI crystal with a PIN diode as a higher energy proton detector is being investigated. Also possible would be adding more telescopes, so that all polarization moments can be measured. The size of the chamber is adequate so that detectors could be mounted out of plane. We look forward to using the polarimeter soon.

9.4 A Barium Fluoride Detector Array for High Energy γ-rays

Z.M. Drebi, S.J. Luke, D.J. Prindle, R. Vandenbosch and K.A.Snover

We are assembling a three-detector barium fluoride scintillator system to measure high energy gamma rays. Two detectors, one from Optovac and the other from Harshaw, have been purchased. Each detector consists of a single right circular cylindrical crystal, 14.5 cm in diameter and 17.5 cm long. Initially both crystals were polished with a mirror finish on all surfaces and wrapped in teflon reflecting material to optimize the pulse hight resolution. Each crystal is coupled to a 5-in Hamamatsu photomultiplier tube model R1251. Each crystal is surrounded by a one-inch thick anti-coincidence plastic scintillator shield. Three 2-inch photomultiplier tubes (Hamamatsu model R329) are coupled to each plastic shield, two on the annulus and one on the front disk.

The optical transmission of the BaF_2 crystals is described in Section 9.5. In spite of the fact that the measured transmissions are poorer than originally specified, our design goal of 10:1 was achieved for the fast/slow pulse amplitude ratio.

We measured the energy resolution of each uncollimated detector for gamma rays at 0.511, 1.275, 0.661, and 6.1 MeV from ^{22}Na,^{137}Cs, and Pu^{13}C sources. The resolution varies from 15% at 662 kev to 5.5% at 6.1 MeV for the Optovac detector, consistent with a dominant contribution from photon statistics. A slightly worse resolution was found for the Harshaw detector. A worsening of resolution was found for a collimated source located off the central axis and along the side of the crystal. In-beam tests using ^{15}N(p,γ) and ^{11}B(p,γ) show resolutions of roughly 8–10% for E_γ = 17–21 MeV.

The time resolution was deduced by measuring γ-γ coincidence using the two BaF_2 detectors and ^{22}Na and ^{60}Co sources. For 1.17–1.33 MeV coincidences, the measured time resolution was 0.84ns FWHM indicating an intrinsic resolution, per detector, of 0.6ns. This was found to vary as $1/\sqrt{E}$ over the energy range 0.5–1.3 MeV.

Operating the plastic shield in anti-coincidence we measured cosmic ray rejection efficiencies over a wide range of energies and with different amounts of lead shield on top and around the detectors. We conducted the measurements in two locations, inside Cave-2 and in the detector lab room. We found that the cosmic ray rejection efficiency outside Cave-2 is around 60% at 10–20 MeV and increases to around 95% as we put 6" of lead shield on top of the detector. These efficiencies increase exponentially with increasing cosmic ray energy. Measurements inside Cave-2 reproduce these results if we assume an effective shielding due to roofing cover equivalent to 2" of lead.

Currently 2 different active base designs are being pursued in order to achieve good gain stability as a function of counting rate.

9.5 Transmission of Ultra-Violet Light Through Large BaF_2 Crystals

E. Abramson,* D. Imre,* S.J. Luke, K.A. Snover and R.P. Swift*

In a previous article,[1] the acquisition of several large BaF_2 scintillator detectors was described. When we received these detectors we were faced with the dilemma of trying to determine the acceptability of these detectors for our purposes. One of the basic questions which concerned us was the transmission of light at the wavelengths of the crystals scintillation. This problem was complicated by two facts. The first was the size of the crystal; since the detectors are rather large (14.5 cm × 17 cm), normal spectrometers were out of the question. Second, BaF_2 scintillates in the ultra-violet, so finding a uv source is not trivial.

We used a molecular spectroscopy laser system to measure the transmission of ultra-violet light in the BaF_2 crystal. The system consisted of a Quanta Ray, DCR Nd:YAG solid state laser which pumped a Lambda Physik FL-2002 Dye Laser. We took the third harmonic of the YAG, 355 nm, to pump the dye laser. The blue output of the dye laser was then doubled in a Lambda Physik BBO frequency doubling crystal. This enables one to get ultra-violet light. The frequency of the light depends upon the dye which is in the FL-2002. BaF_2 scintillates at 210 and 320 nm, we used Coumarin 440 (in methanol) and DCM (end-pumped, in methanol) for the two wavelengths respectively.

We measured the transmission of light at both wavelengths for the crystal obtained from Optovac, Inc. We were able to do a systematic study of the transmission of light as a function of the radial distance from the center, we found that there was a very little difference in the amount of transmission in the center as opposed to the outer regions of the crystal. We did notice that at some parts of the crystal the transmission would go to zero, this was due to inclusions in the crystal itself; but we also discovered that these inclusions did not effect the overall performance of the crystal.[2] The results of our measurement are in the table below. Our 90% result for 330 – 350 nm passes our spec[2] of 83%. However, our results for the two shorter wavelength intervals, referenced to the 330 – 350 transmission, of 0.81 and 0.39, fail to meet our specs[3] of 0.89 and 0.71, respectively.

Wavelength(nm)	*Measured Transmission*	*Ratio to* $\lambda = 330 - 350$	*Spec*
330 – 350	90%		$10^{-.08} = 83\%$
220 – 350	73%	73/90 = 0.81	$10^{-.05} = 89\%$
200 – 220	35%	35/90 = 0.39	$10^{-.15} = 71\%$

*University of Washington, Department of Chemistry.

[1] Section 9.4 of this report.

[2] PO 258881, Section 2.1.

[3] PO 258881, Section 2.2.

9.6 Calibration of LEAR PPACs

T.A. Trainor

In last year's annual report,[1] I described successful installation of an X-Y PPAC beam profile monitor at LEAR as part of the antiproton mass measurement program (Sec. 5.5). This is a double PPAC system. The anode of each PPAC is divided into five 2.5mm wide strips. In slow extraction mode (for diagnostics, $10^5\bar{p}$/sec) the PPACs are operated at high gain (360 V/Torr-cm) and pulses from individual particles drive ten rate meters which provide a 2-D beam profile or provide start signals for a time-of-flight system to measure the $\bar{p}$ energy spectrum. In fast extraction mode (for trapping, $10^8\bar{p}$ in 200nsec.) the PPACs are operated in ion chamber mode (50V/Torr-cm) and the current due to the very high $\bar{p}$ rate is detected.

In ion chamber mode the current signal from any one of the anode segments provides an excellent time record of the pulse from the LEAR ring. Fig. 9.6-1 shows such a time record in which stored $\bar{p}$ in the ring have been cooled, then bunched into four bunches. One of these bunches is then ejected on demand into the PS 196 (mass measurement) beam line. The PPAC system has a rise time less than 5ns even at these lower fields. Fig. 9.6-1 accurately displays the time structure and relative magnitude of a LEAR pulse. This represents the first such information available to LEAR control personnel on an external beam line.

With the reliability of this diagnostic established, the LEAR operators were able to determine that this extraction process was inefficient and time wasting. Bunch forming heats the beam stored in LEAR so that after a single fast extraction pulse is delivered the stored beam must be debunched and cooled. Also the fast extraction pulse from a bunched beam has a larger transverse emittance and so transmission to a target is reduced. LEAR operators were able to show using the PPAC system that simple rapid deflection of the continuous stored beam with a fast kicker magnet (magnetic beam chopper) was better able to deliver a clean, lower emittance pulse to the experimental area. Such a pulse is shown in Fig. 9.6-2. The small peaks on leading and trailing edges are characteristic of a kicker system tuned for optimum transmission and risetime.

Another attractive feature of the PPACs operated in ion chamber mode was the possibility of absolute calibration of the device for the total number of $\bar{p}$. In 1.25mm of 20 Torr isobutane a 5.9 MeV $\bar{p}$ produces about 80e of charge. Calibration experiments with protons and alpha particles in avalanche mode indicated (by an asymmetry in the relationship of signal height to direction of travel of the particle through the counter) that particles enter the counter gas "dressed" with an equilibrium population of delta electrons characteristic of the window material. In the present case this amounts to an additional 6e deposited in the gas. The mean charge deposited per $\bar{p}$ was taken as 87e$\pm$5e.

The current pulse in ion chamber mode has two components. The fast component, due to electron motion, accurately follows any variation of the $\bar{p}$ flux on a time scale longer than 5ns. The slow component, due to positive ion motion ($\sim$1000 times slower) represents an integral of the $\bar{p}$ flux (an upgoing ramp on which the fast component is superposed) followed by a linear fall as the positive ion track moves across the detector gap and is collected by the cathode. These features are evident in Figs. 9.6-1 and 9.6-2.

[1]Nuclear Physics Laboratory Annual Report, University of Washington, p. 54 (1989).

If the entire pulse is integrated ($\sim 1\mu S$) then 1 x $10^6 \bar{p}$ produce 14 pC of charge. Since LEAR pulses typically contain $10^8 \bar{p}$ the detector output typically must be attenuated to provide charge magnitudes compatible with an ADC.

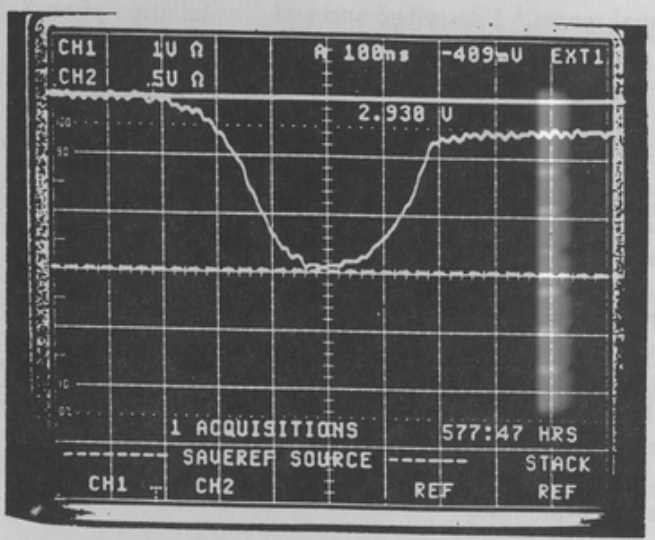

Fig. 9.6-1 PPAC current pulse with $\bar{p}$ pulse prebunched in LEAR. 100ns/div.

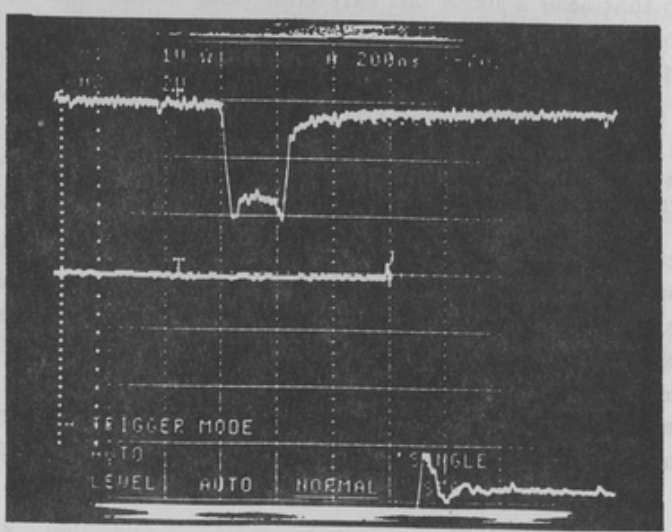

Fig. 9.6-2 PPAC current pulse with $\bar{p}$ pulse produced by fast kicker magnet only. 200ns/div.

9.7 Electron Track Properties in Methane

C.E. Hyde-Wright, T.A. Trainor and S.P. Van Verst

Pursuant to the design of a TPC for study of e^+/e^- pairs in heavy ion collisions we are investigating electron track properties in methane gas. The purpose was to determine whether sufficient position and momentum resolution and data rate could be achieved to provide useful information about the e^+/e^- production mechanism. Our results[1] indicate that methane gas at 150 Torr provides an environment in which electron drift speed, diffusion, and multiple scattering meet the criteria to make the TPC feasible.

In our study of the multiple scattering we discovered an effect, known locally as the chipmunk effect, which is associated with the statistics of the ionization process of minimum ionizing electrons in gas. This effect is discussed here.

A beta spectrometer[2] provided a source of 500 keV electrons which passed across the drift volume of our prototype wire chamber. The e^- tracks were oriented horizontal and perpendicular to the anode wires which are separated by 1 cm. The primary electron generates a start signal in a TDC when it enters a scintillator which acts as an event trigger. The ionization electrons generated by the beta track drift down into the wire plane where they avalanche on an anode wire. This signal generates a stop in the TDC, where the TDC output represents the drift time of the ionization electrons in the gas.

A plot of the correlation between the TDC spectra of two adjacent anode wires is shown in Fig. 9.7-1. Since the tracks are horizontal, the correlation should lie on a 45 degree slope with major axis passing through the origin. Due to multiple scattering, the ionization electron arrival times may be different for the two anode wires, resulting in a slight deviation from the 45 degree slope. Projections of the data onto the T1 and T2 axes provide information on multiple scattering since the widths of the TDC spectra are proportional to deviations of the electron tracks from the horizontal due to multiple scattering.

The width of the correlation figure along an axis oriented parallel to the line $y=-x$ is proportional to the width of the ionization track resulting from the kinematics of the collisions between the primary electron and atomic electrons in the gas. Since these particles have the same mass, it is possible for the primaries to impart a large fraction of their total energy to some secondary electrons. These electrons, known as delta electrons, can then travel some distance in the gas (a few mm) before they are stopped, resulting in a finite width of the ionization track.

The diagonal stripes in the data shown in Fig. 9.7-1 are known as the chipmunk effect and come about from the ionization statistics of electrons in the gas. On average, the 500 keV e^-'s generate about 10 ion pairs/cm. Consider a 1 cm range where 15 ion pairs are generated above anode wire #1. Over wire #2 it is possible that perhaps only 1 or 2 ion pairs are generated. Wire 1 will avalanche and generate a channel number in the output of the TDC (T1). Due to the small number of ionization e^-'s drifting onto wire 2, the signal on wire 2 will be dominated by the ringing due to capacitive coupling with wire 1. An oscilloscope trace depicting this type of event is shown in Fig. 9.7-2. The particular oscillation in the ringing which fires the lower level discriminator of

[1] Nuclear Physics Laboratory Annual Report, University of Washington p. 51 (1989).
[2] *Ibid.*, p. 55.

wire 2 is what determines the channel number of the TDC output for wire 2 (T2). The discreet spacing of the oscillations causes the discreet, or striped, spacing in the correlation spectra.

This process could be reversed of course between wires 1 and 2 resulting in a stripe pattern symmetric about the major axis of the correlation figure. The fraction of events in the stripe pattern resulting from "false" coincidences depends on the amount of coupling between wires and the quality of impedance matching into the wire preamps. In the present case the fraction of bad events was not high enough to prevent proper measurement of track properties.

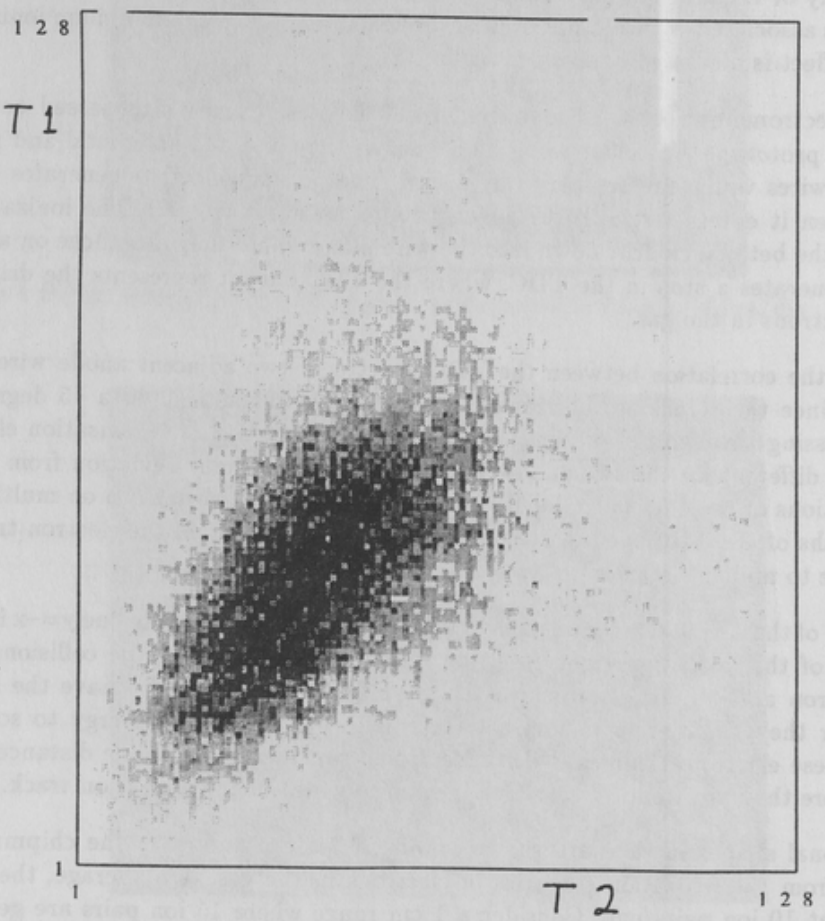

Figure 9.7-1. TDC correlation spectra for two adjacent anode wires generated from β tracks.

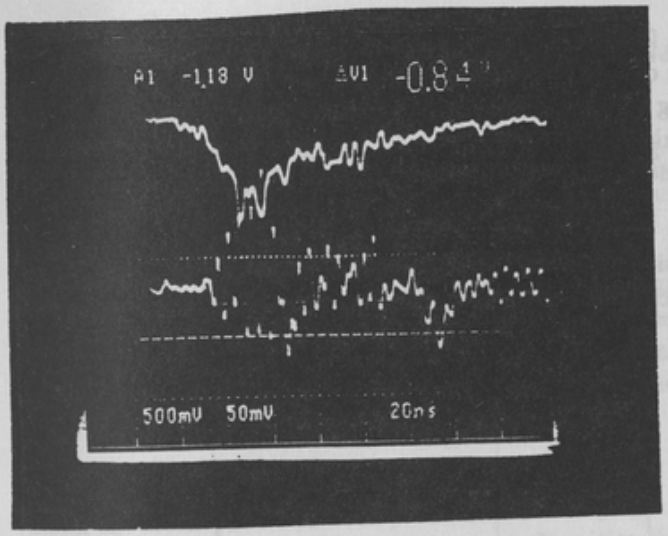

Figure 9.7-2. Oscilloscope trace for anode wire 1 (top) and anode wire 2 (bottom). The signal on wire 2 is ringing (note different voltage scales) due to capacitive coupling with wire 1.

9.8 TPC Design Studies

C.E. Hyde-Wright, T.A. Trainor and S.P. Van Verst

We are developing a Time Projection Chamber[1] (TPC) to investigate the anomalous narrow peaks observed in positron and electron energy spectra in heavy ion collisions at GSI.[2] The TPC has the capability to reconstruct the tracks of leptons produced in the collision, which will test the hypothesis that the e^+/e^- pair results from the two body decay of a previously undetected neutral particle.

A prototype 2-D wire chamber was developed[3] to study electron drift speeds, diffusion, and multiple scattering for the specific conditions of the TPC design.

Recently, the wire chamber was modified to consist of position sensitive anode wires. The anode wires are 20 micron nickel alloy with a resistance of 40 Ω/cm. The signal generated from an electron avalanche is read out on both ends of the anode and input to a charge sensitive ADC which integrates the signals for a time period determined by an external gate. Due to the resistance, the anode acts as a charge divider so that the ratio of the signals from the ends of the wire is proportional to the position of the avalanche on the wire. The position of the hit along the anode is then the ADC channel number from the right side of the wire divided by the sum of the ADC channel numbers from the left and right sides of the wire. This ratio, which lies between 0 and 1, is multiplied by 1024 to generate a position histogram for each wire.

To test this system, an α source was collimated to generate tracks perpendicular to the anode wires. The position spectra for three of the wires are shown in Fig. 9.8-1. The centroids of the peaks occur at the same channel number for all three wires, indicating that the tracks are straight lines oriented perpendicular to the anodes, as expected. The widths of the peaks are due to the finite geometry of the system, determined from the opening of the collimator slits. A resolution of 500 microns was obtained with this setup.

[1] Nuclear Physics Laboratory Annual Report, University of Washington (1989) p. 52.
[2] T. Cowan *et al.*, Phys. Rev. Lett. 56 44 (1986).
[3] Nuclear Physics Laboratory Annual Report, University of Washington (1989) p. 53.

Fig. 9.8-2 shows the position spectra for one anode wire generated with a 500 keV β source. The contribution to the width of the peak due to finite geometry is subtracted out, leaving a width of about 3 mm due to multiple scattering in the horizontal plane. This result is consistent with Moliére's theory of multiple scattering, which predicts a 3.5 mm displacement after 10 cm of travel, and with our single-wire timing measurements which determine multiple scattering in the vertical plane.

We have shown that the position sensitive anode wire is a feasible alternative to determining x-y electron track information for the specific conditions of our proposed TPC.

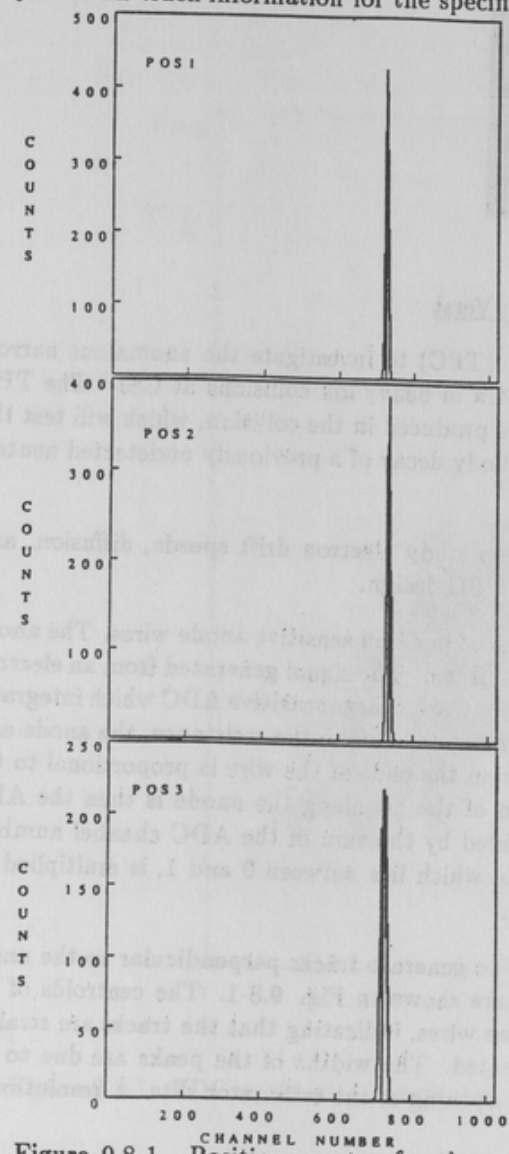

Figure 9.8-1. Position spectra for three adjacent anode wires generated from α tracks. The width of the peaks reflects the finite geometry of the system.

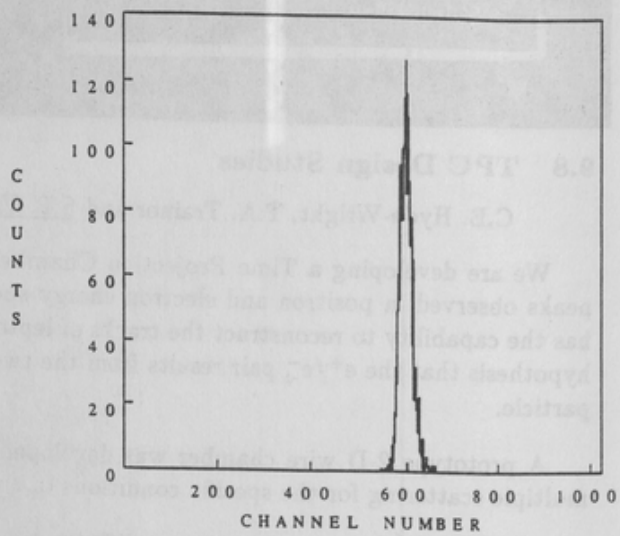

Figure 9.8-2. Position spectra for one anode wire generated from β tracks. The peak width is due to finite geometry plus multiple scattering of the β particle.

9.9 Electron Trajectories in the APEX solenoid

T.A. Trainor

In order to produce alignment criteria for the APEX apparatus, I have considered the consequences of magnetic field nonuniformities and misalignments of the solenoid, target and electron detectors on determination of kinematic quantities.

Ideally, a point source of electrons at the target propagates to line images at the silicon detector arrays. Electrons propagate on helices whose radius and pitch depend on the electron E and θ. Determination of ϕ depends on the azimuthal position of the hit detector segment on the array. E is measured directly by a segment, and θ depends on measurement of E, time of flight and the axial position of the hit segment.

Magnetic field inhomogeneities produce variations in helix radius and guiding center position along the solenoid. To some approximation axially symmetric inhomogeneities produce broadening of the line images while asymmetric nonuniformities shift the images.

Shifts and broadening have three effects. There is loss of total yield if some trajectories fail to hit the detectors, the angle ϕ is incorrectly inferred, and an anisotropy in the electron yield may be incorrectly inferred.

For a perfect solenoid the B field is uniform in magnitude and parallel to the system axis at all points sampled by electron trajectories. Field curvature produces shifts in line images with respect to the target and detectors. For example, suppose a field line radius of curvature of 200 m. Then the line images are displaced by 5mm. This displacement would not reduce the total detection efficiency (this occurs for displacements over 7mm) but would produce an apparent yield anisotropy in ϕ of $\pm 35\%$! To reduce this anisotropy to the statistical level the radius of curvature of the field should be greater than 1km. This is quite feasible with reasonable mechanical positioning of solenoid coils.

Gradient drift of helix guiding centers is produced by transverse gradients in the axial field. The drift is in the opposite sense for electrons and positrons. A gradient of 100mG/cm produces a shift of the line images by N·1mm, where N is the number of turns in a helix (up to 8 for APEX). Again, to keep systematic anisotropies at the statistical level transverse gradients need to be less than 10mG/cm.

Axial gradients produce effects which depend on the apparent time structure of the field variation as seen by the moving electron in relation to the cyclotron frequency. The axial gradients produce both shifts and spreading of the line image, with spreading expected to dominate. A field variation within a 1G range is achievable and will produce no significant systematics.

As a result of this analysis, a reasonable set of mechanical alignment specifications for the field coils and vacuum vessel have been generated. the critical alignment of the silicon detectors with respect to the effective line images would seem to be best accomplished by using a rotating β source positioned at the target beam spot and shifting the detectors in position and angle to minimize apparent ϕ asymmetries.

9.10 APEX Silicon Detector Shroud and Cooling

T.A. Trainor

The two silicon detector arrays for the APEX experiment (Sec. 5.7) each consist of 216 detector segments on a hexagonal array 36cm long and about 3cm in diameter. These arrays need to be cooled to near liquid nitrogen temperature to optimize the energy and time resolutions of the detectors. A system must therefore be provided that cools the detectors and protects them from cryosorbing gases onto the detector surfaces.

We have developed a thin shroud made of 7.6μm kapton to solve this problem. The shroud can withstand pressures up to 400 torr. This permits us to use gas cooling which eliminates the need for a massive cold finger and thereby reduces the absorption of positron annihilation γ-rays, provides uniform cooling and shortens the cooling cycle.

The shroud is manufactured by wrapping the 7.6μm kapton around a split lucite rod. One edge of the kapton sheet is picked up onto the rod by a stripe of rubber cement adjacent to the split. The other edge of the kapton is controlled by a piece of 6mm width square stock to which double sided tape is applied on one surface.

The seam is formed using Armstrong A-12 epoxy. The epoxy is applied to the kapton along the edge attached to the rod. A precise amount is applied using bond paper. Two strips of bond paper 125μm thick are fixed side by side to the kapton by rubber cement with a 500μm gap between. Epoxy is applied to this form and excess scraped off even with the paper surface. The paper is then removed leaving a precise bead of epoxy 1.5mm from the kapton edge. The other edge of the kapton is then drawn down over the epoxy bead and the square stock used to compress the seam against the split rod. This technique produces uniform seams 2.5mm wide and 50μm thick. The seams are quite flexible. When the epoxy is cured one half of the split ring is removed and the kapton tube is released from the rubber cement on the other half with a smaller plastic rod.

A lucite cap and lucite flange are epoxied to the tube ends using an alignment jig. For a 3.56cm diameter tube failure occurs consistently at 0.55 atm. The failure point is at the tube center on the side opposite the seam (the weakest point). The failure pressure is exactly that corresponding to the tensile strength of this kapton: 20k psi.

This technique can also be used with somewhat thicker foils to form self supporting gas cells for nuclear physics experiments. The resulting gas cell has no post to block scattered particles.

The gas cooling system will use recirculated N_2 gas which passes through a LN_2 heat exchanger and heater in a closed cycle system providing temperature and pressure regulation.

9.11 Electronic Equipment

R. Barry, J.M. LaCroix, R.E. Stowell and T.D. Van Wechel

Due to personnel reductions in the electronics shop, a larger portion of the shops time was spent on maintenance and repair of existing equipment and less on design of new equipment this year.

The design that was started last year[1] on a new upcharge control system for the tandem belt was completed. The controller has been built and installed on the tandem. (See Sect. 10.7.)

Some additional projects that were undertaken included:

a. Construction of a dual 2kV 5 mA regulated power supply to update the older neutron monitors in the cave areas.

b. Two additional regulated constant current 5 amp computer controlled bipolar power supplies were built for additional steering magnets used on the Linac.

c. A universal laboratory power supply was designed and constructed that will operate in either the constant voltage or constant current mode over a 0 to 30 voltage range at a current of 0 to 6 amps.

d. New printed circuit boards were made and installed in the 60 inch chamber readout chassis to correct a long standing intermittent problem in the arm angle readouts.

e. Several under/over voltage glitch detectors were designed and built for fault detection on the Linac refrigerator compressors and some systems on the polarized ion source.

f. A NIM packaged two quadrant analog divider circuit was designed and constructed.

g. A very low frequency (100 Hz) beam chopper with variable duty cycle was designed and constructed for the AMS group.

h. A general purpose NIM packaged 12 channel fast pulse transformer coupled isolation/inverter module was constructed.

i. A protective over-power circuit with automatic shutdown was designed and built for the Linac low energy buncher.

j. Two NIM modular universal logic boxes were designed and constructed to perform the logical AND, NAND, OR, NOR functions. One was a four input two output device, the other was a four channel two input, two output device.

Commercial electronic NIM/CAMAC modules purchased this year included: 1 Phillips 706 16 channel discriminator; 2 Phillips 776 16 channel preamps; 3 Ortec 427A delay amps; 2 Ortec 473A constant fraction disc.; 2 Ortec 551 timing SCA's; 2 Ortec 579 fast filter amps; 1 Ortec 566 TAC; 1 Piel 112 pulse-shape discriminator; 1 LeCroy 2249SG 12 channel ADC; 1 Phillips 7186 16 channel TDC; and 4 Ortec 4001C/402D power bins.

[1]Nuclear Physics Laboratory Annual Report, University of Washington (1989) p. 57.

10 ACCELERATORS AND ION SOURCES

10.1 Van de Graaff Accelerator Operations and Development

C.E. Linder and W.G. Weitkamp

During the 10.5 months from April 16, 1989 to February 28, 1990 the tandem operated 3597 hours. Additional statistics of accelerator operations are given in Table 10.1-1. Among the improvements made to the tandem were the charging system improvements described in Sections 10.7 and 10.8 and the generating voltmeter improvements described in Section 10.10.

We have been conducting tests on a suitable replacement for our 15 year old column resistors, as described in our last year's Annual Report.[2] We prepared test resistor assemblies containing 2, 3 or 4 resistors in a PVC tube similar to our previous design.[3] The resistors were either Kobra[4] or ROX[5] resistors with values selected to give 400 MΩ for each assembly. The test resistor assemblies have now been in the machine for more than 9 months. There have been no failures, the resistance values have typically decreased about 5% and the dispersion of resistance values has typically stayed under about 1.5%. This is satisfactory performance. These results show that these two types of resistors are superior in this configuration to the commonly used Caddock MG815 resistor, which was tested earlier. The first of MG815 failed after 3 months and the remaining resistors changed an average of 40% in value after 4 months. In the near future we will select the best resistor configuration, basing our decision on both performance and ease of installation, and begin manufacturing a complete set of new resistors for the tandem. We expect parts for these resistor assemblies to cost less than $50 each.

As part of the project described in Sec. 10.7 and 10.8 to improve the operation of the charging system, we have rebuilt the chassis which houses all the controls and diagnostics for the charging system. Among the features of this new panel are:

- Circuit breakers which were formerly hidden behind the panel are now out in plain view on the front of the panel.
- Three side-by-side edge meters read the high and low energy column currents and the down charge current. This has been very helpful in diagnosing belt charging problems.
- BNC connectors are located near each of the meters displaying currents so that the respective currents can be readily examined with a chart recorder or an oscilloscope.
- The high energy vacuum gauge, to which the charging system is interlocked, is displayed.
- Digital current meters display the current on each leg of the drive motor circuit.
- Lights indicate the status of the 4 interlocks which must be satisfied to run the belt drive motor and the 2 interlocks which must be satisfied to before charge can be applied to the belt.

[2] Nuclear Physics Laboratory Annual Report, University of Washington (1989) p. 39.
[3] *Ibid.*, (1975) p. 5.
[4] K&M Electronics, West Springfield MA 01089.
[5] Dale Electronics, Columbus NE 68601.

Table 10.1-1
Tandem Accelerator Operations
April 16, 1989 to February 28, 1990

Activity	*Days Scheduled*	*Percent*
A. Nuclear Physics Research, Tandem Alone		
Light Ions	49	15
Polarized Ions	18	6
Heavy Ions	15	5
Accelerator Mass Spectrometry	30	9
Subtotal	112	35
B. Nuclear Physics Research, Booster and Tandem Coupled		
Light Ions	3	1
Polarized Ions	6	2
Heavy Ions	35	11
Subtotal	44	14
B. Outside Users		
Rocketdyne Corporation	1	<1
University of Washington Division of Nuclear Medicine	1	<1
Boeing Corporation	12	4
Subtotal	14	4
C. Other Operations		
Tandem Development	26	8
Tandem Maintenance	63	20
Booster Development	13	4
Unscheduled Time	47	15
Subtotal	149	47
Total	319	100

10.2 Booster Operations

J.F. Amsbaugh, D.T.Corcoran, G.C. Harper, M.A. Howe, D.W. Storm and D.I. Will

During the last year the booster was scheduled for 16 different experimental runs. The total time scheduled and run was 52 days. The *new* beams provided are listed along with the corresponding maximum energy and maximum energy per nucleon. See last year's report[1] for other beams, many of which were repeated this year. Asterisks indicate maximum energies which met the experimenter's requirements without requiring the full linac.

^{1}H	^{2}H	^{3}He	^{6}Li	^{7}Li	^{9}Be	^{14}N	
28*	36	27*	87*	91	53*	109*	MeV
28*	18	9*	14.5*	13	5.9*	7.8*	MeV/AMU

We continue to learn how to tune the linac faster, and the graduate students are becoming competent operators. Improvements in the control computer program which facilitate tuning are described in section 10.4. There has been little unscheduled downtime. The rf controllers are now all working well. We have an occasional amplifier failure, which is readily corrected by replacement and subsequent repair in our electronic shop. The cryogenic system is reliable.

During the year two more couplers stuck in positions where they do not function. At the beginning of the year there was one such stuck coupler. Consequently we scheduled a six week period during which all the cryostats with problem couplers were serviced and then restored to operational status. However, as we finish the year a different coupler has stuck.

We still have difficulties with two resonators multipacting, in spite of warming, baking, and reconditioning them. The next step will be to re-plate these resonators. We still operate the low-β resonators at an average field of 2.8 MV/m and the high-β ones at an average of 2.4 MV/m. Tests of plating techniques (see section 10.4) have not been particularly successful, even when attempting to repeat our standard technique. We have refrained from re-plating resonators used in the linac until we obtain reproducibly successful results in tests.

We have been able to improve the transmission through the linac. It appears that at least part of the problem had to do with bunching. The time structure monitor has been improved (see section 10.7) so that the background has been substantially reduced. This permits us to adjust the low energy buncher to obtain a narrow bunch with a minimum beam outside the bunch. Previously we had too much beam outside the bunch; such beam is not accelerated properly and does not survive the first 90° bend after the low-β section of the linac. Additional improvement in transmission results from better alignment of the low-β section. Finally, we installed two more vertical steering magnets. Now we are able to obtain over 50% transmission from the linac entrance to the middle of the 180° bend. This loss includes the loss of the beam outside the bunch. The transmission from that point to the linac exit (before the final 90° bend) is nearly 100%, and we have achieved 83% transmission around the final 90° bend.

We have not yet had to shut down the linac due to a mechanical failure in the cryogenic system. Nor have we had to cancel or terminate a run due to any linac failure. But our three RS compressors now have between 23 and 32 thousand operating hours. The normal lifetime is expected to be about 30 thousand hours.

[1]Nuclear Physics Laboratory Annual Report, University of Washington (1989) p 62.

We are pursuing the resonator plating issues, and as soon as we are confident that we can successfully re-plate them we will remove the worst resonators from the linac and re-plate them. This should improve our average fields.

10.3 Cryogenic Operations

D.I. Will and J.A. Wootress

The booster linac is cooled by liquid helium which is thermally shielded by liquid nitrogen. In 1989 liquid nitrogen consumption increased 5% to 210,000 gallons.[1] The helium is purchased as high purity bulk gas and liquified by our helium refrigerator. Usage of 147,000 SCF in 1989 was 65,000 SCF more than that in 1988 due to an increase in the frequency of purging contaminants from charcoal beds. In past years we have managed to limit complete coldbox warmups to semiannual events, each of less than 24 hours (from cessation of liquid helium production to reestablishment of liquid helium production) by purging beds at least weekly. During such short warmups, all our cryostats remain below 40° K. In October, 1989, we were forced to warmup and purge the refrigerator and the dewar together for the first time since we began regular helium refrigeration of our booster in August, 1985. This event lasted some 50 hours, and all resonators reached 70° K. Of our thirty six resonators, five required multipactor conditioning for less than a day and one needed conditioning for three days. The following table summarizes our routine maintenance for 1989:

Item	Use	Major Services	Times Performed
Refrigerator			
Cold Box	98%	warm/derime	2
Top Expander	~4800 Hrs	warm/derime	15
	~120 RPM	main seals	2
		wristpin bearings/pins	2
		crankpin bearings	2
		valve seals	2
		flywheel bearings	1
Middle Expander	~7000 Hrs	warm/derime	4
	~130 RPM	main seals	2
		wristpin bearings/pins	1
		crankpin bearings	2
		valve seals	1
		flywheel bearings	2
Wet Expander	~2800 Hrs	warm/derime	8
	~50 RPM	main seals	2
Screw Compressors			
RS 1	8700 Hrs	replace charcoal	1
RS 2	7300 Hrs	none	
RS 3	2600 Hrs	none	
Distribution System		warm/derime	4

[1]Nuclear Physics Laboratory Annual Report, University of Washington (1989) p. 68.

10.4 Resonator Plating and Testing

J.F. Amsbaugh, M.R. Bryce, D.T. Corcoran, G.C. Harper and D.W. Storm

During the past year we began to explore different lead-plating techniques in order to see if we can achieve better performance from the resonators. Successful results have been reported[1] for thin layers of lead plated with no polishing. During the construction of the booster, we used an older technique[2] which involved plating approximately 10 μmeters of lead and then removing more than half of it with a chemical polish. Various rinsing and stabilizing procedures have been applied to the lead plated surfaces at different laboratories. Again, we had been using the older technique, which involved rinsing with EDTA solutions, amonium hydroxide solution, and finishing with an acetone rinse to dry the lead.

During the past year, we performed 5 different platings which produced lead surfaces of satisfactory appearance. These included both thin plating and our older technique, and involved two different low-β resonator bodies. Each of these was subjected to a series of rf tests. In the first 4 cases, the performance was unsatisfactory because the Q factor fell rapidly with field. Although the low field Q factors varied from 1.2×10^8 to 4.9×10^8 (which is among the highest we have ever obtained), by the time the average accelerating field was raised to 2 MV/m, the Q factors had fallen to 0.3×10^8 to 1.1×10^8. In the best of these cases we were able to achieve 3 MV/m with power of 9 Watts. In previous tests we had achieved 3 MV/m with 3 to 6 Watts. Something was clearly wrong. We determined that the same plating bath had been used for all these tests. Furthermore, at the beginning of the test period this bath had been used by mistake with reverse polarity and so was probably contaminated with some copper.

We replaced the bath and have done one more plating and testing, using our standard technique. This last time the low-field Q was only 1.0×10^8, but the rate of decrease of Q with field was much lower than it had been for the cases with the old plating bath. See Figure 10.4-1. The Q factor at 3 MV/m was 0.6×10^8, which corresponds to a load of 9 W. This is still unacceptable performance. We have found some other problems with the plating system, which are being fixed. We plan to pursue the plating work in the near future.

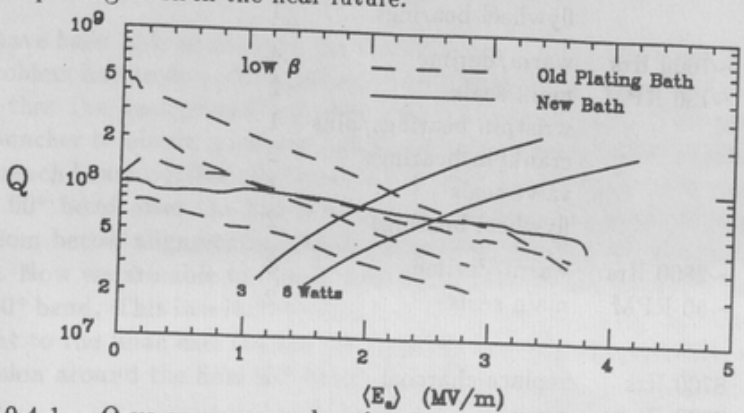

Fig. 10.4-1. Q vs average accelerating field for the five tests.

[1] J.R. Delayan, Rev. Sci. Instrum. **57** (1986) 766.

[2] D.W. Storm, J.M. Brennan, and I. Ben-Zvi, IEEE Trans. Nucl Sci **NS-32** (1985) p 3607; W.W. Burt, Adv. Cryog. Eng. Mater. **29** (1983) p 159; G.J. Dick, J.R. Delayan, and H.C. Yen, IEEE Trans. Nucl Sci **NS-24** (1977) p 1130.

10.5 Time Structure Monitor Modifications

J.F. Amsbaugh and D. W. Storm

Two different bunchers are used to inject beam from the Tandem Van de Graaff into the Linac.[1] The first is located before the Tandem and provides bunches at 12.5 or 50 MHz. The second buncher, one of our 150-MHz low-β superconducting resonators,[2] is about 3 meters upstream of the linac and rebunches the beam to match the time energy phase space acceptance of the linac.

The time structure monitor (TSM) is designed to measure the relative arrival time and time distribution of the beam pulse at the entrance of the Linac. With the second buncher off, this information is used to adjust the pre-tandem buncher for minimum time spread, typically about 1–2 nsec FWHM. Then the second buncher is tuned by finding the phase offset that does not shift the arrival time and is bunching. Finally, the second buncher amplitude is adjusted for minimum time spread, typically 700–300 psec. The performance of the TSM affects its usefulness as a diagnostic. Poor performance leads to poor beam quality.

The TSM consist of two assemblies mounted on 6" O.D. Conflat flanges, inserted in the top and right sides of a chamber in the beamline. The top assembly has a stepper motor and voltage feedthrough for positioning a biased 0.0082" dia. tungsten wire in or out of the beam. Coaxial with the wire when centered in the beam is a grounded cylindrical cage 2" O.D.× 3.5" long. This cage has two holes for the beam to pass thru and one for secondary electrons, created by beam striking the wires to exit. A 25 mm dia. Channeltron[3] electron multiplier array (CEMA) is mounted on the right flange to detect these electrons. The CEMA is a two stage multiplier that operates at −1800 to −2400 volts with the 50Ω electron collection anode near ground. The wire is biased negative one to five hundred volts with respect to the CEMA input electrode. The CEMA signal is used to start a TAC which is stopped by a signal of either 12.5 or 50 MHz, obtained from the 150-MHz Linac clock.

Initial tests indicated that the x-rays generated by the electrons striking the grounded cage were being detected and were broadening the time signal. Better results were obtained by removing the grounded cage and surrounding the CEMA with a Ta and Al shield. However, performance was found to depend strongly on the steering and focusing of the beam. The advantages of the cage is that it shapes the electric field so that transit time spread of the secondaries is reduced. Biasing the cage reduces the energies of the x-rays produced. To reinstall a biased cage required redesign of the CEMA mounting.

A crack in the second stage multiplier array was discovered and the CEMA was replaced. Further tests showed the count rate was too high, swamping the CEMA. Reduction of both the beam intensity and electron exit hole improved time resolution. The exit hole, a 0.2 ×0.4 inch slot, was reduced to 0.024" diameter. The cage must be biased positive with respect to the CEMA input face to prevent the secondary electrons created at the exit hole from being accelerated into the CEMA. The resolution is optimum for wire to cage potential of about +400 V and wire to CEMA input of about +200 V. Typical time spreads range from 770 to 390 psec.

---

[1] D. W. Storm *et al.*, IEEE Tran. Nucl. Sci. **NS-32** (1985) 3262.

[2] Storm *et al.*, Rev. Sci. Instrum. **57(5)** (1986) 773.

[3] Channeltron is a registered trade mark of the Galileo Electro-Optics Corp., Sturbridge, Mass.

10.6 The Tandem Emittance

M.A. Howe, H.L. Qian* and W.G. Weitkamp

Continuing work reported last year,[1] we have been using a Danfysik Beam Emittance Measuring System 590 to measure the emittance of beams from the tandem. The measurements have been performed on the beam after it passes through the first magnet at the end of the tandem.

The emittance measuring system uses a slit and a set of parallel wires (a 'harp') both of which are mounted 38 mm offset on rotating shafts. The harp is located about 1 m downstream from the slit. Emittance is measured by rotating the slit and harp across the beam stepwise and measuring the charge intercepted by each wire of the harp during each step. The slit and harp are tilted at 45° with respect to the shaft axis, so both horizontal and vertical emittances can be measured. A computer program calibrates and applies several corrections to the emittance data and calculates the area of the contour on the r-θ plot containing 90% of the beam.

After performing the measurements reported last year, we checked the dependence of the measured emittance on the focus of the beam, i.e., whether the emittance figure in the r-θ plane is a long narrow line or a compact spot. This dependence can be very large, as much as a factor of 2, with the smallest emittance when the figure is as compact as possible. This occurs when the angular divergence of the beam is minimized. In the horizontal plane, the limited resolution of the harp wires causes the the emittance to grow as the emittance figure becomes elongated. In the vertical direction vertical jitter induced on the beam by the inclined beam tubes in the tandem also causes the emittance to grow as the figure elongates. We found that we could obtain fairly reproducible and reasonable measurements by producing a compact spot in the r-θ plane. With the available focussing elements at the location we had placed the emittance monitor, it was not possible to do this in the horizontal plane, so our measurements were restricted to the vertical plane.

We also found that effects such as ripple on beam focussing elements, changes in tandem stripper foil condition and interception of the beam by apertures could also change the emittance by significant and sometimes uncontrollable amounts, limiting the precision of the measurements. These effects throw considerable suspicion on our previous conclusions concerning the emittance properties of the beam. Consequently we have remeasured a number points in the vertical plane. Our conclusions at this point are as follows.

The proton emittance falls from a value of 8.5 π mm mrad MeV$^{1/2}$ at a terminal voltage of 3 MV to a value of 3.8 π mm mrad MeV$^{1/2}$ at 8 MV.

The emittance for the oxygen beam formed from OH^- ions from the direct extraction ion source drops from 20 to 14 π mm mrad MeV$^{1/2}$ as the terminal voltage rises from 6 to 8 MV. The oxygen beam from the 860 sputter source is fairly constant at 19 π mm mrad MeV$^{1/2}$ for terminal voltages from 4 to 8 MV. To a precision of about 10% there is no evidence for dependence on charge state.

The Si beam emittance with a terminal voltage of 8 MV rises from 21 to 30 π mm mrad MeV$^{1/2}$ as the charge state increases from 7 to 9.

We are planning to begin measurements at the exit of the booster in the near future.

*Present address: Tulane University, New Orleans LA.

[1]Nuclear Physics Laboratory Annual Report, University of Washington (1989) p. 45.

10.7 New Belt Charge Controller for Van de Graaff

T.D. Van Wechel

Last year when the new control panel for the Van de Graaff was installed, the belt charge controller was also updated. Previously a motor driven variac with a raise/lower switch on the control panel determined the belt charge setpoint. The output of the variac was transformer coupled to the control grid of a cascode vacuum tube amplifier in series between the belt upcharge screen and a 25 kilovolt d.c. power supply. The belt charge current was zero when the output of the variac was 50Vac and increased to a maximum belt charge current of approximately 500μA at a variac voltage of 8Vac.

The function of the motor driven variac has been replaced with electronics. The new belt charge controller has a new feature that can be used if desired, to help compensate for drift of the operating parameters of the tandem. The corona current is monitored by a dead band amplifier. The deadband is centered at 50μA and has a width setable from 0 to $\pm$20μA about the center. If the corona current drifts out of the dead band the controller can increase or lower the belt charge current by up to $\pm$15% of the setpoint to compensate.

The setpoint reference is provided by a DAC, whose digital input is from an up/down counter that is incremented or decremented by the front panel raise/lower switch. The output of the deadband amplifier drives the control input of a pulse width modulator that varies the setpoint reference level signal to provide setpoint compensation as described above. A wien bridge oscillator provides a sine wave that drives a gain controlled transconductance amplifier. The output of the transconductance amplifier is amplified by a power op-amp and is coupled by a step-up transformer to provide the same ac voltage levels as that of the motor driven variac. The setpoint reference level from the pulse width modulator is scaled and offset to drive the control input of the transconductance amplifier. The controller is setup to provide an ac voltage at the output of the stepup transformer, that varies from 50Vac when zero belt charge is desired to 8Vac for maximum belt charge current. The cascode amplifier is in series between the 25kV power supply and the belt upcharge screen as before.

10.8 Tandem Belt Charge System

T.A. Trainor.

A year ago I reported that I had identified the two sources of terminal voltage noise in a belt-charged tandem Van de Graaff. These are belt edge flutter and belt surface bumpiness. The first produces large amplitude noise at the belt fundamental f_o(=2.4Hz). The second produces smaller amplitude noise at $12f_o$ and harmonics corresponding to the rubber cure pattern on the belt.

The edge flutter noise contribution was essentially eliminated by switching from standard mesh charging screens to shim stock. The shim stock is much more compliant than mesh and tracks the edge flutter very well, maintaining good contact with the belt surface. More recently I suggested that the belt noise fine structure at $12f_o$ was due to belt surface bumpiness causing the screens to lose contact with the belt surface. This bumpiness is so slight as to elude simple observation. However, the screen moving over the belt surface at 1000 in/sec is extremely sensitive to very small surface height variations.

Fig. 10.8-1a shows the high energy column current (HECC) signal last Fall with a single layer of 3 mil thick SS screen 1.5 inches long installed at the upcharge position. On this time scale the HECC is essentially the time derivative of the charging belt current. While the edge flutter was completely eliminated by this compliant screen configuration, the fine structure in Fig. 10.8-1a was noticeably larger than had been observed previously. The prominent dispersion shapes (at $12f_o$) are interpreted as gaps in the belt charge distribution. From this figure the gaps are determined to be 12 cm (5 ms) wide. Such gaps exactly explain the shape and magnitude of the correction signals required for the corona and terminal regulator systems.

Given this apparent confirmation of my hypothesis about screen bounce over surface bumps I explored the possibility of an optimum screen configuration to minimize this noise component. Using a linear programming approach I found that the system does have an optimum configuration. Analyzing the shim stock screen as a deflected plate I determined the resonant frequency and spring constant of the plate in terms of the modulus of elasticity and dimensions of the plate material. I then developed constraint equations for the bandwidth and the total force applied to the belt by the screen in its quiescent position. These relations are represented in Fig. 10.8-2.

The constraint diagram shows that there is a tradeoff between bandwidth and range of compliance for a given applied force. This suggests a two-component screen design. A short, thin section follows the very rapid but small-amplitude surface bumpiness while a larger, thicker section follows the large amplitude but relatively slow edge flutter. Both sections must have dimension ratios which correspond to the same force applied to the belt so that they both deflect to the middle of their motion range under quiescent conditions.

The performance of such a composite screen design is shown in Fig. 10.8-1b. Traces in parts a) and b) are placed in phase to show reproducible fine structure. This is a laminate of 4 mil and 2 mil SS shim stock. The overall length is 2 inches, and the 2 mil shim protrudes 1/4 inch beyond the 4 mil shim as the bottom layer. The two layers are spot welded together in a random pattern with weld-to-weld distance typically 1/2 inch. The sharp reduction in $12f_o$ noise (2–3 x) confirms both the original mechanism for $12f_o$ noise production by loss of screen contact and the linear programming approach to screen design. Further improvement of ~2 x is likely as we optimize the screen design.

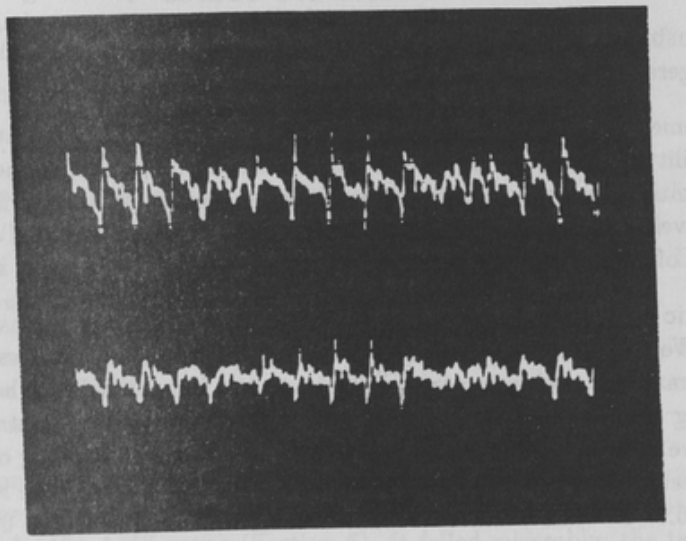

Figure 10.8-1. High Energy Column Current, 9 MV Terminal, 400μA upcharge. **Span 500 ms, 100mV/cm. a) Oct.**, 1989, 3 mil SS screen. b) Feb., 1990, composite screen.

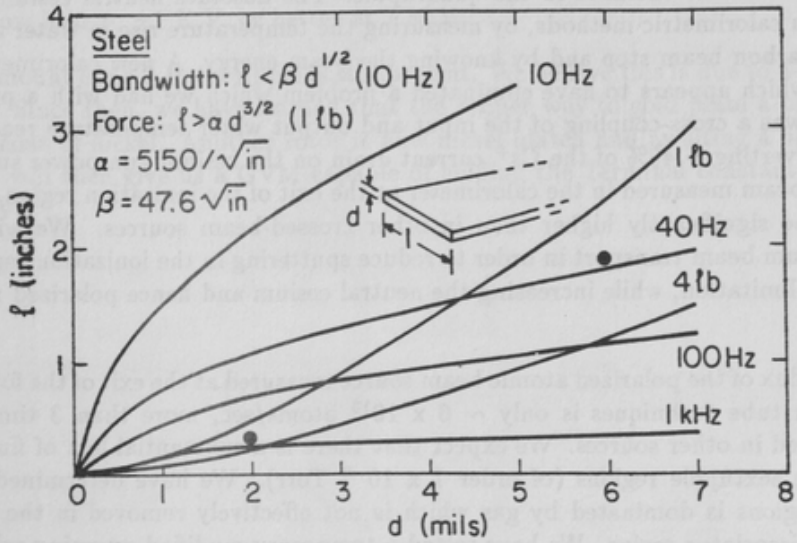

Figure 10.8-2. Constraint diagram for charging screens.

10.9 The Crossed-Beams Polarized Ion Source

J.F. Amsbaugh, D.R. Balsley, D.T. Corcoran, J.K. Eisenberg, C.A. Gossett, G.C. Harper, J.A.Rogers and K.B. Swartz

The development of the crossed-beams polarized ion source has been steadily progressing. The reliability, stability and ease of operation have been improving while the intensity has been increasing. Our main efforts in the past year have been concentrated on final optimization of the polarization, development of the cesium beam and improved cesium beam diagnostics, study of the low output flux of the atomic beam source and completion of the control system.

The magnetic field profile in the radio frequency transition region has been carefully mapped and adjusted. We found that in the original configuration of the rf cavities the slope of the field in the weak field transition region was in opposition to the fringing field of the strong field transitions causing a strong coupling of the weak field transition tuning with the strong field magnetic field setting. We have reversed the weak field cavity and find that the tuning of the rf cavities and the magnetic field settings are now quite reproducible from run to run. We routinely observe proton polarization of 0.9 (1 = max) and deuteron vector polarization of $it_{11} = 0.47$ (0.57 = max).

We have also been working to improve the cesium beam tuning and diagnostics. A four sectored aperture has been installed at the exit of the cesium beam quadrupole triplet. The current on each sector may be monitored in order to center the cesium beam at this point. We plan to install a similar aperture at the entrance to the quadrupole. The absolute neutral cesium beam flux is determined with calorimetric methods, by measuring the temperature rise in water at a given flow rate cooling a carbon beam stop and by knowing the beam energy. A new calorimeter paddle has been installed which appears to have eliminated a problem which we had with a previous design in which there was a cross-coupling of the input and output water temperature readings. At this time we are converting $\sim$ 40% of the Cs^+ current drain on the cesium gun power supply to useful neutral cesium beam measured in the calorimeter at the exit of the ionization region. This fraction is believed to be significantly higher than in other crossed-beam sources. We will continue to develop the cesium beam transport in order to reduce sputtering in the ionization region, presently our main beam limitation, while increasing the neutral cesium and hence polarized negative beam flux.

The output flux of the polarized atomic beam source measured at the exit of the fourth sextupole via compression tube techniques is only $\sim$ 6 x 10^{15} atoms/sec, more than 3 times lower than typically observed in other sources. We expect that there is a substantial loss of flux due to poor pressures in the sextupole regions (of order 7 x 10^{-6} Torr). We have determined that the gas load in these regions is dominated by gas which is not effectively removed in the first pumping chamber—the dissociator region. We have tested a temporary modified pumping scheme in which the first chamber was separated into a region enclosing the dissociator and a second pumping stage between two skimmer-collimators. The results of this test are quite encouraging and we plan to design a more permanent differential pumping arrangement in our continuing effort to increase the atomic beam flux.

The polarized source control system is essentially complete (see Sec. 11.3). The microprocessor system for the spin precessor and beam transport has been developed and completed within the last year. Remote and local analog control of the source via a knob box system has also been

implemented. The tuning of the polarized beam for injection into the tandem and for transport through the tandem has been greatly improved.

10.10 Tandem Energy Control—The Generating Voltmeter

T. Brown, D. Corcoran, F.H. Schmidt and T. Van Wechel

Last year (Section 9.7) we reported a surprising double beat frequency which caused the Terminal potential to oscillate with a period of about 44 seconds. The oscillation was caused by a beat between the GVM rotor frequency (58.8 Hertz), 60 Hertz pickup, and 2.4 Hertz induced by the Tandem charging belt.

The 58.8–60.0 Hertz beat frequency was easily eliminated and consequently the 1.2–2.4 beat, but residual ripple from the GVM rotor was overloading the control system so as to prevent full utilization of the feed-back gain.

A newly designed, precisely machined GVM rotor was constructed in the Physics Department machine shop using a new programmable milling machine. After gold plating, it was installed in the Tandem and tested by the AMS group (Section 6). It failed miserably; the terminal potential "jumped about" over a 15–20 kilovolt range at 7 M.V.

The rotor appeared to have a slightly blemished gold surface; so a spare rotor was gold plated using greater care. It was installed in the Tandem and it is almost a total success: The terminal potential is now held to ± 1 K.V. or better at 7 M.V.

A small amount of 58.8 Hertz ripple is still present. We believe this is due to a-less-than-perfect layer of gold. Since then, we have learned that the proper way to gold plate a brass surface is to first apply a coat of nickel. Another rotor is now nickel plated and awaiting a final gold coating. We hope this will then give us a GVM capable of holding the Terminal constant to $\pm$ 300 to 500 volts at 7 M.V.

11 COMPUTER SYSTEMS

11.1 Acquisition System Developments

M.A. Howe, C. Hyde-Wright, H.P. Readdy and R.J. Seymour

Our principal data acquisition hardware consists of a dozen Tracor Northern TN-1213 ADCs connected to input registers installed in a BiRa MBD-11 controlled CAMAC crate. The MBD-11 is controlled by a DEC VAXStation 3200 running VMS version 4.7 with VWS/UIS as the "windowing" software. The VAXStation has 8 megabytes of memory, a 19 inch monochrome screen and a Q-bus extension cable to a BA23-CC expansion box containing a 760 megabyte Maxtor disk drive on an Aviv DFC 904 controller, another Aviv controller for a Telex 9251 6250 bpi tape drive, a TTI CTS-8000 8mm tape system, a DEC IEQ11 IEEE-488 bus controller, a DEC DRV11-J and an MDB DWQ11 Q-bus to UNIBUS converter. The other end of the DWQ11 converter is in one of our old 11/60's UNIBUS cabinets, where the MBD-11, a DR11-C and our Printronix's lineprinter controller are still attached. Additional CAMAC space is available for our LeCroy 2249's, 2228's and 2551's.

A second acquisition system has been assembled for the Time Projection Chamber project (see section 9.7). It consists of another monochrome VAXStation 3200, an Aviv/Maxtor 760 megabyte disk system, an Able Qniverter and an MBD-11. Unlike our main system, this dedicated system has no additional lab-built electronics for event synchronization, interfacing or scalers. It simply uses LeCroy 2449a ADCs' LAMs to trigger readout and analysis. Event recording is direct to disk, and subsequent event taping and printing duties are performed by other VAXStations available across the lab's DECnet network.

To correct the Qbus Interface Chip problem described last year, all of our VAXStation 3200s had their CPU boards replaced by Digital.

Our principal acquisition software is TUNL's XSYS, with major modifications to their DISPLAY program. Since the Display program is the principal user interface to the system, it receives the most continuous development. The arrival of a color VAXstation (see next section) has spawned the addition of color contour displays. We have also added the ability to directly generate 1-d and 2-d (with grey scale, Fig. 9.7-1) PostScript plots of the XSYS DISPLAY window. We have implemented a multiple spectrum display by allowing up to nine miniature windows to share the screen, although only one (the "active" window) is affected by the mouse or typed commands.

XSYS's extended capabilities have greatly increased our "average" experiment's amount of event data collected, compared to the MULTI/QDA system we ran on the PDP 11/60. We try to provide about 500,000 free disk blocks for an experimenter, and they often fill, tape and refill that space in the course of a run.

XSYS's greater acquisition capacity combined with the sudden increase of on-site disk space swamped our abilities to tape and archive data. We had been investigating optical disk storage, but the price, features and capacities never approached our needs. The advent and acceptance of "8mm" systems seemed more appropriate. Each 8mm cartridge can hold over 2 gigabytes of data. All 8mm systems are based upon an Exabyte Corporation modification of a Sony 8mm video camera tapedrive. Many companies match that Exabyte drive with differing styles of controller electronics

to produce a tape "system". The basic Exabyte drive has a complete lack of activity indication. We had tried a Dilog system as a demo. Since Dilog, like most system suppliers, simply adds a controller inside the VAX, we experienced long delays while waiting for operations which never completed. Based upon that test, we chose the Transitional Technologies Inc. (TTI) CTS-8000 system. It provides a numeric display of drive activity, tape-remaining and error rate. The 8mm tape system was initially justified by magtape cost savings alone. It has proven a fast, reliable and capacious system for both backup of large event files previously recorded on disk, and for direct recording of events with large event sizes. Some care and patience is required to avoid "confusing" the system, but as long as the drive shows "ready" before an operation is attempted, it works well. We find that we occasionally crash the VAXStation when attempting extensive VMS Backup operation while acquisition is underway. We suspect this is due to some bus latency problems exacerbated by the VAXStation's limited Qbus address translation cache, but have not isolated the problem.

Different hardware, usage experience and gradual changes are causing the generation and expansion of locally-written documentation for XSYS. This included restructuring of XSYS's online HELP into a tree system.

Our PDP-11 screen-menu Momentum Filter control programs have been moved to the VAXStation environment.

With the purchase of a second MBD-11 for the TPC system, our original (1978 vintage) MBD-11 was finally freed to be sent back to BiRa to bring it to current revision level and to attempt to correct intermittent errors. Even their replacement of 17 components (and the addition of 5), the MBD still would occasionally hang (it seemed to miss the VAXStation's NPG signal granting Qbus access). Finally one memory chip failed completely and all symptoms disappeared with its replacement.

In a related, but distant, note: our versions of MULTI/QDA and SINGLES are currently installed and running at TANDAR, Argentina's vertical tandem Van de Graaff center in Buenos Aires. They have ported them to RSX-11M v4.2 on a PDP-11/34.

11.2 Analysis and Support System Developments

M.A. Howe, C. Hyde-Wright, H.P. Readdy and R.J. Seymour

Our principal interactive system is still an 8 megabyte VAX 11/780 running VMS version 4.7, with connections to thirty-odd local terminals. It is connected via ethernet to eight VAXStation 3200's, one VAXStation 2000, one color VAXStation 3100 and a color DECStation 3100 in our building, and via fiber optic ethernet to the rest of the campus. We do not usually run the systems as a cluster.

The VAXStation 3100 and DECStation 3100 were received under Charles Hyde-Wright's Presidential Young Investigator (PYI) grant from Digital. They arrived completely diskless. They have each been given SCSI 766 megabyte Imprimis Wren 6 drives. A VaxStation 3200 obtained last year under the Digital PYI grant has been temporary located at SLAC for the PEGASYS project.

The 11/780 now has two Maxtor 760 megabyte drives on its Qbus extension, and we finally have a Maxtor on all but one of the VAXStation 3200's.

A test installation of our second TTI/Exabyte 8mm tape system on the 11/780's Qbus extension worked perfectly. The 8mm system is normally installed on a faster VAXstation 3200 to provide better service for both offline analysis, display and network-wide backups. In the last two years our on-site formatted disk capacity has quintupled from about 1500 megabytes to 7500 megabytes. Given a single 6250 bpi tapedrive among the offline systems, 9-track techniques were woefully inadequate to handle our backup, archiving and analysis demands. The 8mm tape system makes incremental backups simple, and full backups remain feasible.

With our disks often running over 90% full, disk fragmentation has been of unending concern. Over the years we have tested commercial defragmentors such as Raxco's Rabbit-7 and, most recently, Executive Software's Diskeeper. To aid our analysis of our problem and their performance, we have written diskspace analysis programs which provide single-page maps of every cluster on the disk, rendered in run-length encoded gray-scale PostScript, with the darkness of gray indicating number of fragments for each file shown. Although Diskeeper eventually achieved a near-perfect level of file defragmentation, it was unable (over the course of a month) to consolidate our freespace. Thus newly created (or restored) large (100 to 300 thousand block) event files could not be created contiguously. We're still investigating approaches to our particular problems with disk space optimization.

XSYS is our primary offline analysis package, although we also run LAMPF's Q on a VAXStation in support of Douglas Rosenzweig's work (see section 7.2).

We served as a beta-test site for the VMS version of Wolfram's Mathematica package. It required bringing a VAX to VMS v5.2 with DECWindows. Wolfram has since generated a VMS v4.7 version. The VMS upgrade was relatively uneventful, and later allowed the booting of our newly-delivered VAXStation 3100 as a diskless cluster member. The regime of DECWindows coupled with VMS v5.2's increased security produces an operating environment which is noticeably less casual for inter-user and inter-machine file transfers. Part of this is obviously "tuning", and will improve with experience, but some symptoms seem inherent from the design of the facilities. Since the end of the Mathematica beta-test period, the 3100 has been converted to VWS/UIS in lieu of DECWindows.

With the arrival of the color DECStation 3100, we now have Ultrix, Digital's version of Unix, in the lab. We shall be installing Mathematica on this platform in view of its higher speed.

We now have TGV's MultiNet communications package running on all of the VAXes. This provides us with direct Internet access, and complies with the campus' goal of removing pure DECnet from the cross-campus fiber optic network. Our principal Internet address is npl.npl.washington.edu.

As demonstrated by the disk space analysis program and XSYS's DISPLAY, we have been adding native PostScript generation subroutines to many of our graphics-oriented application packages. It seems to take about two weeks to go from brute-strength PostScript imaging to fairly streamlined and optimized PostScript file structures. The optimization techniques often vary based upon the kind of image being created.

We have imported TRIUMF's PLOTDATA and OPDATA packages, and they are gradually developing a following. A modified version of SLAC's TopDrawer, based upon their UGS, is still

our flagship general graphics generator.

The random pieces of hardware and software we accumulate over the years periodically get used in new and unexpected ways. An example of this was the use of our LaserMaster laserprinter, which has been functionally replaced by our Apple LaserWriter, for generating computed holograms. A physics masters student had generated the patterns on our VAX as part of his thesis project.[1] He moved them via DECnet/ethernet to the PC-AT clone hosting our LaserMaster. Since the LaserMaster uses a card and rasterizing processor internal to the PC for its image generation, a page-filling interference pattern could be coded, transferred and printed in less than two minutes. These were then photographed onto 35-mm slides for illumination by a laser.

Likewise, our 7-track tapedrive was converted to a "rabbit" system for Alejandro García's experiment (see section 3.2).

Since the end of its warranty period, we have self-maintained the 11/780. This has ranged from calling Digital for occasional board swaps or upgrades, to individual component isolation and replacement. A failure this year was repaired by the purchase of a complete 11/780 CPU circuit card set for $1200 from a used equipment vendor. One card from that set saved the work of isolating the failing component. Since then the card set has served to repair another failure. The rest of the 11/780's problems have been caused by aging electrolytic capacitors.

We still provide management for the Nuclear Theory group's three VAXStation 3200's.

11.3 Polarized Ion Source Computer Control System

C.A. Gossett, G.C. Harper, M.A. Howe and R.W. Stout

Work directed toward placing the operation of the polarized ion source completely under computer control with both remote and local access is essentially complete. This includes development of the ANAC 700 microprocessor controlled system for the spin precessor, the knob box project, and connection of the remaining atomic beam system and cesium system parameters.

Acquisition of additional ANAC multiplexor units and a spare microprocessor controller from Yale University provided the required hardware for the completion of the spin precessor system. The software for the spin precessor controller was developed in house and modeled after the atomic beam and cesium systems. Commissioning of the spin precessor controller immediately allowed complete computer control over the interlock system of the entire source. ADC and DAC multiplexors were put into operation after completion of the first knob box. All source parameters were also made accessible through the CSX program on the LINAC μvax control computer for both monitor and control.

A knob box system was designed and built for tuning source parameters from a central location. The system consists of an IBM PC computer, power supply and floppy disk drive mounted in a 5.25 inch by 19 inch rack mount chassis, a knob box, and a 40 foot long rolled and shielded ribbon cable for interconnection. The knob box itself is a 7 inch by 13 inch, lightweight, aluminum box with 16 pushbuttons for parameter selection and 4 optically encoded rotational motion transducers for parameter adjustment on the front panel. A 20 character vacuum fluorescent display for each

[1] S.E. Horn, M.S. thesis, University of Washington (1989) unpublished.

knob provides information concerning the parameter to which the knob is mounted, the parameter setpoint, or a system message.

Two knob box systems are now complete and operational. After completion of the first, the 10 turn pot tuning system of the spin precessor parameters was discarded. The knob boxes can now be connected to any ANAC 700 system controlled parameter on the source. The 16 buttons on the knob boxes connect parameters to the 4 knobs in a left to right sequence similar to the beam development. In this manner, the entire source may be tuned from one position by simply stepping through the sequence of source parameters.

In the present software configuration, the CSX program senses a button push and issues one or more keyboard commands through a command file dedicated to that button. In this manner, a pushbutton can mount a set of knobs to a set of analog parameters, toggle 2-state parameters, issue store and recall commands, or even remap the button configuration. This last feature has allowed operation of the injector deck ion sources and the low energy buncher using the same knob box by sequencing through a linked list of systems using one of the buttons. Source parameters are changed incrementally so that connecting or disconnecting a knob and activating or deactivating a display does not change the value in the database.

Further development includes activating the few remaining unconnected source parameters and a labeling system for the 77 parameters which may, at this time, be connected.

11.4 Improvements to the Main Control System

G.C. Harper and M.A. Howe

During 1989 considerable work was done to make the booster master control program (CSX) faster and more efficient. This was accomplished by restructuring some of the message handling data structures to allow shorter internal messages and a consolidation of message handling routines with simular functions so that message processing was more efficient. The graphics updating routines were made more intelligent so that the global data base is scanned less often and the touch screen parameter increment/decrement routines were combined with the routines that handle parameter changes initiated by the knob boxes. These changes have resulted in a noticeable increase in screen drawing and updating speed.

Two new knob boxes were added for controlling the polarized ion source (PIS). [2] There are sixteen buttons on each knob box which are used to activate a CSX command file containing any legal CSX keyboard command. Several new commands were specifically created to make the buttons more functional. For example, there is a parameter save/restore command, a cup toggle in/out command, a knob display refresh command, and a button file directory change command (so that buttons can have multiple functions).

During the new knob box development a serious bug was found in CSX which prevented proper CSX-knob box signal handshaking and could cause the knobs to get ahead of a slow satellite and fill up the buffers in the satellite. Thus under some conditions the satellite would continue to change the parameter long after the user stopped turning the knob. This error has been corrected.

[2] See Section 11.3, this report

our flagship general graphics generator.

The random pieces of hardware and software we accumulate over the years periodically get used in new and unexpected ways. An example of this was the use of our LaserMaster laserprinter, which has been functionally replaced by our Apple LaserWriter, for generating computed holograms. A physics masters student had generated the patterns on our VAX as part of his thesis project.[1] He moved them via DECnet/ethernet to the PC-AT clone hosting our LaserMaster. Since the LaserMaster uses a card and rasterizing processor internal to the PC for its image generation, a page-filling interference pattern could be coded, transferred and printed in less than two minutes. These were then photographed onto 35-mm slides for illumination by a laser.

Likewise, our 7-track tapedrive was converted to a "rabbit" system for Alejandro García's experiment (see section 3.2).

Since the end of its warranty period, we have self-maintained the 11/780. This has ranged from calling Digital for occasional board swaps or upgrades, to individual component isolation and replacement. A failure this year was repaired by the purchase of a complete 11/780 CPU circuit card set for $1200 from a used equipment vendor. One card from that set saved the work of isolating the failing component. Since then the card set has served to repair another failure. The rest of the 11/780's problems have been caused by aging electrolytic capacitors.

We still provide management for the Nuclear Theory group's three VAXStation 3200's.

11.3 Polarized Ion Source Computer Control System

C.A. Gossett, G.C. Harper, M.A. Howe and R.W. Stout

Work directed toward placing the operation of the polarized ion source completely under computer control with both remote and local access is essentially complete. This includes development of the ANAC 700 microprocessor controlled system for the spin precessor, the knob box project, and connection of the remaining atomic beam system and cesium system parameters.

Acquisition of additional ANAC multiplexor units and a spare microprocessor controller from Yale University provided the required hardware for the completion of the spin precessor system. The software for the spin precessor controller was developed in house and modeled after the atomic beam and cesium systems. Commissioning of the spin precessor controller immediately allowed complete computer control over the interlock system of the entire source. ADC and DAC multiplexors were put into operation after completion of the first knob box. All source parameters were also made accessible through the CSX program on the LINAC μvax control computer for both monitor and control.

A knob box system was designed and built for tuning source parameters from a central location. The system consists of an IBM PC computer, power supply and floppy disk drive mounted in a 5.25 inch by 19 inch rack mount chassis, a knob box, and a 40 foot long rolled and shielded ribbon cable for interconnection. The knob box itself is a 7 inch by 13 inch, lightweight, aluminum box with 16 pushbuttons for parameter selection and 4 optically encoded rotational motion transducers for parameter adjustment on the front panel. A 20 character vacuum fluorescent display for each

[1] S.E. Horn, M.S. thesis, University of Washington (1989) unpublished.

knob provides information concerning the parameter to which the knob is mounted, the parameter setpoint, or a system message.

Two knob box systems are now complete and operational. After completion of the first, the 10 turn pot tuning system of the spin precessor parameters was discarded. The knob boxes can now be connected to any ANAC 700 system controlled parameter on the source. The 16 buttons on the knob boxes connect parameters to the 4 knobs in a left to right sequence similar to the beam development. In this manner, the entire source may be tuned from one position by simply stepping through the sequence of source parameters.

In the present software configuration, the CSX program senses a button push and issues one or more keyboard commands through a command file dedicated to that button. In this manner, a pushbutton can mount a set of knobs to a set of analog parameters, toggle 2-state parameters, issue store and recall commands, or even remap the button configuration. This last feature has allowed operation of the injector deck ion sources and the low energy buncher using the same knob box by sequencing through a linked list of systems using one of the buttons. Source parameters are changed incrementally so that connecting or disconnecting a knob and activating or deactivating a display does not change the value in the database.

Further development includes activating the few remaining unconnected source parameters and a labeling system for the 77 parameters which may, at this time, be connected.

11.4 Improvements to the Main Control System

G.C. Harper and M.A. Howe

During 1989 considerable work was done to make the booster master control program (CSX) faster and more efficient. This was accomplished by restructuring some of the message handling data structures to allow shorter internal messages and a consolidation of message handling routines with simular functions so that message processing was more efficient. The graphics updating routines were made more intelligent so that the global data base is scanned less often and the touch screen parameter increment/decrement routines were combined with the routines that handle parameter changes initiated by the knob boxes. These changes have resulted in a noticeable increase in screen drawing and updating speed.

Two new knob boxes were added for controlling the polarized ion source (PIS). [2] There are sixteen buttons on each knob box which are used to activate a CSX command file containing any legal CSX keyboard command. Several new commands were specifically created to make the buttons more functional. For example, there is a parameter save/restore command, a cup toggle in/out command, a knob display refresh command, and a button file directory change command (so that buttons can have multiple functions).

During the new knob box development a serious bug was found in CSX which prevented proper CSX-knob box signal handshaking and could cause the knobs to get ahead of a slow satellite and fill up the buffers in the satellite. Thus under some conditions the satellite would continue to change the parameter long after the user stopped turning the knob. This error has been corrected.

[2] See Section 11.3, this report

Controls were added for the PIS spin precessor and the knob sensitivity was carefully adjusted for each source parameter to make tuning easier. The software for the PIS is now complete.

Touch screen control of the injector deck was enhanced so that the external terminal is no longer required. A subpage was created to give control of the deck slits and touch screen access to the learn function was added. In addition, a separate page was developed for controlling the beam chopper hardware.

Two vertical steering magnets were added to the booster beamline. The steering magnet page was modified to give control of those magnets. An ADC card was added to the MicroVAX and software written to read and display data from the new scanner current integrator.

The alarm system was expanded to allow a user to set up custom alarms on most booster parameters. A display page was developed to alert users to vacuum system gatevalve changes.

12 APPENDIX

12.1 Nuclear Physics Laboratory Personnel

Faculty

Eric G. Adelberger, Professor
John G. Cramer, Professor
George W. Farwell, Professor Emeritus
Cynthia A. Gossett, Research Assistant Professor
Pieter M. Grootes, Joint Senior Research Associate, Geological Sciences
Isaac Halpern, Professor
Charles E. Hyde-Wright, Assistant Professor
Fred H. Schmidt, Professor Emeritus
Kurt A. Snover, Research Professor
Derek W. Storm, Research Professor; Director, Nuclear Physics Laboratory
Thomas A. Trainor, Research Associate Professor
Robert Vandenbosch, Professor
William G. Weitkamp, Research Professor; Technical Director, Nuclear Physics Laboratory

Research Staff

Ludwig de Braeckeleer, Research Associate
Marc Frodyma, Research Associate
Swaminathan Kailas, Research Associate[1]
Mitchell Kaplan, Research Associate
Christopher W. Stubbs, Research Associate[2]
Scott Van Verst, Research Associate
Douglas Wells, Research Associate

Predoctoral Research Associates

John A. Behr
Cecilia Bitz[3]
Thomas A. Brown
Aaron Charlop
Ziad M. Drebi
Jon Eisenberg
Alejandro García
Jens H. Gundlach
Weidong Jiang
Yihan Liu
Michael Leskovar[3]
S. John Luke
Diane Markoff
Brian McLain
Douglas P. Rosenzweig
Gregory Smith
Yue Su
Kenneth Swartz
Philip Williams
Peter Wong

[1]Present address: Nuclear Physics Division, Bhabha Atomic Research Center, Bombay 400085 India.
[2]Present address: Center for Particle Astrophysics, 301 Leconte Hall, UC Berkeley, Berkeley, CA 94720.
[3]Now at: Physics Department, University of Washington, Seattle, WA 98195.

Professional Staff

John F. Amsbaugh, Research Engineer
David Balsley, Research Engineer[3]
Gregory C. Harper, Research Engineer
David J. Hodgkins, Research Engineer[4]
Mark A. Howe, Research Engineer
Duncan Prindle, Research Scientist
H. Pamela Readdy, Computer Systems Engineer[5]
Richard J. Seymour, Computer Systems Manager
Rod E. Stowell, Electronics Engineer/Electronics Shop Supervisor
H. Erik Swanson, Research Physicist
Timothy D. Van Wechel, Electronics Engineer
Douglas I. Will, Research Engineer

Technical Staff

Robert L. Cooper, Instrument Maker
Dean T. Corcoran, Engineering Technician
Louis L. Geissel, Instrument Maker, Student Shop Leadman
John M. LaCroix, Electronics Technician[6]
Carl E. Linder, Engineering Technician
Hendrik Simons, Instrument Maker, Shop Supervisor
John A. Wootress, Accelerator Technician

Administrative Staff

María G. Ramírez, Administrative Assistant
Ida M. Tess, Technical Secretary

Part Time Staff

Kevin Arnal
Richard Barry
Melanie Bryce
Matthew Carson
W. Brian Christman
Wendy Kameoka
Kevin McMurry
Spas Muleshov
Johannes Ritter
John A. Rogers
Manish Rohila
Patrick J. Santos
Eric C. Torrence

[3]Present address: 6561 4th Ave NE, #204, Seattle, WA 98115.
[4]Present address: Los Alamos National Lab, PO 1663, M/S H21, Los Alamos, NM 87545.
[5]Present address: 11549 Holmes Point Drive, Kirkland, WA.
[6]Present address: 2318 2nd Ave, Seattle, WA 98121.

12.2 Degrees Granted, Academic Year 1989-1990

Ph. D. Degrees:

"Shapes of Excited Rotating Medium Mass Nuclei Determined from Giant Dipole Resonance Gamma Decays," Jens Horst Gundlach, Ph. D. Thesis, University of Washington (1990).

12.3 List of Publications

Published Papers:

"Searching for New Macroscopic Forces", E.G. Adelberger and C.W. Stubbs, Physics News in 1988, Physics Today, **42**, S-53 (1989).

"Radiocarbon Dating of Pollen by Accelerator Mass Spectrometry", Thomas A. Brown, D. Erle Nelson, Rolf W. Matthewes, John S. Vogel, and John R. Southon, Quaternary Research **32**, 205 (1989).

"Quasielastic Reaction Mechanism Studied Using the Reaction $^{12}C(e, e'p)$", L.B. Weinstein, H. Baghaei, W. Bertozzi, J.M. Finn, J. Glickman, C.E. Hyde-Wright, N. Kalantar-Nayestanaki, R.W. Lourie, J.A. Nelson, W.W. Sapp, C.P. Sargent, P.E. Ulmer, B.H. Cottman, L. Ghedira, E.J. Winhold, J.R. Calarco, J. Wise, P. Boberg, C.C. Chang, D. Zhang, K. Aniol, M.B. Epstein, D.J. Margaziotis, C. Perdrisat, and V. Punjabi, Phys. Rev. Lett. **64**, 1646 (1990).

"γ Width of the Unbound 5.17 MeV Level on ^{14}O and the "hot" CNO Cycle", P.B. Fernandez, E.G. Adelberger and A. Garcia, Phys. Rev. **C40**, 5 (1989).

"Improved Beam-energy Calibration Technique for Heavy-ion Accelerators", A.M.J. Ferrero, A. Garcia, S. Gil, A. Etchegoyen, M. DiTada, A.J. Pacheco, D. Abriola, D.E. DiGregorio, M. Elgue, M.C. Etchegoyen, J.O. Fernandez Niello, A.O. Macchiavelli, and J.E. Testoni, Nuc. Inst. and Meth. in Physics Research **B42**, 389 (1989).

"Barkas Effect Observed with Antiprotons and Protons", G. Gabrielse, X. Fei, L.A. Orozco, S.L. Rolston, R.L. Tjoelker, T.A. Trainor, J. Haas, H. Kalinowsky and W. Kells, Phys. Rev. A. **A40**, 481 (1989).

"Cooling and Slowing Trapped Antiprotons Below 100 Milli-eV", G. Gabrielse, X. Fei, L.A. Orozco, R.L. Tjoelker, J. Haas, H. Kalinowsky, T.A. Trainor and W. Kells, Phys. Rev. Lett. **63**, 1360 (1989).

"First Capture of Antiprotons in an Ion Trap; Progress toward a Precision Measurement and Antihydrogen", G. Gabrielse, X. Fei, L. Haarsma, S.L. Roston, R.L. Tjoelker, T.A. Trainor, H. Kalinowsky, J. Haas and W. Kells, Physica Scripta **T22**, 36 (1988).

"Low Lying States in ^{127}Xe: Implications for the Efficiency of an ^{127}I Solar Neutrino Detector", A. Garcia, E.G. Adelberger, A. Charlop , S. Gil, J.H. Gundlach, and S. Kailas, Phys. Rev. **C41**, 775 (1990).

"The University of Washington Polarized Ion Source", C.A. Gossett, D.R. Balsley, G.C. Harper, C.M. Bitz, J.K. Eisenberg,and J.A. Rogers, Rev. Sci. Instrum. **61**, 445 (1990).

"Rapid Response of Tree Cellulose Radiocarbon Content to Changes in Atmospheric $^{14}CO_2$ Concentration", P.M. Grootes, G.W. Farwell, F.H. Schmidt, D.D. Leach, and M. Stuiver, Tellus, **41B**, 134–148 (1989).

"Experimental Bounds on Interactions Mediated by Ultra-Low Mass Bosons," B.R. Heckel, E.G. Adelberger, C.W. Stubbs, Y. Su, H.E. Swanson, G. Smith, and W.F. Rogers, Phys. Rev. Lett. **63**, 2705 (1989).

"Density Dependence in the Two-Nucleon Effective Interaction at 135 MeV", J.J. Kelly, W. Bertozzi, T.N. Buti, J.M. Finn, F.W. Hersman, C.E. Hyde-Wright, M.V. Hynes, M.A. Kovash, B. Murdock, B.E. Norum, B. Pugh, F.N. Rad, A.D. Bacher, G.T. Emery, C.C. Foster, W.P. Jones, D.W. Miller, B.L. Berman, J.A. Carr, and F. Petrovich, Phys. Rev. **C39**, 1222 (1989).

"Electroexcitation of Rotational Bands in ^{18}O" D.M. Manley, D.J. Millener, B.L. Berman, W. Bertozzi, T.N. Buti, J.M. Finn, F.W. Hersman, C.E. Hyde-Wright, M.V. Hynes, J.J. Kelly, M.A. Kovash, S. Kowalski, R.W. Lourie, B. Murdock, B.E. Norum, B. Pugh, and C. P. Sargent, Phys. Rev. C41 448 (1990).

"High-performance Low-maintenance Sputter Source", T.A. Trainor, G.C. Harper and D.J. Hodgkins, Nucl. Inst. and Meths. **A287**, 176 (1990).

"A Precision Injector for the Tandem-Booster System at Seattle", T.A. Trainor, J.G. Douglas, G.C. Harper, D.J. Hodgkins and L.B. van Houten, Nucl. Inst. and Meths. **A287**, 184 (1990).

"Charging Belt Noise in a Van de Graaff Accelerator", T.A. Trainor, Nucl. Inst. and Meths., **A287**, 103 (1989).

"Nuclear Fission: What have we Learned in 50 Years?", R. Vandenbosch, Nucl. Phys. **A502**, 1c–20c (1989).

"Beam Diagnostics for the University of Washington Superconducting Booster", W.G. Weitkamp, J.F. Amsbaugh, R.C. Connolly, H.Fauska, T.J. Irwin, M.A. Howe, J.M. LaCroix, D.D. Leach, and H.P. Readdy, Nucl. Inst. and Meth. **A287**, 283 (1990).

Papers Submitted or to be Published:

"^{37}Ca β^+ Decay and the Efficiency of the ^{37}Cl Detector for High Energy Neutrinos", A. Garcia, E.G. Adelberger, H.E. Swanson, T.F. Lang and D.M. Moltz, submitted to Phys. Rev. C.

"Importance of Biospheric CO_2 in a Subcanopy Atmosphere Deduced from ^{14}C AMS Measurements", P.M. Grootes, G.W. Farwell, F.H. Schmidt, D.D. Leach, and M. Stuiver, Radiocarbon **30**, No. 3 (1989), in press.

"Spin Dependence of the Giant Dipole Resonance Strength Function in Highly Excited Nuclei in the Mass Region A=39–45", M. Kicínska-Habior, K.A. Snover, J.A. Behr, G. Feldman, C.A. Gossett, and J.H. Gundlach, submitted to Phys. Rev. C, in press.

"Giant Nuclear Resonances", K.A. Snover, McGraw-Hill Encyclopedia of Science and Technology, Seventh Edition, to be published.

Published Conference Proceedings, and Invited Talks:

"A New Look at an Old Problem: Testing the Equivalence Principle in the Field of the Earth", E.G. Adelberger, in *Fundamental Symmetries in Nuclei and Particles*, ed. H. Henrikson and P. Vogel, World Scientific Publ. Co., Teaneck, NJ (1990).

"Experimental Tests of the Universality of Free Fall and of the Inverse Square Law", E.G. Adelberger, to be published in the Proceedings of the 12th International Conference on General

Relativity and Gravitation.

"Is there a Fifth Force?", E.G. Adelberger, Proceedings of the XXIII Yamada Conference, *Nuclear Weak Process and Nuclear Structure*, ed. M. Morita, H. Ejiri, H. Ohtsubo and T. Sato, World Scientific, Singapore, p. 570, (1989).

"High-Sensitivity Hillside Results from the Eöt-Wash Experiment," E.G. Adelberger, Proceedings of the XXIVth Rencontre de Moriond, *Tests of Fundamental Laws in Physics*, ed. O. Fackler and J. Tran Thanh Van, p. 485, (1989).

"Recent Development of the University of Washington Colliding Beams Polarized Ion Source", C.A. Gossett, International Workshop on Polarized Ion Sources and Polarized Gas Jets, Feb. 12–17, 1990, National Laboratory for High Energy Physics (KEK), Japan. Invited talk, to be published.

"Exclusive and Inclusive Virtual Compton Scattering", C.E. Hyde-Wright, Topical Conference on Electronuclear Physics with Internal Targets, Jan. 9–12, 1989, S.L.A.C., CA. R.G. Arnold, ed, World Scientific, 1989.

"New Results on Deformation and on Isospin Mixing from Giant Dipole Decays in Highly Excited Nuclei", K.A. Snover, Bull. Am. Phys. Soc. **35**, 1032 (1990).

"The Giant Dipole Resonance in Highly Excited Nuclei", K.A. Snover, Workshop on Nuclear Structure in the Era of New Spectroscopy, Niels Bohr Institute, Copenhagen, Denmark, Nov. 1989.

"Fission: The First 50 Years", R. Vandenbosch, in Proceedings of International Conference on Nuclear Reaction Mechanisms, Calcutta, India, Jan. 1989, S. Mukherjee, ed., World Scientific, 1989, pp 217–227.

"Fission Isomers", R. Vandenbosch, presented at "50 Years with Nuclear Fission", J.W. Behrens and A.D. Carloon, eds, American Nuclear Society, 1989, p.161.

"Nuclear Fission: What have we Learned in 50 Years?", R. Vandenbosch, presented at the International Conference Fifty Years Research in Nuclear Fission, Berlin, Germany, Apr. 3–7, 1989.

Abstracts and other Conference Presentations:

"High Energy γ-rays from ^{14}N + Ag at 35 MeV/A", S.J. Luke, R. Vandenbosch, W. Benenson, J. Clayton, D. Kiofcheck, T.K. Murakami, and J. Stevenson, Bull. Am. Phys. Soc. **34**, No. 8, 1818 (1989).

"Giant Dipole Radiation and Isospin Purity in Highly Excited Compound Nuclei", J.A. Behr, K.A. Snover, C.A. Gossett, J.H. Gundlach, W.T. Hering, Bull. Am. Phys. Soc. **34**, 1832 (1989).

"Giant Dipole Radiation and Isospin Purity in Highly Excited Compound Nuclei", J.A. Behr, N.S.F. – M.S.U. Nuclear Physics Summer School, Gull Lake, Michigan, July 30–Aug. 11, 1989.

"The University of Washington AMS System: A 6-Year Technical Update", T.A. Brown, G.W.

Farwell, P.M. Grootes, and F.H. Schmidt, Fifth International Conference on Accelerator Mass Spectrometry, Paris, France, Apr. 23–27, 1990.

"^{14}C AMS at the University of Washington: Measurements in a Shared Facility at the 1% level on 0.4 mg Samples", T.A. Brown, G.W. Farwell, P.M. Grootes, P.D. Quay, F.H. Schmidt, and M. Stuiver, Fifth International Conference on Accelerator Mass Spectrometry, Paris, France, Apr. 23–27, 1990.

"Angular Momentum of Low-lying States in 127 Xe", A. Garcia, E.G. Adelberger, A. Charlop, S. Gil, J.H. Gundlach, and S. Kailas, Bull. Am. Phys. Soc., Series II, Vol. 34, No. 8, Sept. 1989.

"Missing 3+ State in 18 Ne", A. Garcia, E.G. Adelberger, D.M. Markoff, and K.B. Swartz, Bull. Am. Phys. Soc., Series II, Vol. 34, No. 8, Sep. 1989.

"Spin Distributions at Near-Barrier Energies for ^{28}Si + ^{154}Sm", S. Gil, D. Abriola, D.E. Di Gregorio, M. di Tada, M. Elgue, A. Etchegoyen, M.C. Etchegoyen, J. Fernandez Niello, A.M.J. Ferrero, A.O. Macchiavelli, A.J. Pacheco, J.E. Testoni, P. Silveira Gomes, V.R. Vanin, A. Charlop, A. Garcia, S. Kailas, S.J. Luke, and R. Vandenbosch, XII Workshop on Nuclear Physics – Iguazu Fall, Argentina, Aug. 28–Sep. 1, 1989.

"Giant Dipole Gamma-rays and Dynamic Shape Changes in Highly Excited Nuclei near A=90", J.H. Gundlach, K.A. Snover, J.A. Behr, C.A. Gossett, M. Kicinska-Habior and K.T. Lesko, International Nuclear Physics Conference, São Paulo, Brazil, Aug. 20–26, 1989.

"Giant Dipole γ-Ray and Dynamic Shape Changes in Highly Excited Nuclei near A=90", J.H. Gundlach, K.A. Snover, J.A. Behr, C.A. Gossett, M. Kicinska-Habior and K.T. Lesko, Bull. Am. Phys. Soc. **34**, 1154 (1989).

"Perturbative QCD Calculations of Exclusive Virtual Compton Scattering" C.E. Hyde-Wright, G.R. Farrar, and K. Van Bibber, Submitted to PANIC, MIT, Massachusetts, June 25–29, 1990.

"Fission Angular Distributions for the Systems ^{9}Be + ^{232}Th, ^{235}U", S. Kailas, V.S. Ramamurthy, R. Vandenbosch, A. Charlop, S.J. Luke, D. Prindle, and S.P. Van Verst, Symposium on Nuclear Physics, Aligarh, India, 1989.

"Fusion Cross Section for the System ^{6}Li + ^{28}Si at E_{Li} = 36 MeV", S. Kailas, A. Charlop, A. Garcia, S. Gil, S.J. Luke, B.T. McLain, D. Prindle and R. Vandenbosch, Symposium on Nuclear Physics, Aligarh, India, 1989.

"Charging Screen Improvements and Resistor Tests at the University of Washington FN Tandem", C.E. Linder, T.A. Trainor, and W.G. Weitkamp, to be published in Proceedings of the Symposium of Northeastern Accelerator Personnel, Oak Ridge, 1989.

"Recent Experience with Shim Stock Belt Charge Applicators", T.A. Trainor, to be published in Proceedings of the Symposium of Northeastern Accelerator Personnel, Oak Ridge, 1989.

FRONT ROW: W. KAMEOKA, Z, DREBI, A. GARCIA, D. CORCORAN, T. TRAINOR, J. LUKE, R. COOPER, W. WEITKAMP, J. BEHR, K. SWARTZ, F. SCHMIDT, C. HYDE-WRIGHT, D. ROSENZWEIG, R. VANDENBOSCH

MIDDLE ROW: M. KAPLAN, D. MARKOFF, E. SWANSON, Y. LIU, M. RAMIREZ, H. SIMONS, R. SEYMOUR, G. FARWELL, R. STOWELL, J. ROGERS, G. HARPER, L. de BRAECKELEER, L. GEISSEL

BACK ROW: K. SNOVER, J. GUNDLACH, D. WILL, D. WELLS, SHELL POINT VANVERST, P. WONG, D. STORM, P. WILLIAMS, A. CHARLOP, G. SMITH, T. BROWN, W. JIANG, M. HOWE, P. GROOTES, B. MCLAIN, D, PRINDLE

THIS YEAR, DUE TO TECHNICAL DIFFICULTIES, WE HAD TO ASSEMBLE IN FRONT OF THE LAB FOR THREE ATTEMPTS AT THIS GROUP PHOTO. E. ADELBERGER, J. AMSBAUGH, J. CRAMER, M. FRODYMA, C. GOSSETT, C. LINDER, I. TESS AND J. WOOTRESS POSED IN THE FIRST AND/OR SECOND ATTEMPTS.